

**DESIGN AND APPLICATION OF GENETICALLY ENCODED PROBES  
TO STUDY NEUROLOGICAL DISORDERS**

by

**Saranya Radhakrishnan**

**A Dissertation**

*Submitted to the Faculty of Purdue University*

*In Partial Fulfillment of the Requirements for the degree of*

**Doctor of Philosophy**



Department of Chemistry

West Lafayette, Indiana

August 2020

**THE PURDUE UNIVERSITY GRADUATE SCHOOL**  
**STATEMENT OF COMMITTEE APPROVAL**

**Dr. Mathew Tantama, Chair**

Department of Chemistry

**Dr. Angeline Lyon**

Department of Chemistry

**Dr. Jason Cannon**

Department of Toxicology

**Dr. Daniel Suter**

Department of Biological Sciences

**Dr. Alex Chubykin**

Department of Biological Sciences

**Approved by:**

Dr. Christine Hrycyna

*Dedicated to my mentor, Mathew  
my mother, Hemalatha  
my cat, Mama*

## ACKNOWLEDGMENTS

This has been a long and arduous journey and I could not have done this without the support structure offered by my friends and family, and the guidance I received from all my mentors. I also thank all the people who set up fascinating research questions for me to explore and allowed me to pursue this endeavor by standing on the shoulders of giants.

First and foremost, I would like to thank my advisor, Mathew. His passion and drive for science is infectious and has inspired me to approach scientific challenges with excitement. He has helped me identify my strengths and flourish into a confident and independent researcher. He has gone above and beyond to support me during this five-year long journey and I could not have asked for a more kind and thoughtful mentor. When he had to leave Purdue in my last year of graduate school, Angeline took my under her wing and provided a space for me to recognize my potential and I am grateful for her constant encouragement. I would also like to thank some of my other mentors after undergraduate who believed in me and took a chance on me. Dr. Sunita Setlur at BWH offered me one of my first positions after undergrad and this was instrumental in opening a lot of doors for me. Following this, Dr. Shyamala Mani offered me a lot of independence and trusted me with challenging and fascinating neuroscience that cemented my interest in the field. I cannot thank them both enough for creating the stepping stones that have finally gotten me here into graduate school.

This was a tremendous character-building experience and I am happy that I had excellent peers alongside with me on this journey. Thank you Keelan Trull, Stevie Norcross, Emily Haynes, Dan Cholger for being fantastic labmates that livened up every day in the lab; Dr. Jason Conley and Dr. Alex French for providing constructive criticism and expertise. I am especially grateful to Dr. Megha Rajendran who has been like a second mentor and has always reminded me to put myself first. My undergraduate Nathan Leroy has grown into an excellent and capable researcher and I am grateful for all his contributions to this project. I also thank my committee members, Dr. Daniel Suter, Dr. Jason Cannon and Dr. Alex Chubykin for being readily available for advice and guidance.

Finally, I would be remiss if I do not acknowledge the huge contribution of my friends and family. My parents have ensured that I had the access to the best education and they went beyond their means to provide me with the opportunities to succeed. They have constantly stressed the importance of education, and it is apparent to me that the values of hardwork and persistence that they have instilled in me, has brought me to this point. My sister, Srividhya has been an absolute rock and is always around to catch me when I fall. I have looked up to her all my life and I still have a lot of catching up to do to measure up to her. My best friend Swetha has been by my side since day 1 of undergrad and it has been a wild journey that has brought us both to the finish line at graduate school, side by side, as peers and sisters for life. I thank my friends Bharath, Kaushik, Apurupa and Aditya for their constant support and for all the good times. Thank you Ganesh for always keeping me grounded and well-fed during stressful work days. I am especially excited that I got to savour and complete this journey with my partner, Adharsh by my side. He inspires me everyday with his zest for science and incredible work ethic. My little family, with our cats Trillian and Moomoo, has helped me keep my sanity and has reminded me everyday that life is wonderful and anything is possible.

# TABLE OF CONTENTS

LIST OF TABLES .....	10
LIST OF FIGURES .....	11
ABSTRACT .....	13
CHAPTER 1. INTRODUCTION .....	14
1.1 Neurodegenerative disorders .....	14
1.2 Parkinson’s disease .....	15
1.3 LRRK2 in Parkinson’s Disease .....	16
1.4 Mitochondrial Dysfunction and Oxidative Stress.....	17
1.5 Redox Measurements.....	19
1.6 Genetically-encoded fluorescent sensors.....	22
1.7 Genetically-encoded redox probes.....	23
1.8 Neurotrauma and neuroinflammation.....	26
1.9 Purinergic signaling .....	27
1.10 ATP measurements.....	28
CHAPTER 2. IMAGING EXTRACELLULAR ATP WITH A GENETICALLY-ENCODED, RATIOMETRIC SENSOR.....	30
2.1 Abstract.....	30
2.2 Introduction.....	31
2.3 Materials and Methods.....	33
2.3.1 Materials .....	33
2.3.2 Sensor construction.....	33
ecAT3.10. ....	33
ecAT1.03-YEMK. ....	34
2.3.3 ATeam3.10 expression and purification.....	34
2.3.4 Purified AT3.10 in vitro spectroscopy.....	35
2.3.5 Cell line maintenance and transfection.....	35
2.3.6 Live-cell fluorescence microscopy and image analysis.....	35
2.3.7 Data collection and analysis .....	37
2.4 Results.....	37

2.4.1	Sensor construction and characterization .....	37
2.4.2	ecAT3.10 reports extracellular ATP turnover by ectonucleotidase activity.....	44
2.4.3	ecAT3.10 detects nucleotide-stimulated endogenous ATP release.....	47
2.5	Discussion.....	53
CHAPTER 3. DEVELOPMENT OF 2 <sup>ND</sup> GENERATION RED-SHIFTED FLUORESCENT REDOX SENSOR .....		57
3.1	Abstract.....	57
3.2	Introduction.....	57
3.3	Materials and Methods.....	60
3.3.1	Materials .....	60
3.3.2	Molecular Biology .....	60
3.3.3	Protein Expression and Purification .....	60
3.3.4	Steady-State Fluorescence Spectroscopy .....	61
3.3.5	Time-Resolved Fluorescence Spectroscopy .....	62
3.3.6	Cell Culture and Transfections .....	62
3.3.7	Live-Cell Imaging.....	63
3.3.8	Data Analysis.....	63
3.4	Results and Discussion .....	64
3.4.1	Sensor Design of 2 <sup>nd</sup> generation roGRFP2 sensor.....	64
3.4.2	Generation of Sensor Library .....	65
3.4.3	Screening and Characterization of Sensor Library .....	67
3.4.4	Proof-of-Concept studies in HEK293 cell line.....	71
3.4.5	Two-Photon Imaging.....	73
3.4.6	Grx1 and Orp1 .....	74
3.5	Conclusion .....	75
CHAPTER 4. NEURON ACTIVITY-DEPENDENT REDOX COMPARTMENTATION REVEALED WITH A SECOND GENERATION RED-SHIFTED RATIOMETRIC SENSOR		76
4.1	Abstract.....	76
4.2	Introduction.....	76
4.3	Materials and Methods.....	79
4.3.1	Materials .....	79

4.3.2	Molecular Biology .....	79
4.3.3	Lentivirus production.....	79
4.3.4	Cell Culture and Transfections .....	80
4.3.5	Live-Cell Imaging.....	80
4.3.6	Data Analysis.....	81
4.4	Results and Discussion .....	81
4.4.1	Dual Compartment Redox Imaging in Hippocampal Neurons.....	81
4.4.2	Assay Optimization .....	82
4.4.3	Neuron Activity-Dependent Redox Dynamics .....	86
4.4.4	pH dependence.....	87
4.4.5	Antioxidant rescue .....	87
4.4.6	Single-Cell Analysis of Redox Compartmentation .....	89
4.4.7	Rotenone Treatment.....	92
4.4.8	Neuron-Astrocyte Co-Culture .....	93
4.4.9	Fly Retina Imaging .....	95
4.5	Conclusion .....	97
<b>CHAPTER 5. EXPLORING THE RELATIONSHIP BETWEEN LRRK2 AND OXIDATIVE STRESS IN PARKINSON'S DISEASE .....</b>		<b>99</b>
5.1	Abstract.....	99
5.2	Introduction.....	99
5.3	Results.....	103
5.3.1	LRRK2 mutants in HEK293 cells .....	103
5.3.2	SH-SY5Y model.....	109
5.3.3	Primary hippocampal neurons .....	114
5.4	Conclusions and Future Directions.....	117
5.5	Materials and Methods.....	119
5.5.1	Materials .....	119
5.5.2	Molecular Biology.....	119
5.5.3	Cell Culture and Transfections .....	120
	HEK293 cells .....	120
	SH-SY5Y cells .....	120

Cultured Primary Mouse Neurons.....	120
5.5.4 Live-Cell Imaging.....	121
5.5.5 Data Analysis.....	121
CHAPTER 6. FUTURE PERSPECTIVES.....	122
6.1 Moving Towards In Situ and In Vivo Redox Imaging.....	122
6.2 Models for Studying LRRK2.....	123
6.3 Sensor Design and Protein Engineering.....	125
REFERENCES.....	127
VITA.....	157
PUBLICATIONS.....	158

## LIST OF TABLES

Table 1.1. Genetically encoded redox probes .....	24
Table 3.1. Linker variation for construct library.....	66

## LIST OF FIGURES

Figure 1.1. LRRK2 domains and mutations .....	17
Figure 1.2. Ratiometric and intensimetric fluorescent probes .....	23
Figure 2.1. ecATeam3.10 sensor detects extracellular ATP.....	38
Figure 2.2. Surface-localized ecAT3.10 responds to the addition of extracellular ATP .....	40
Figure 2.3. Characterization of ATP affinity and response kinetics.....	43
Figure 2.4. ecATeam3.10 detects ATP hydrolysis by ectonucleotidases. ....	46
Figure 2.5. ecAT3.10 detects nucleotide-stimulated release of ATP from cells .....	49
Figure 2.6. ecATeam3.10 detects ADP-stimulated release of endogenous ATP .....	51
Figure 2.7. ADP-stimulated release of ATP release .....	52
Figure 3.1. Diagram of the FRET relay from the roGFP donor to the RFP acceptor.....	64
Figure 3.2. Design of the rogRFP2 sensor library .....	64
Figure 3.3. Steady-state spectroscopy screen of a0GG4g.....	67
Figure 3.4. Redox titration and dynamic range measurement of a0GG4g .....	69
Figure 3.5. Linker and RFP acceptor library screen .....	70
Figure 3.6. Characterization of the second generation rogRFP2 sensor.....	71
Figure 3.7. Proof of concept dual compartment imaging in HEK293 cells.....	73
Figure 3.8. Two-photon cross sections of purified rogRFP2.....	74
Figure 4.1. Compartment specific expression of redox sensors .....	82
Figure 4.2. Stimulating neuronal activity using KCl and Glutamate.....	83
Figure 4.3. Optimization of oxidizing agent for calibration .....	85
Figure 4.4. Neuron activity-dependent redox compartmentation .....	86
Figure 4.5. Measurement of pH changes using BCECF-AM .....	87
Figure 4.6. NAc antioxidant treatment .....	88
Figure 4.7. Neuron activity-dependent redox compartmentation and antioxidant rescue. ....	89
Figure 4.8. Single-cell analysis of activity-dependent redox compartmentation.....	90
Figure 4.9. Antioxidants block the redox response in neurons.....	91
Figure 4.10. Rotenone attenuates activity-dependent redox responses in both compartments ....	93

Figure 4.11. Astrocytes attenuate mitochondrial oxidative stress in neurons.....	95
Figure 4.12. Fly retina autofluorescence interferes with green fluorescence imaging .....	96
Figure 4.13. Ratiometric imaging in <i>Drosophila</i> retina.....	97
Figure 5.1. LRRK2 mutants and Grx1roGFP2 in HEK293 cells .....	103
Figure 5.2. Grx1-roGFP2 response in LRRK2 mutants .....	106
Figure 5.3. Redox challenge in LRRK2 mutants.....	108
Figure 5.4. SH-SY5Y differentiation.....	110
Figure 5.5. Stimulation of differentiated SH-SY5Y cells.....	111
Figure 5.6. Calcium imaging of differentiated SH-SY5Y .....	112
Figure 5.7. Hydrogen peroxide challenge on SH-SY5Y cells.....	113
Figure 5.8. SH-SY5Y response to peroxide challenge and rotenone treatment .....	114
Figure 5.9. Redox responses in hippocampal neurons.....	115
Figure 5.10 LRRK2 redox response to glutamate stimulation. ....	116
Figure 5.11. Dopaminergic neurons in midbrain culture.....	118
Figure 5.12 Tracking mitochondrial movement .....	118

## ABSTRACT

Oxidative stress is a hallmark of several aging and trauma related neurological disorders, but the precise details of how altered neuronal activity elicits subcellular redox changes have remained difficult to resolve. Current redox sensitive dyes and fluorescent proteins can quantify spatially distinct changes in reactive oxygen species levels, but multicolor probes are needed to accurately analyze compartment-specific redox dynamics in single cells that can be masked by population averaging. Our lab previously engineered a genetically-encoded red-shifted redox-sensitive fluorescent protein sensors using a Förster resonance energy transfer relay strategy. Here, we developed a second-generation excitation ratiometric sensor called rogRFP2 with improved red emission for quantitative live-cell imaging. Using this sensor to measure activity-dependent redox changes in individual cultured neurons, we observed an anticorrelation in which mitochondrial oxidation was accompanied by a concurrent reduction in the cytosol. This behavior was dependent on the activity of Complex I of the mitochondrial electron transport chain and could be modulated by the presence of co-cultured astrocytes. We also demonstrated that the red fluorescent rogRFP2 facilitates ratiometric redox imaging in *Drosophila* retinas. The proof-of-concept studies reported here demonstrate that this new rogRFP2 redox sensor can be a powerful tool for understanding redox biology both in vitro and in vivo across model organisms. In addition, we have used these tools that monitor cellular redox, to study oxidative stress and ROS changes in Parkinson's disease models. Here, we have established cellular models for studying Parkinson's disease causing LRRK2 mutations to create a platform for future work to explore the relationship between PD associated LRRK2 variants and oxidative stress.

# CHAPTER 1. INTRODUCTION

My work in the Tantama lab has primarily revolved around developing genetically encoded redox probes and applying them in different biological contexts to study neurological disorders, specifically of the neurodegenerative nature. Here, I developed a genetically encoded red-shifted redox sensor rogRFP2, which has been applied in neuronal models. Using the repertoire of toolsets available, we study oxidative stress and ROS changes in Parkinson's disease models. In addition, I worked on developing and characterizing ecATeam, which is a genetically encoded extracellular ATP sensor.

## 1.1 Neurodegenerative disorders

Neurodegeneration is the process of neuronal deterioration in the brain and spinal cord that progressively leads to loss of brain function and a decline in cognitive abilities. It is a multifactorial process that is usually induced by cellular dysfunctions such as oxidative stress, mitochondrial dysfunction, excitotoxicity, calcium deregulation, protein aggregation and neuroinflammation (Glass et al, 2010; Lin & Beal, 2006). Some of the common neurodegenerative disorders are Alzheimer's disease (AD), Parkinson's disease (PD), Huntington's disease, amyotrophic lateral sclerosis (ALS) and Frontotemporal dementia. This cluster of neurodegenerative diseases that affect cognitive and motor functions are quickly ascending to become a critical health issue, especially with an increasingly aging population (Gammon, 2014). It is vital to study them as they are irreversible, lack effective therapeutic interventions, and pose a significant social and economic burden.

These diseases target specific neuronal subpopulations, which leads to the failure of specific brain regions, thereby compromising their function. For example, in both early onset and late onset AD one of the first regions that exhibit neuronal loss is the entorhinal cortex followed by hippocampus resulting in the hallmark symptom of memory loss seen in AD (van Hoesen, Hyman, & Damasio, 1991). ALS is caused by the degeneration of motor neurons (Martin, 1999) and in HD, the neuronal loss is predominantly observed in the striatal neurons of the basal ganglia and the cortex (Larsson et al., 1998). In PD, the degeneration occurs in the dopaminergic neurons of the substantia nigra.

The selective vulnerability of different neuronal subtypes in the brain makes them susceptible to stress when presented with environmental insults or trauma (Saxena & Caroni, 2011). Among these diseases, the genetic cause of HD is attributed to the inherited defect in a single gene, whereas most of the other neurodegenerative diseases result from a combination of genetic and environmental factors. These diseases typically progress slowly, taking years to develop, and the neurological damage is already quite prevalent and irreparable before the onset of symptoms, making them especially challenging to detect and treat.

## 1.2 Parkinson's disease

PD is the second most common neurodegenerative disorder, and it affects over 6 million people globally (Ray Dorsey et al., 2018); currently, there are nearly 1 million people in the US suffering from PD (Marras et al., 2018). The disorder was first recognized by James Parkinson over 200 years ago who termed it the 'Shaking Palsy' or 'Paralysis Agitans' and described it in his work, 'Essay on the Shaking Palsy'. He highlights the defining characteristics of the disease as *tremor coactus* which refers to resting tremors and *scelotyrbie festinans*, referring to the classic parkinsonian feature of festinating gait (Parkinson, 1817). Half a century later, the eponym Parkinson's disease was coined by Jean-Martin Charcot, who was pivotal in distinguishing resting tremors from the action tremors in other diseases like multiple sclerosis and ALS, which shared similar motor defects (Charcot, Bourneville, & Brissaud, 1887). He further characterized some of the motor symptoms of the disease like bradykinesia and rigidity and also recognized some non-motor symptoms. To this day, the hallmark of the disease is rigidity, bradykinesia, and resting tremors of the motor symptoms, which are accompanied by some issues with balance and coordination. The 'invisible symptoms' or non-motor symptoms such as pain, constipation, autonomic dysfunction, sleep irregularities, and mood changes also severely impact the quality of life (Charcot et al., 1887).

The pathological features of PD were discovered much later, like the link between PD and the substantia nigra as well as the observance of inclusion bodies in the substantia nigra. Following this, the role of dopamine was identified serendipitously when the treatment of L-DOPA reversed reserpine-induced Parkinsonism in animal models (Carlsson, Lindqvist, Magnusson, & Waldeck, 1958). Upon the discovery of the localization of dopamine in the brain, it was hypothesized that

the presence of dopamine in the corpus striatum was relevant to the control of movement (Bertler & Rosengren, 1959). It is now understood and acknowledged that the pathological hallmarks of PD are the presence of Lewy bodies and loss of dopamine caused by neurodegeneration in the substantia nigra pars compacta (SNc) (Hughes et al, 1992). The origins of these pathological presentations have been difficult to delineate, making it hard to design effective treatments or early interventions for PD. Current treatment for PD are drugs like levodopa that are used for dopamine replacement therapies (Goetz et al, 2005) or deep brain stimulation (Groiss et al, 2009) but all of these treatments are only used to manage the symptoms and are not effective in slowing the progression of the disease.

Age is the dominant factor for PD, and people over the age of 60 are primarily affected by the disease. A majority of PD cases are sporadic, but some heritable mutations have also been identified (Thomas & Flint Beal, 2007). Monogenic forms of the disease are cases where the phenotype can develop due to a mutation in a single gene. These are rare types of PD but account for around 30% of familial and 3-5% of sporadic cases (Klein & Westenberger, 2012a). Some of the common monogenic mutations of PD include LRRK2, SNCA, UCHL1, which are autosomal-dominant, PINK1, Parkin, and DJ-1, which are autosomal-recessive (Klein & Westenberger, 2012a). Despite their relatively rare occurrence, it is important to understand the development of the disease in genetic forms of PD due to the pathological similarities shared with the idiopathic forms of PD. Environmental factors and gene-environment interactions are also responsible for the development of PD disease pathogenesis (Kiebertz & Wunderle, 2013). Some of the common examples of these are pesticides (J. W. Langston & Ballard, 1983), metals like iron and manganese (Harischandra et al., 2019; Montgomery, 1995), industry by-products like PCBs (Hatcher-Martin et al., 2012), and dietary and lifestyle factors (Powers et al., 2009).

### **1.3 LRRK2 in Parkinson's Disease**

Leucine-rich repeat kinase 2 (LRRK2) gene is the most common genetic cause of PD. LRRK2 is a large and complex protein with multiple functional domains whose normal cellular function is not completely understood. LRRK2 is a pleomorphic risk locus with several variants that have differential effects on the pathogenicity of the protein and potentially vary in the mechanism of causation (Paisán-Ruíz et al., 2004; Zimprich et al., 2004).

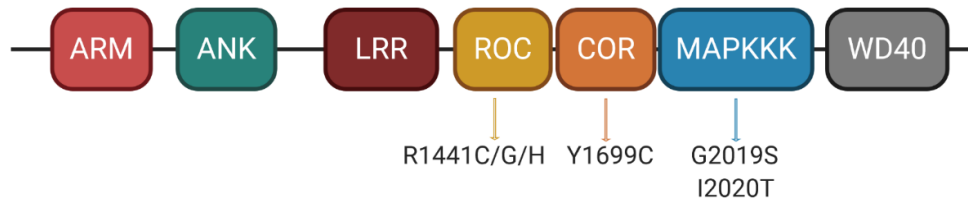


Figure 1.1. LRRK2 domains and mutations

LRRK2, also known as dardarin is a 2458 amino acid protein and is encoded by a coding sequence of ~7.5 kb. The protein has a Ras-related guanosine triphosphate (GTP)-binding domain (*Ras of complex proteins, Roc*), a kinase domain belonging to the mitogen-activated protein kinase kinase kinase (MAPKKK) subfamily and a region called C-terminal of Ras (COR) domain which make up the central catalytic region. Outside of this, it has armadillo, ankyrin, and leucine-rich repeats in the N-terminal region, and WD 40 repeats at the C-terminus, and these serve as modules for protein-protein interactions (Cookson, 2016b). Around 20 different PD associated mutations, of which at least 8 are pathogenic, have been identified in LRRK2. Among these, the mutations of particular interest are the R1441C/G/H mutation near the Roc domain, the Y1669C in the COR domain, and the mutations G2019S and I2020T in the kinase domain (Deng et al., 2006; Zimprich et al., 2004). When compared to the wild type protein, the I2020T and G2019S mutants show a minor but significant increase in net kinase activity and are considered gain of function mutations (Gloeckner et al., 2006; West et al., 2005b).

#### 1.4 Mitochondrial Dysfunction and Oxidative Stress

Several aging disorders commonly present with evidence of oxidative damage, and this has also been observed in PD tissue and animal models (Andersen, 2004). There is also a continued accumulation of data suggesting that mitochondria play an important role in the pathogenesis of the disease. Toxins like rotenone and MPTP that are used to reproduce features of PD in animal models are known to affect the mitochondria, specifically the mitochondrial complex I (Betarbet et al., 2000; J. Langston, Ballard, Tetrud, & Irwin, 1983; Sherer et al., 2003). Reduced coenzyme Q10 (CoQ10) and complex I activity have been observed in brain tissues of PD patients (Keeney, 2006; Schapira et al., 1990; Shults et al., 1997). Since mitochondria are a major source of reactive

oxygen species (ROS) in the cell, it is imperative to look at the possibility of mitochondrial dysfunction induced oxidative stress.

Mitochondria are essential for cellular metabolism and function as they are the site of energy production in the cell through mitochondrial respiration and they produce adenosine triphosphate (ATP) through the citric acid cycle and oxidative phosphorylation (Fornie, Carrari, & Sweetlove, 2004). Oxidative phosphorylation that occurs in the inner mitochondrial membrane, produces a majority of ATP. Here, the electron transport chain that consists of protein complexes I, II, III, IV, mitochondrial membrane bound coenzyme Q and soluble electron carrier cytochrome c, transfers electrons from electron donors to electron acceptors like oxygen. Protons are produced from these redox reactions and are pumped across the inner mitochondrial membrane. The production of ATP by ATP synthase is powered by the energy provided by the electric potential and pH gradient.

Some of the common redox by products of mitochondrial respiration are hydrogen peroxide and superoxide anion radical. The superoxide is released into the inner mitochondrial membrane, where it is converted by Mn-superoxide dismutase (SOD2) to hydrogen peroxide (Candas & Li, 2014) which can easily penetrate the membrane. These and other redox molecules play an important role in maintaining redox homeostasis in the cells and redox signaling across compartments. ROS accumulation can lead to mitochondrial outer membrane permeabilization which can lead to the activation of the cellular apoptotic pathway (Kamata et al., 2005; Tajeddine, 2016).

In PD, mature dopamine neurons in the SNc region have high levels of basal mitochondrial oxidative stress (Sulzer & Surmeier, 2013). These cells experience increased susceptibility to oxidative stress due to autonomous pacemaking properties that engage L-type calcium channels, causing a calcium influx (Goldberg et al., 2012; D. J. Surmeier, Guzman, Sanchez-Padilla, & Schumacker, 2011). The removal of this excess calcium is an energy-expensive process and is aided by oxidative phosphorylation in the mitochondria, thereby increasing the probability of generating ROS as by-products of this mechanism. Due to this metabolic burden, mature dopaminergic neurons in the SNc region have higher mitochondrial oxidative stress than dopaminergic neurons in the VTA region (Guzman et al., 2010). Elevated oxidative stress is

observed both in the somatic and dendritic regions of the dopaminergic neurons (Guzman et al., 2010).

Mutations in PD associated genes affect proteins involved in mitochondrial dynamics and cause defects in mitophagy. Parkin and PINK1 encode for proteins that regulate mitophagy, the process by which damaged mitochondria are cleared from the cell (Jin & Youle, 2012). DJ-1 is a redox-sensitive protein that is enriched in the mitochondria, and this confers the ability to act as a cellular redox sensor that can signal oxidative stress and direct oxidative defense mechanisms in the mitochondria (Hao, Giasson, & Bonini, 2010). Loss of function mutations in DJ1 could impede the ability of DJ1 to regulate oxidative stress by compromising mitochondrial uncoupling (Hao et al., 2010). PD mutations in these genes result in the accumulation of damaged mitochondria, which could additionally result in a buildup of oxidative stress and neurodegeneration. LRRK2 mutations have also been observed to cause delays in mitochondrial clearance, affect mitochondrial fission and mitophagy (Hsieh et al., 2016; Niu, Yu, Wang, & Xu, 2012). Complex I defects and oxidative stress have also been observed with the accumulation of  $\alpha$ -synuclein inside mitochondria (Bender et al., 2013; Devi et al, 2008). Additionally,  $\alpha$ -syn also induced mitochondrial fragmentation and changes in mitochondrial morphology (Kamp et al., 2010; Xie & Chung, 2012).

Increases in ROS can propagate mitochondrial dysfunction and vice versa. It is imperative to delineate this cycle of oxidative stress and mitochondrial dysfunction to understand the etiology of Parkinson's disease. To study this, we need tools that can be used in cellular and tissue models of PD to observe the propagation of ROS leading up to neurodegeneration. In our lab, we are interested in developing tools for redox measurements and use these in different cellular models to study Parkinson's disease.

## **1.5 Redox Measurements**

From the earlier description of oxidative stress and the integral role it plays in neurodegenerative disorders, it is clear that we need effective methods for measuring cellular redox changes to understand these diseases. Oxidative stress can be measured in the following ways: (a) direct measurement of the levels of ROS, (b) measurements of antioxidant levels, (c) measuring the levels of the oxidative damage to biomolecules, (d) indirect measurements of downstream effects

on gene expression and signaling(Ellerby & Bredesen, 2000). Some of the earlier methods for measuring oxidative stress depended on measuring the products of oxidative stress like lipid peroxidation products or markers of protein and DNA damage. Assays that measure antioxidant levels, usually measure the activity of antioxidant enzymes like superoxide dismutase and catalase.

ROS molecules cause oxidation of amino acid residues like proline, lysine, threonine, and arginine and oxidation of protein backbones resulting in the generation of protein carbonyls (Levine et al., 1990). These are usually used as biomarkers of oxidative modification of proteins and can be measured by ELISA, Mass spectrometry, immunoblots, and spectrophotometric methods and HPLC (Levine et al., 1990). An alternate to protein oxidation measurements is the detection of DNA damage. Some of the ROS modifications on DNA generate DNA oxidation products like the nucleobase 8-oxo-7,8-dihydroguanine (8-oxoGua) (Cadet & Richard Wagner, 2013) which is considered as one of the main DNA biomarkers used to measure oxidative stress in cellular DNA and samples of biological fluids (Evans, Dizdaroglu, & Cooke, 2004; Shigenaga, Park, Cundy, Gimeno, & Ames, 1990). These products are usually measured by methods such as HPLC coupled with electrochemical detection or mass spectroscopy (Shigenaga et al., 1990). Some other markers for oxidative stress are 8-hydroxy-2'-Deoxyguanosine (8-OHdG) and 4-hydroxynonenal (HNE) which is an end product of lipid peroxidation (Ayala et al, 2014)

The other method of detecting oxidative stress was to measure levels of antioxidants. In cells, there is usually a balance maintained between ROS and antioxidants. One of the main functions of antioxidants is to sequester excessive ROS to protect the cell against damage, effectively maintaining redox homeostasis (Birben et al., 2012). Glutathione, present in its reduced form (GSH), is one of the most vital antioxidants in the cell (Lushchak, 2012). Under physiological conditions, reduced GSH is present at nearly 10-100-fold concentrations over the oxidized form (oxidized GSH, GSSG) and helps reduce ROS and protein disulfides (Aquilano, Baldelli, & Ciriolo, 2014). The ratio of the reduced and oxidized form, referred to as glutathione redox potential, is an effective indicator of cellular redox and measured by spectrophotometry or HPLC (Rahman, Kode, & Biswas, 2007). Some other common cellular antioxidants are enzymes like superoxide dismutase (SOD) and catalase (J. Sedlak & Lindsay, 1968). SOD catalyzes the conversion of superoxide to hydrogen peroxide, and catalase catalyzes the decomposition of

hydrogen peroxide to water. The enzyme activity for these antioxidants can be measured using commercially available assays (Weydert & Cullen, 2010). One of the drawbacks of these types of indirect measurements is that the oxidative stress is usually quantitated using endpoint measurements of oxidized/reduced thiol ratio, oxidized macromolecules, and lipids but these do not help us gain any insight into the interplay of redox activities between a cell in a spatially resolved manner.

An interesting alternative to these types of measurements is the direct measurement of ROS in cells instead of the measurement of ROS initiated effects like biomolecular damage. Some of these methods are spin trapping, fluorescence, and enzymatic techniques, and chemiluminescence (Halliwell & Whiteman, 2004). Electron paramagnetic resonance (EPR) spectroscopy, also known as electron spin resonance, is a popular method for direct ROS measurements (Halliwell & Gutteridge, 2015). It is used to detect molecules with unpaired electrons and when combined with spin trapping, it can be used to measure short lived ROS species like  $O_2^{\cdot-}$ ,  $\cdot OH$ , and NO (Halliwell & Whiteman, 2004). A major advantage of this method is that it can be used for imaging redox in whole live animals in a non-invasive manner (Shulaev & Oliver, 2006). The spin traps react covalently to these ROS and form a stable adduct and the ESR spectrum of these adducts will reveal the identity of the trapped ROS (Suzen, Gurer-Orhan, & Saso, 2017). However, these adducts are often unstable in biological environments and the images have low spatial resolution (Halliwell & Whiteman, 2004; Villamena & Zweier, 2004).

Another common method for ROS measurements, is the use of fluorescent dyes and they are particularly useful for live cell imaging. These dyes have a fluorescent readout when they come in contact with ROS. The most commonly used fluorescent redox probe is Dichlorodihydrofluorescein (DCFH) and the acetylated derivative DCFH-DA is cell permeable and used for intracellular measurements. The deacetylation of DCFH-DA is catalyzed by intracellular esterases followed by oxidation to the fluorescent product DCF (X. Chen, Zhong, Xu, Chen, & Wang, 2010). Some other popular probes are dihydroethidium (DHE) and Mito-DHE (commercially available as mitoSOX) (Rothe & Valet, 1990; Xianhua Wang et al., 2013). With all these probes, there is rapid photo oxidation, which can lead to high background fluorescence (Zielonka & Kalyanaraman, 2010). While these probes are widely used to measure cellular ROS,

there have also been developments of probes that are specific to different reactive species like the boronate-based probes (Chang, Pralle, Isacoff, & Chang, 2004). The use of these probes can be advantageous as they circumvent the need for any genetic manipulation and can be directly applied to different types of samples. However, some of the disadvantages of these probes are their irreversibility, lack of specificity and inability to penetrate/target to multiple cellular compartments. These dyes can also exhibit cross reactivity. Despite the availability of mitochondrial specific probes like mitoSOX, they are not ideal as they can overload the mitochondria at high concentrations and disrupt mitochondrial function (Robinson et al., 2006). We are interested in studying cell type and compartment specific redox and we need an effective alternative to these dyes that can be successfully targeted and expressed in different subcellular compartments.

## 1.6 Genetically-encoded fluorescent sensors

Osamu Shimomura isolated the green fluorescent protein from jellyfish (*Aequorea Victoria*) in 1962. It is a 27kDa protein made up of 238 amino acids that form a  $\beta$ -barrel structure around a central  $\alpha$ -helix. The chromophore is protected from the external medium and comprises of 3 amino acids. The chromophore of the wtGFP consists of the residues SYG (S65/Y66/G67) and the cyclicized backbone of these residues forms the imidazolidone ring. Cyclization followed by oxidation results in the formation of a conjugated system of  $\pi$ -electrons and confers the property of absorbing and emitting visible light. Depending on whether the Y66 is in its anionic phenolate form or in its neutral phenol form, the fluorophore absorbs light at 470nm or 395nm (Tsien, 1998). Therefore, wtGFP can have two excitations peaks based on the protonation state of the phenol group on Y66 and this property of GFP makes it useful for designing genetically encoded sensors like the redox sensitive roGFPs (Tsien, 1998). A variant of GFP was designed by introducing the S65T mutation that shifted the chromophore absorption to 488nm, which is now referred to as eGFP (Heim & Tsien, 1996).

Genetically encoded fluorescent probes are designed using fluorescent proteins that can be encoded in a sequence and expressed in cells (J. Zhang, Campbell, Ting, & Tsien, 2002). These sensors can be classified based on the type of output they produce or the number of FPs in the probe. Single FP probes typically signal changes in the environment due to engineered changes within the FP (pH and redox sensing) or contain ligand binding domain with a circularly permuted

FP (cpFP) or split FP (Nagai, Sawano, Eun Sun Park, & Miyawaki, 2001; Tantama, Hung, & Yellen, 2011). Another classification of these probes is based on optical output where intensimetric sensors are probes where ligand binding or environment induced fluorescent changes are measured at a single wavelength (Figure 1.2). These sensors tend to have high dynamic ranges and signal to noise ratio but unfortunately cannot easily be used for quantitative measurements and can be affected by expression levels and imaging artifacts. Another category of sensors is ratiometric sensors that are engineered to exhibit dual excitation behavior (Figure 1.2). For example, in Figure 1.2 you can notice that due to the dual excitation behavior of the ratiometric sensor, we have emission values for two different excitation wavelengths and any change in environment is signaled by changes at both these wavelengths, enabling a self-normalizing quantitative measurement. These sensors can, therefore, be corrected for expression level, bleaching, and experimental artifacts.

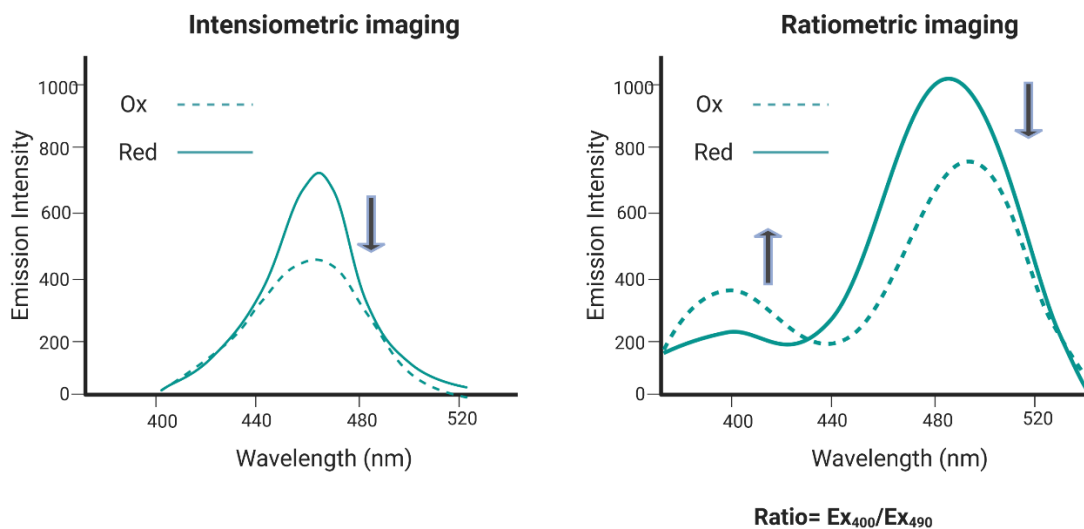


Figure 1.2. Ratiometric and intensimetric fluorescent probes

### 1.7 Genetically-encoded redox probes

The above-mentioned limitations of small-molecule dyes can be overcome with the development of genetically encoded probes that enable the dynamic measurements of redox in cells (Ezeriņa, Morgan, & Dick, 2014). One of the major advantages of genetically encoded probes is the ability to be accurately targeted to multiple subcellular locations (Albrecht et al., 2014). In addition, the

greater redox specificity of some of these probes makes them an exciting alternative to redox sensitive dyes. The probes are reversible, have low toxicity and can be targeted to subcellular regions by fusing them to specific targeting sequences (Albrecht et al., 2014). Not all of the currently available genetically encoded probes are redox species-specific, but oxidant-specific protein domains can be incorporated into the probes, making them redox species-specific (Morgan, Sobotta, & Dick, 2011).

Table 1.1. Genetically encoded redox probes

Redox Sensor	FP	Sensing domain	Ratiometric	Specificity	Reference
roGFP1	GFP	FP	Yes	GSSG/GSH	(Hanson et al., 2004)
roGFP2	EGFP	FP	Yes	GSSG/GSH	(Hanson et al., 2004)
Grx1-roGFP2	EGFP	Grx1, FP	Yes	GSSG/GSH	(Gutscher et al., 2008)
roGFP2-Orp1	EGFP	Orp1, FP	Yes	H <sub>2</sub> O <sub>2</sub>	(Gutscher et al., 2009)
rxYFP	YFP	FP	No	GSSG/GSH	(Østergaard et al., 2001)
HyPer	cpYFP	OxyR	Yes	H <sub>2</sub> O <sub>2</sub>	(Belousov et al., 2006a)
HyPerRed	cpRFP	OxyR	No	H <sub>2</sub> O <sub>2</sub>	(Belousov et al., 2014)
RedoxFlour	Cerulean /Citrine	Peptide linker with 4 Cys	Yes	H <sub>2</sub> O <sub>2</sub> , GSH/GSSG, Trx	(Yano et al., 2010)
rxRFP	cpRFP	FP	No	Thiol/disulfide equilibrium	(Fan & Ai, 2016; Fan, Chen, & Ai, 2015)
TrxRFP	RFP	Trx, FP	No	Thiol/disulfide equilibrium	(Fan, Makar, Wang, & Ai, 2017a)

The first fluorescent protein based redox sensor was created by modifying the yellow fluorescent protein (YFP) and inserting a pair of cysteines onto the surface of the  $\beta$ -barrel (Østergaard, Henriksen, Hansen, & Winther, 2001b). Upon oxidation, a reversible disulfide bridge is formed between the two residues, resulting in a change in fluorescence when compared to the reduced state. A similar modification was introduced in green fluorescent proteins (GFP) by Hanson et al to create the roGFP that is redox sensitive and ratiometric (Hanson et al., 2004). More recently, red fluorescent redox sensors, rxRFPs have been created by modifying a circularly permuted red FP by the placement of cysteines on the N and C termini of the FP (Fan & Ai, 2016). This method of modifying the FPs to make them redox sensitive has yielded the most widely used fluorescence redox probes.

The roGFP sensors are designed using the GFP as a scaffold and engineering two cysteine residues, S147 and Q204, near the chromophore (Hanson et al., 2004). The disulfide formation at these residues causes a chromophore protonation shift. The redox sensitive FPs, roGFP1 and roGFP2 were created using the wtGFP and S65T mutant, respectively and they are excitation ratiometric. In the roGFP2, based on S65T variant, the chromophore is preferentially deprotonated in reduced roGFP2 and upon oxidation it is preferentially protonated which enhances excitation at 405nm in addition to the excitation at 488nm (Hanson et al., 2004). The advantages of the ratiometric nature of the roGFPs are that the readout can now be controlled for factors like expression level, illumination, bleaching, etc. which makes them better to use than single excitation intensimetric sensors. The midpoint potentials for the roGFP1 is -291mV and -280mV for roGFP2 (Hanson et al., 2004). These low midpoint potentials made them suitable for subcellular measurements in different compartments like the cytosol, mitochondria, nucleus and peroxisomes.

Another type of redox probe is one where the FP is not redox sensitive, but it is fused to a redox sensitive protein domain and responds to a conformational change in the domain. The best example for this is the redox sensitive probe HyPer used for measuring intracellular H<sub>2</sub>O<sub>2</sub> where the cpYFP is fused to the sensing domain OxyR (Belousov et al., 2006b). HyPer has also been used to measure micromolar levels of intracellular H<sub>2</sub>O<sub>2</sub> levels and has can detect nanomolar changes *in vitro*. However, when compared to the roGFPs, HyPer is significantly more pH sensitive making it less suitable for use in measuring intracellular redox (Belousov et al., 2006b).

In order to improve the specificity of the redox sensitive FPs discussed earlier, the FPs are fused with other redox enzymes. This helps engineer a redox relay between the redox sensitive FP and the enzyme to equilibrate with a specific redox pair. This approach has been used in sensors such as the rxYFP-yGrx1 (Björnberg, Østergaard, & Winther, 2006), Grx1-roGFP2 (Gutscher et al., 2008), roGFP2-Orp1 (Gutscher et al., 2009) and more recently the Trx-RFP (Fan, Makar, Wang, & Ai, 2017b). In Grx1-roGFP2, roGFP2 is fused to glutaredoxin-1 (Grx1) and the sensor is now highly glutathione specific and more importantly, has superior kinetics as compared to the parent roGFP2 sensor. The roGFP2 was also fused to the sensing oxidant receptor peroxidase 1 (Orp1), to generate the roGFP2-Orp1 sensor which is now sensitive and specific to H<sub>2</sub>O<sub>2</sub>. Both these probes

have been used in *in vivo* models in *Drosophila* and *in vivo* and in slice in rodent models (Albrecht, Barata, Großhans, Teleman, & Dick, 2011a).

Genetically encoded probes allow the dynamic measurement of redox changes in single cells and subcellular levels with compartment specific targeting. However, due to the limited emission range of these probes, we can only monitor one or two compartments or redox parameters at a time. For the simultaneous measurement of multiple compartments, we need multicolor probes that can be targeted to specific subcellular regions. The currently available redox sensors in the red spectrum like the rxRFPs, roKate, grx1-roCherry, rxmRuby, Trx-RFP have allowed for the kind of multicolor imaging that helps understand redox dynamics between compartments but these sensors are single excitation intensimetric sensors and there is still a need for ratiometric redox sensors for quantitative measurement of intracellular redox levels (Fan & Ai, 2016; Fan et al., 2017a; Piattoni et al., 2019; A. G. Shokhina, Belousov, & Bilan, 2019; Arina G. Shokhina et al., 2019). Additionally, the optical window of 650-1100nm is preferred for the deep imaging of tissues, and there is also a dearth of far red or near infrared sensors for redox imaging. Still, the availability of such a varied toolbox of probes for redox imaging with high spatial and temporal resolution, has facilitated the study of redox processes in cells and whole organisms and will continue to allow new insights into cellular redox system.

## **1.8 Neurotrauma and neuroinflammation**

Though a lot of neurodegenerative disorders are typically observed to be age-associated, neurodegeneration can also occur during neurotrauma or in neuropsychiatric illnesses. Some of the common diseases arising from neurotrauma include, epilepsy, stroke, traumatic brain injury (TBI) and spinal cord injury (SCI) (Arundine & Tymianski, 2004; Rama & Garcia Rodriguez, 2012). Traumatic brain injury also increases extracellular levels of glutamate and this is a major contributor to neuronal damage after traumatic injury (Arundine & Tymianski, 2004). After traumatic injury or ischaemic injury to the brains, there is an increase in the levels of extracellular ATP which are actively released from living cells (Melani et al., 2005). One of the essential functions of astroglia is to sequester and recycle extracellular glutamate (Nedergaard et al., 2003) but recent studies have shown that astrocytes also release glutamate (Parpura 1994) and ATP (Newman 2001). This neuroglial communication can signal neuroinflammation, affect neuronal

activity (Fellin 2004) and neuronal survival (Ding et al 2007). Purinergic receptors P2X2 and P2Y1 are activated by ATP release from astrocytes which encounter mechanical trauma (Neary, Kang, Willoughby, & Ellis, 2003).

## 1.9 Purinergic signaling

Adenosine triphosphate (ATP) is widely recognized as a critical intracellular energy source. However, its role as a ubiquitous signaling molecule involved in purinergic signaling is not as well defined despite being studied over the last 40 years (Burnstock, 2006a). ATP release into extracellular space occurs by leakage of intracellular ATP during apoptosis and cellular damage and by non-lytic mechanisms like stimulated exocytosis. Extracellular ATP modulates purinergic signaling by activating receptors in both an autocrine and paracrine manner (Corriden & Insel, 2010b). Extracellular ATP is rapidly hydrolysed by ectonucleotidases into ADP, AMP and Adenosine and these components selectively activate specific subtypes of purinergic receptors to effect different downstream signaling events (Signaling, Harden, Boyer, & Nicholas, 1995).

Purinergic receptor subtypes are broadly categorized into two families, the P1 family of receptors that are G-protein coupled and are selectively activated by adenosine and P2 family which respond to ATP and its metabolites (Ralevic & Burnstock, 1998). The P2 family of receptors is further subclassified into P2X receptors (ionotropic) and P2Y receptors (G-protein coupled) (Ralevic & Burnstock, 1998). Purinergic signaling has been observed in several cell types including cardiac cells, epithelial, immune cells and in neuron-glia communication (Burnstock, 2006b; Cekic & Linden, 2016).

Its role as a key gliotransmitter has recently gained importance after studies showed extracellular ATP release at tri-partite synapses regulates neurotransmitter release from neurons. In CA1 synapses, glutamate release from the presynaptic terminals can activate mGluR5 receptors on the astrocytes which caused an elevation of astrocytic  $Ca^{2+}$  (Panatier et al., 2011). This evoked an extracellular ATP release which regulates neurotransmitter release in the post synaptic terminal. Similarly, adaptive increases to  $CO_2$  accumulation during respiration was observed when chemosensitive astrocytes responded to the physiological decrease in pH by increasing intracellular  $Ca^{2+}$  (Davalos et al., 2005a). This also stimulated an ATP release which then caused the purinergic

activation of chemoreceptor neurons in the retrotrapezoid nucleus. Extracellular ATP also mediates microglial chemotactic response to injury, but it is unclear if ATP itself acts as the chemoattractant or stimulates the release of other chemo-attractants through a purinergic mechanism (Davalos et al., 2005b). ATP, its hydrolysis components and extracellular ATPase are hypothesized to form a self-regulating loop in synapses but several questions remain regarding the specific conditions under which extracellular ATP release occurs, the nature of this self-stimulated release of ATP and primarily whether the ATP release observed in tri-partite synapses is released from glial cells

### **1.10 ATP measurements**

Real time imaging of purinergic signaling in astrocytes has been challenging so far due to the lack of tools for imaging extracellular ATP release from live cells. Purinergic signaling has been measured using secondary messengers from downstream signaling events and using pharmacological modulators but these techniques used are either invasive, have poor spatiotemporal resolution or are unable to follow the ATP signaling in live cells (Rajendran, Dane, Conley, & Tantama, 2016). Genetically encoded fluorescent sensors can be used for live-cell imaging and detection of analytes with high spatial and temporal resolution. They can also be targeted to subcellular compartments and the extra cellular membrane for measuring real-time changes in analyte concentration to study gliotransmission of ATP.

Some of the available fluorescent probes for ATP measurement are Perceval, the ATeam sensors and Queen sensors (Berg, Hung, & Yellen, 2009; Hiromi Imamura et al., 2009; Tantama, Martínez-François, Mongeon, & Yellen, 2013; Yaginuma et al., 2014). Perceval is a ratiometric sensor with a cpmVenus that can measure the ATP to ADP ratio inside cells (Berg et al., 2009). Imamura et al, developed a set of Förster resonance energy transfer (FRET) based indicators named ATeam to visualize and monitor the levels of ATP inside live cells in real-time. These consisted of a cyan and yellow fluorescent protein pair as the reporter and the epsilon subunit of the bacterial  $F_0F_1$ -ATP synthase, which is the sensing domain. ATP binding causes a conformation change in the sensing domain that creates a FRET response, which is measured as a fluorescence readout (Hiromi Imamura et al., 2009). The Queen family of ATP sensors utilizes the same epsilon subunits as the sensing domain, but uses a single fluorescent protein, cpEGFP, as the reporter

(Yaginuma et al., 2014). Here, we have used the FRET-based ATP sensor ATeam to engineer a surface tethered ATP sensor that can be used to study purinergic signaling at the cell membrane.

My thesis will begin with a chapter highlighting my work on the genetically encoded extracellular ATP sensor, ecATeam. Following that, the subsequent chapters will focus on the development and application of genetically encoded redox probes in biological contexts. Chapters III and IV will highlight the development and characterization of the red-shifted redox probe, rogRFP2 and the observation of activity-dependent redox compartmentation using this sensor. Chapter V will discuss the work that went into establishing cellular models to study LRRK2 and its relationship with ROS using redox probes.

## CHAPTER 2. IMAGING EXTRACELLULAR ATP WITH A GENETICALLY-ENCODED, RATIOMETRIC SENSOR

\*This work has been published and is reproduced with permission from Conley, J. M., Radhakrishnan, S., Valentino, S. A. & Tantama, M. Imaging extracellular ATP with a genetically-encoded, ratiometric fluorescent sensor. *PLOS ONE* **12**, e0187481 (2017).

### 2.1 Abstract

Extracellular adenosine 5'triphosphate (ATP) is a fundamental component of purinergic signaling that contributes to wide ranging physiological processes and pathophysiological conditions. New methods that enable direct measurement of extracellular ATP dynamics with high spatial and temporal resolution are expected to advance our understanding of purinergic signaling mechanisms in healthy and pathological states. Several distinct classes of fluorescent protein-based biosensors have emerged as powerful molecular tools that report real time intracellular ATP dynamics with single cell and subcellular resolution, but there are no reports of leveraging such technology for the detection of extracellular ATP. Therefore, the focus of this study was to develop and characterize a series of fluorescent protein-based biosensors for the detection of extracellular ATP. Our strategy was to anchor several candidate ATP biosensors to the plasma membrane and to position the biosensor in the extracellular space, allowing for the detection of extracellular ATP. We present the extensive characterization of one such cell surface tethered candidate biosensor. Live cell fluorescence microscopy was used to verify biosensor expression and localization at the cell surface and to measure sensor response to exogenous application of ATP when expressed by cell types, including Neuro2A and HEK293 cells. Furthermore, we present progress using this sensor to measure extracellular ATP dynamics that are modulated by cellular processes, including ligand stimulated cellular release of ATP and degradation of ATP by ectonucleotidase activity. In conclusion, we developed a genetically encoded fluorescent protein-based biosensor that currently demonstrates the ability to measure dynamic changes in extracellular ATP levels in live cell proof of concept studies.

## 2.2 Introduction

Extracellular adenosine triphosphate (ATP) is a central component of purinergic signaling. Purinergic signaling contributes to a vast array of fundamental physiological processes and pathophysiological conditions including neuron-glia communication (Araque et al., 2014; Fields & Burnstock, 2006; Khakh & North, 2012), immune responses (Cekic & Linden, 2016; Junger, 2011), inflammation (Eltzschig, Sitkovsky, & Robson, 2012; Idzko, Ferrari, & Eltzschig, 2014), and cancer (Bastid et al., 2015; Ghiringhelli et al., 2009). ATP is released from cells into the extracellular space by a variety of mechanisms such as stimulated exocytosis and conductive passage through hemichannels (Elliott et al., 2009; Lazarowski, 2012; Lazarowski, Boucher, & Harden, 2003; Praetorius & Leipziger, 2009). Following the release, extracellular ATP directly modulates purinergic receptors in an autocrine and paracrine manner (Corriden & Insel, 2010a). For example, in an immune context ATP leakage from apoptotic cells in healthy tissue (Chekeni et al., 2010; Elliott et al., 2009) or from damaged cells in injured tissue acts as a chemotactic signal for clearance by phagocytes (Davalos et al., 2005b; Haynes et al., 2006; Lou et al., 2016). In the context of nervous tissue, ATP released by astrocytes (Bowser & Khakh, 2007) can regulate synaptic and network excitability (Gourine et al., 2010; Pougnet et al., 2014; Shigetomi, Kracun, Sofroniew, & Khakh, 2010; Tan et al., 2017; Torres et al., 2012). Furthermore, extracellular ATP is central to purinergic signaling not only because of its direct effects but also because of extracellular ectonucleotidases, such as CD39 (Bastid et al., 2015) and CD73 (P. S. Murphy et al., 2017), hydrolyze it to the additional purinergic signaling molecules ADP, AMP, and adenosine (Robson, Sévigny, & Zimmermann, 2006). Depending on the physiological context (Y. Chen et al., 2006; Lovatt et al., 2012), these metabolites uniquely modulate distinct sets of ATP-gated ionotropic P2X receptors, ATP and ADP-modulated metabotropic P2Y receptors, and P1 adenosine receptors (Abbracchio et al., 2006; Coddou, Yan, Obsil, Pablo Huidobro-Toro, & Stojilkovic, 2011; Ralevic & Burnstock, 1998). It is important to understand extracellular ATP dynamics as a fundamental aspect of physiology and because ATP-dependent receptors, as well as the ATP release and clearance machinery, are potential therapeutic targets (Burma et al., 2017; Danquah et al., 2016). However, deficiencies in our understanding of the broad concentration ranges, timescales, and distances over which extracellular ATP acts currently obscures the roles of purinergic signaling in both healthy and diseased tissue. Therefore, in order to establish a clear picture of purinergic signaling in physiology, it is necessary to distinguish the role of extracellular

ATP from its hydrolysis products and to quantitatively measure extracellular ATP dynamics directly.

Direct measurements of extracellular ATP employ diverse techniques including biochemical endpoint assays, microelectrode sensors, and fluorescent ATP analogues (Corriden & Insel, 2010a; Rajendran et al., 2016). In particular, membrane-tethered luciferase continues to provide critical new knowledge about purinergic signaling in cancer biology, immunology, and beyond (Barberà-Cremades et al., 2012; Loo et al., 2015; Michaud et al., 2011; Pellegatti et al., 2008; Pietrocola et al., 2016; Weber et al., 2010; Wilhelm et al., 2010). These methods have yielded invaluable insight into ATP signaling; however, new methods are needed to push beyond the current limitations in spatial and temporal resolution. These limitations prevent the precise understanding of changes in extracellular ATP levels that occur within seconds and minutes at cellular and subcellular length scales. For example, current techniques are limited in their applications to complex tissue because they require chemical additives, damage tissue with an invasive probe, or consume ATP upon measurement. More recently, genetically-encoded fluorescent protein-based sensors have been developed as relatively non-invasive tools with high spatiotemporal resolution to study intracellular ATP. These include the ATeam family of sensors that report intracellular ATP dynamics by a change in Förster resonance energy transfer (FRET) between two fluorescent proteins (H Imamura et al., 2009), and the QUEEN (Yaginuma et al., 2014) and Perceval (Berg et al., 2009; Tantama et al., 2013) sensors that use a single circularly-permuted fluorescent protein. Though exploited in a number of intracellular contexts, these sensors have not been used to detect extracellular ATP.

Here, we re-engineer a ratiometric ATeam FRET-based ATP sensor by targeting it to the cell surface and report its use as a genetically-encoded fluorescent sensor of extracellular ATP. We report its design, characterization, and proof-of-principle that it can be used to image and monitor real-time changes in extracellular ATP levels caused by endogenous clearance and release mechanisms in cell culture, using Neuro2A cells as a principal test platform for the sensor.

## 2.3 Materials and Methods

### 2.3.1 Materials

Standard chemicals and cell culture reagents were purchased from Sigma and ThermoFisher. ARL67156, suramin, and PPADS were purchased from Tocris.

### 2.3.2 Sensor construction

#### *ecAT3.10.*

The pCMV(MinDis).iGluSnFR plasmid (Addgene plasmid #41732), a modified version of the pDisplay vector that has the hemagglutinin (HA) tag removed and contains the iGluSnFR glutamate sensor, was used as a template for construction of the ecATeam sensors. The plasmid was restriction enzyme digested with BglII and SalI for removal of iGluSnFR sequence, but retention of the coding region for the IgK leader sequence and PDGFR transmembrane domain. The ATeam3.10 insert was prepared, as follows. The pRSetB-ATeam3.10 vector (from H. Imamura) was restriction enzyme digested with XbaI and EcoRI to divide the ATeam3.10 sequence into 2 fragments that separate the homologous cyan and yellow fluorescent protein sequences to allow for specific PCR amplification. Subsequently, the N-terminal ATeam3.10 fragment was amplified with the 5'-CAGGTTCCACTGGTGACAGAATGGTGAGCAAGGGCG-3' and 5'-CACCATGAATTCCTTCATTTTCGGCAACG-3' oligonucleotide primer pair and the C-terminal fragment was amplified with the 5'-GAAATGAAGGAATTCATGGTGAGCAAGGGC-3' and 5'-GATGAGTTTTTGTTCGTCGACCTTGTACAGCTCGTCCATGC-3' oligonucleotide primer pair using Phusion polymerase (Fisher Scientific). Upon gel purification, the pCMV(MinDis) vector fragment and the two PCR-amplified ATeam3.10 fragments were used for a 3-fragment Gibson Assembly reaction (NEBuilder Gibson Assembly, New England Biolabs) that yielded the pCMV(MinDis)-ATeam3.10 construct (ecAT3.10).

### ***ecAT1.03-YEMK.***

The pCMV(MinDis).iGluSnFR plasmid was also used as a template for construction of the ecAT1.03-YEMK construct. Here, 5'-CCGCCACAACATCGAGTACCTGCAGGTTGACGAACAAAACTCATCTC-3' and 5'-TTGCTCACCATACTCGAGTAGTCACCAGTGGAACCTG-3' oligonucleotide primers were used with Phusion polymerase to PCR amplify a fragment of the pCMV(MinDis).iGluSnFR plasmid that retains the IgK leader sequence and PDGFR transmembrane domain, but is devoid of the iGluSnFR sequence. The insert fragment containing AT1.03-YEMK was prepared by restriction enzyme digest of pcDNA-AT1.03(YEMK) (from H. Imamura) with XbaI and HindIII. The final pCMV(MinDis)-AT1.03-YEMK (ecAT1.03-YEMK) construct was generated by Gibson Assembly (NEBuilder, New England Biolabs) of the insert fragment with the PCR amplified pCMV(MinDis) vector fragment.

Upon preparation of plasmid DNA, all coding sequences of the final ecATeam constructs were confirmed by Sanger sequencing at Genewiz (South Plainfield, NJ).

### **2.3.3 ATeam3.10 expression and purification**

*E. coli* strain BL-21 expressing pRSetB-ATeam3.10 was cultured in Auto Induction Media (AIM) at 37°C for 12h then at room temp for 36h. Cells were then pelleted, resuspended in lysis buffer (25 mM Sodium Phosphate Buffer [pH 7.8], 500 mM NaCl, 10 mM Imidazole, 5% Glycerol, 0.1% Triton X-100, 1mM PMSF, 1mM DTT, and 0.2 mg/mL Lysozyme), and lysed by sonication. Lysate was then centrifuged at 30,000xg for 30min at 4°C, and passed through a 0.45 µm syringe. The sample was then run over a Ni column (GE Chelating Sepharose column charged with Ni<sup>2+</sup>). The column was then washed with wash buffer A (25 mM Sodium Phosphate Buffer [pH 7.8], 500 mM NaCl, 20 mM Imidazole, 5% Glycerol), wash buffer B (25 mM Sodium Phosphate Buffer [pH 7.8], 500 mM NaCl, 40 mM Imidazole, 5% Glycerol), then elution buffer (25 mM Sodium Phosphate Buffer [pH 7.8], 500 mM NaCl, 150 mM Imidazole, 5% Glycerol). The fractions containing purified ATeam 3.10 were dialyzed in storage buffer (5 mM MOPS Buffer [pH 7.3], 300 mM NaCl, 10% Glycerol), with two changes at 4°C and stored at -80°C for future use.

### **2.3.4 Purified AT3.10 in vitro spectroscopy**

Protein concentration was determined using a standard procedure micro Bradford Assay (Thermo Scientific). The protein was diluted to 0.125  $\mu$ M in assay buffer (50 mM MOPS-KOH, pH 7.3, 50 mM KCl, 0.5 mM MgCl<sub>2</sub>, and 0.05% Triton X-100) and fluorescence was measured using a BioTek Synergy H4 microplate reader at room temperature, in the absence and presence of ATP, ADP, ARL67156, PPADS, or Suramin. For all filter-based measurements, a 420/50 nm excitation and 485/20 and 528/20 nm emission filters were used.

### **2.3.5 Cell line maintenance and transfection**

N2A cells (ATCC CCL-131), HEK293 cells (ATCC CRL-1573), and SK-MEL-5 (ATCC HTB-70) were cultured in Dulbecco's modified Eagle's medium containing 4.5 g/L glucose, 2 mM glutamine, and supplemented with 10% cosmic calf serum or 10% fetal bovine serum and were maintained at 37°C and 5% CO<sub>2</sub> in a humidified incubator. N2A cells were confirmed to be mycoplasma free as assessed by the Universal Mycoplasma Testing Kit (ATCC). For imaging experiments, cells were seeded, as indicated, onto nitric acid-cleaned and washed 18-mm #1.5 coverslips, or into Cellvis 12-well or 24-well glass bottom plates with high performance #1.5 cover glass that were cleaned with NaOH/H<sub>2</sub>O<sub>2</sub>, washed, and pre-coated with poly-D-lysine. Cells were then transfected with plasmid DNA for expression of ecATeam sensors by living cells using the Effectene (Qiagen) transfection reagent as described in the manufacturer's protocol.

### **2.3.6 Live-cell fluorescence microscopy and image analysis**

Cells were prepared for microscopy by exchanging cell growth media for imaging solution consisting of 15 mM HEPES, 1.25 mM NaH<sub>2</sub>PO<sub>4</sub>, 10 mM glucose, 120 mM NaCl, 3 mM KCl, 2 mM CaCl<sub>2</sub>, 1 mM MgCl<sub>2</sub>, and 3 mM NaHCO<sub>3</sub> (pH 7.3) and cells were equilibrated at room temperature for at least 20 min prior to imaging. All microscopy experiments were performed at ambient room temperature, either during continuous perfusion (~1.5 mL/min flow rate) of imaging solution (or indicated treatment), or in the presence of a static bath of imaging solution where treatments were added by pipette to the bulk solution of the static bath. Cells were imaged using an Olympus IX83 fluorescence microscope with a 20X/0.75 NA objective illuminated by a Lumencor SpectraX light engine and equipped with an Andor Zyla 4.2 sCMOS camera. The

ecATeam sensor activity was measured by examining the fluorescence intensities in CFP, CFP-YFP FRET, and YFP channels. Specifically, the ATeams were excited in the CFP and CFP-YFP FRET channels using a 438/29 nm bandpass filter, and emission was collected through 470/24 and 540/30 nm bandpass filters for the CFP and CFP-YFP FRET channels, respectively. The fluorescence in the YFP channel was excited using a 510/10 nm bandpass filter and emission was collected through a 540/30 nm bandpass filter. Excitation light from all fluorescence channel measurements was blocked by the ET-ECFP/EYFP/mCherry multiband beamsplitter (Chroma 69008bs). The microscope components and image acquisition were controlled by the Andor iQ3 software and the ImageJ/FIJI software package was used to analyze all images for each experiment, as specified. For fluorescence images, the mean and standard deviation of background intensities were measured for each fluorescence channel in every field of view. For each fluorescence channel, the mean background intensity was subtracted from every image of the associated imaging set. Background masks were then created with minimum thresholds of two times the mean background intensity. The background masks were applied to the fluorescence intensity images and fluorescence ratio images were created by pixel-by-pixel division of the background masked individual fluorescence channels. Regions of interest that encompassed whole cells or cell membranes, as indicated, were drawn and the mean fluorescence ratios of pixels within each region of interest were calculated.

For kinetic measurements, experiments were performed at ambient room temperature using a diamond-shaped laminar flow fast perfusion chamber (Warner RC-25F). Imaging solution was perfused at a rate of 5 mL/min, and inhibitors were not used. Images were collected at 2 second intervals for the FRET and YFP fluorescence emission channels. Data was fit to a two-exponential association function,  $y = y_0 + A_1 \cdot (1 - e^{(-t/\tau_1)}) + A_2 \cdot (1 - e^{(-t/\tau_2)})$ .

Confocal microscopy was carried out on a Nikon A1 confocal system with a Ti-E microscope base, using a 60X/1.49 NA Nikon apo TIRF objective at room temperature. The 457 nm line of a multi-argon laser was used for excitation, and CFP and FRET channel fluorescence intensities were collected using 482/35 nm and 525/50 nm bandpass filters.

### **2.3.7 Data collection and analysis**

Unpaired, two-tailed Student's t-test was used to test for differences in means. Mean values are reported with standard errors of the mean (mean  $\pm$  sem).

## **2.4 Results**

### **2.4.1 Sensor construction and characterization**

To generate a sensor of extracellular ATP, we targeted a soluble ATeam ATP sensor to the cell surface. The ATeam family of sensors, first developed by Imamura and co-workers, are generally composed of an  $\epsilon$  subunit from a bacterial  $F_0F_1$ -ATP synthase that is fused between a cyan fluorescent protein (CFP) and a yellow fluorescent protein (YFP) (H Imamura et al., 2009). ATP binding induces a conformational change that increases Förster-type resonance energy transfer (FRET) between the CFP donor and YFP acceptor (H Imamura et al., 2009). The soluble ATeam3.10 sensor was chosen as a starting point because it can provide a ratiometric fluorescence readout, which facilitates quantitative and longitudinal live-cell imaging studies by normalizing for expression level and decreasing signal drift. It is also a higher-affinity variant that better matches the estimated physiological range of extracellular ATP. In order to target the soluble ATeam3.10 sensor to the cell surface, we employed a strategy previously used to engineer extracellular glutamate sensors (Hires, Zhu, & Tsien, 2008; Marvin et al., 2013; Okumoto et al., 2005). The ATeam3.10 sensor was fused between an IgK leader sequence (Coloma, Hastings, Wims, & Morrison, 1992) on the N-terminus and a transmembrane anchor domain from the platelet-derived growth factor receptor (PDGFR) (Gronwald et al., 1988) on the C-terminus. These modifications direct the sensor to the secretory pathway and tether the sensor to the extracellular face of the plasma membrane, respectively (Fig 2.1). The resulting membrane-tethered sensor was termed ecAT3.10 (extracellular ATeam3.10).

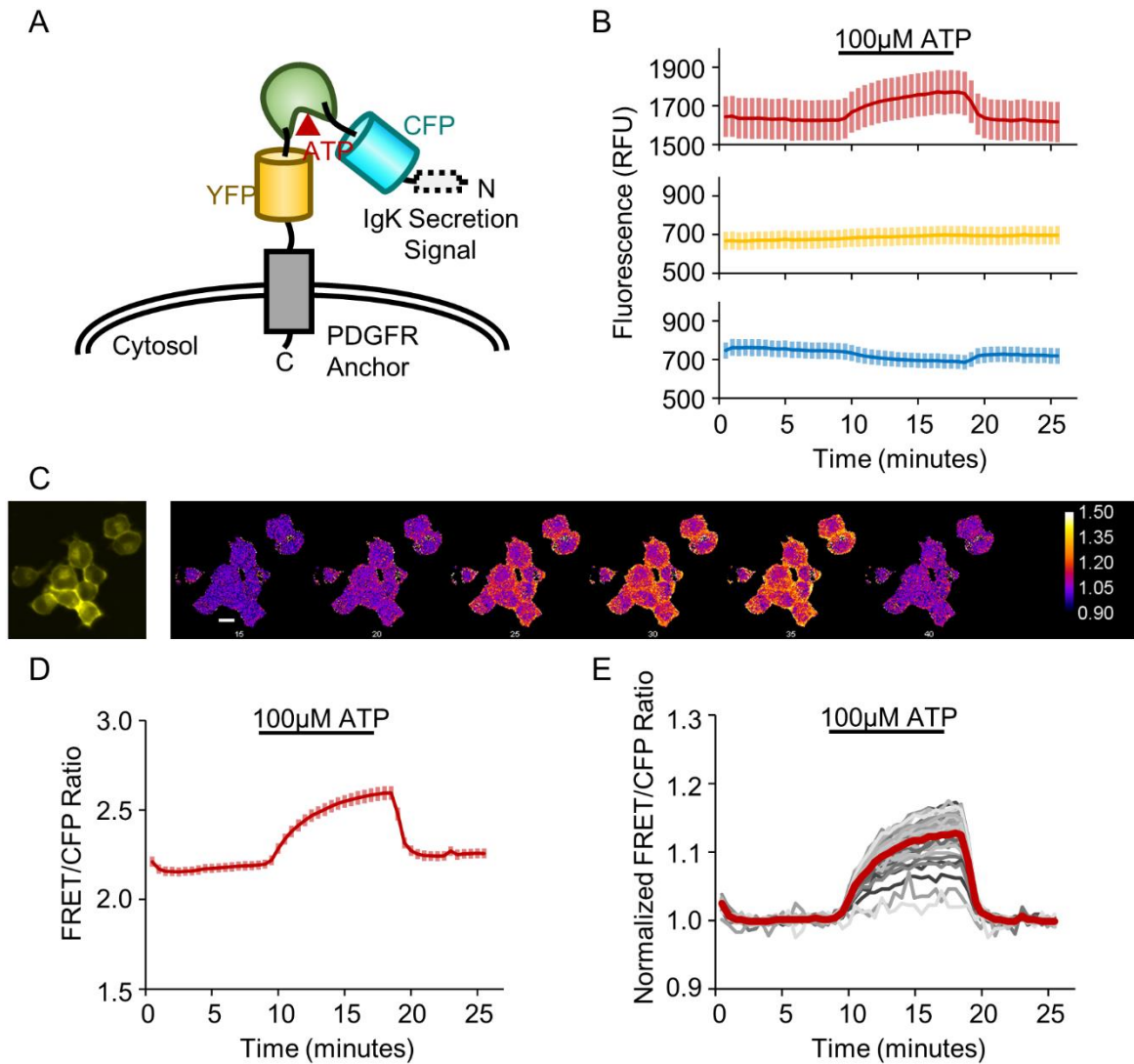


Figure 2.1. ecATeam3.10 sensor detects extracellular ATP

(A) Schematic of ecAT3.10 design in which the ATeam3.10 FRET-based ATP sensor is displayed on the cell surface via a PDGFR transmembrane anchor. (B) Fluorescence intensity in the FRET channel increases upon wash-in of 100  $\mu$ M ATP while the CFP donor intensity decreases. As expected, the YFP direct acceptor channel does not show an ATP-dependent change. Cells were imaged under continuous perfusion. (C) Representative widefield fluorescence images for the cells analyzed in (D-E). The first panel in the YFP channel shows morphology, the subsequent panels are false colored to show the change in the normalized FRET/CFP pixel-by-pixel ratio signal. Scale bar is 20 $\mu$ m. (D) The average FRET/CFP emission ratio, which we refer to as the ratio signal, shows a robust increase of  $0.27 \pm 0.01$  ( $n = 41$  cells). Values and solid line traces are cell means, and errors and error bars are standard errors of the means. (E) To account for drift, a linear baseline was fitted, and the ratio signal was normalized on a cell-by-cell basis (individual cells, gray), showing an average fold change of  $1.127 \pm 0.005$  (population average, red). *Sensor design and conceptualization by Jason Conley and Mathew Tantama.*

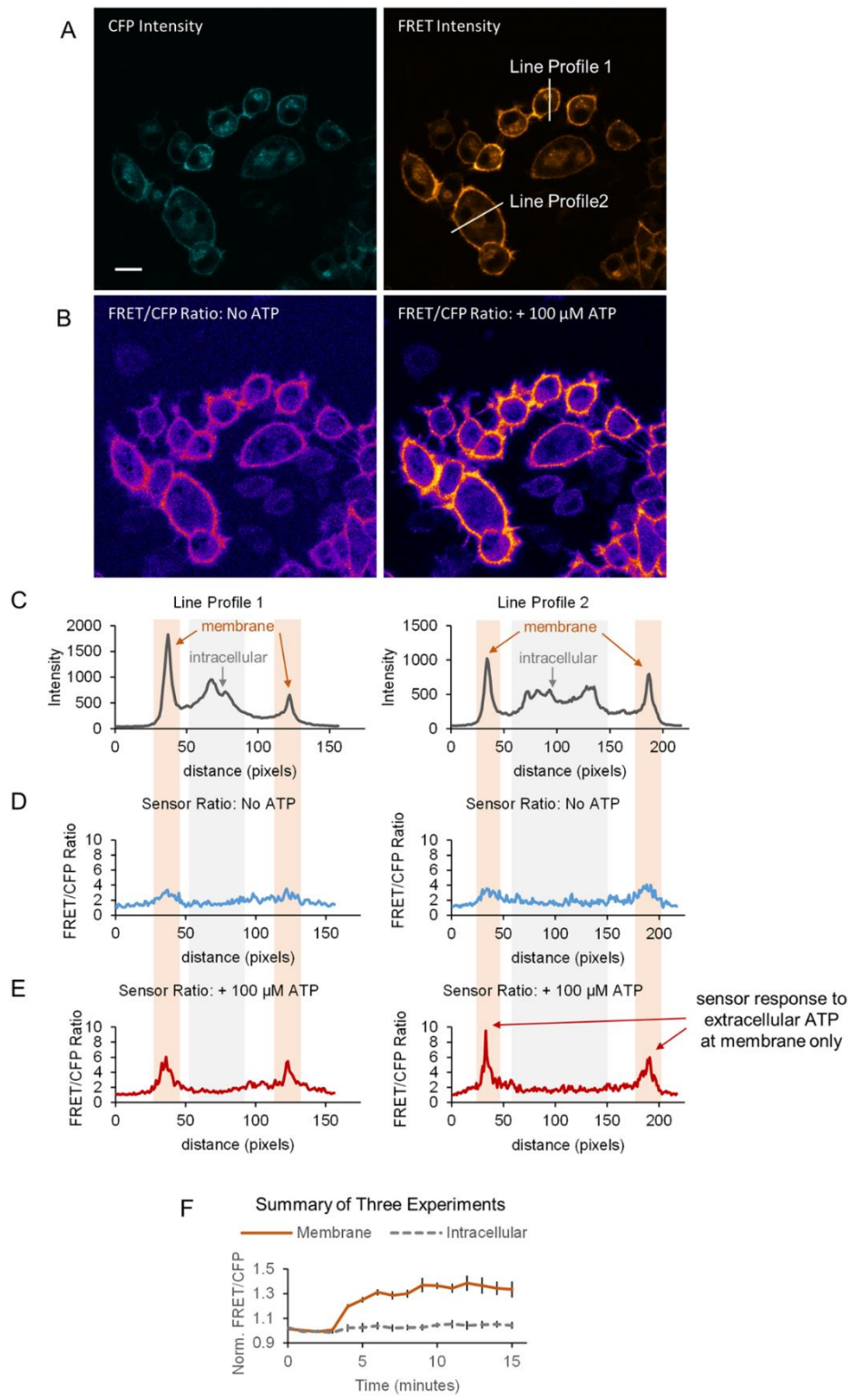
Initially, the ecAT3.10 sensor was expressed in cultured mammalian cells to test for expression at the cell surface and for a response to exogenous ATP. Even in widefield imaging mode, the fluorescence signals were clearly localized to the cell perimeter of Neuro2A cells, indicating successful targeting of ecAT3.10 to the plasma membrane (Fig 2.1). Furthermore, under continuous bath perfusion conditions, wash-in of 100  $\mu$ M ATP resulted in an increase in FRET emission intensity and a decrease in CFP donor fluorescence intensity, which is consistent with the expected increase in FRET upon ATP binding (Fig 2.1). At the cell population level, the ecAT3.10 FRET/CFP emission ratio signal (referred to as the “ratio signal”) reached a maximal increase of  $0.27 \pm 0.01$  (Fig 2.1), representing a peak fold-increase of  $1.127 \pm 0.005$  (mean  $\pm$  sem,  $n = 41$  cells) in the presence of ATP relative to the ratio signal in the absence of ATP (Fig 2.1.D). Upon washout of extracellular ATP from the bath, the ecAT3.10 ratio signal returned to baseline, demonstrating that the sensor can be used to reversibly detect changes in extracellular ATP. Interestingly, ecAT3.10 was able to detect significant cell-to-cell variability in the response magnitude (Fig 2.1.E), which may be related to physical characteristics of the cell surface or endogenous activity under these slow-perfusion conditions in the absence of inhibitors (Trouillon & Ewing, 2013). It is important to note that the variability is not caused by differences in sensor expression levels because the ratio signal is independent of the concentration of the sensor.

After demonstrating the reversibility of the sensor, we examined the spatial profile of the ecAT3.10 response in greater detail to show that ecAT3.10 is a faithful reporter of extracellular ATP. The sensor exhibited strong surface-targeted fluorescence signals, but intracellular punctate fluorescence was also apparent (Figs 2.1 and 2.2). Intracellular punctae have been observed during overexpression of fluorescent protein sensors by other groups, and it is attributed to excess protein resident in the endoplasmic reticulum (Marvin et al., 2013). Sensor responses were therefore analyzed for ratio signal changes within subcellular ROIs, including the cell membrane and intracellular regions of interest using confocal microscopy. The confocal analysis confirmed that the fluorescence response originates exclusively from the membrane (Fig 2.2). Furthermore, even in widefield imaging mode, the whole-cell fluorescence signal response is reflective of the membrane response. Thus, ecAT3.10 can be conveniently used with either confocal or widefield microscopy, and the subsequent experiments presented here utilized widefield microscopy.

Figure 2.2. Surface-localized ecAT3.10 responds to the addition of extracellular ATP

High magnification confocal microscopy demonstrates that the ecAT3.10 ratio signal response to extracellular ATP occurs exclusively at the membrane. (A) Representative confocal fluorescence intensity images in the CFP and FRET channels show strong membrane localized signal and some intracellular puncta. Scale bar is 20  $\mu\text{m}$ . (B) Pixel-by-pixel FRET/CFP ratio images before (left) and after addition of 100  $\mu\text{M}$  ATP (right) illustrates a response at the membrane only. (C-E) Line profile analysis for the two example cells shown in (A). A 5-pixel width line region of interest was drawn through the membrane and peak areas of intracellular fluorescence. (C) The fluorescence intensity line profiles exhibit peaks at the membrane and also from intracellular locations that are likely ER/Golgi in origin. The line profiles from the ratio images shown in (B) before (D) and after (E) the addition of extracellular ATP clearly show that the ecAT3.10 ratio signal increases at the membrane and not from the intracellular sites. (F) After 3 minutes, 100  $\mu\text{M}$  ATP was added. The time course shows that the membrane-localized ratio signals increase, but the signals from intracellular regions do not change (mean  $\pm$  sem for three experiments with  $n = 32$  cells,  $n = 60$  cells, and  $n = 46$  cells). *Data collected and analyzed by Jason Conley and Mathew Tantama*

Figure 2.2 continued



After our initial tests, we characterized the concentration range in which ecAT3.10 can detect extracellular ATP. Live Neuro2A cells expressing ecAT3.10 were imaged at room temperature with continuous bath perfusion to minimize cell-to-cell variability. Increasing concentrations of exogenous ATP from 0  $\mu\text{M}$  to 1000  $\mu\text{M}$  were washed onto the cells during real-time image acquisition, and steady-state was achieved before changing the extracellular ATP concentration (Fig 2.3). The sensor “on-cell” responses exhibited concentration-dependent increases of the ecAT3.10 ratio signal, and an apparent affinity equilibrium constant,  $K_{\text{app}}$  of  $12 \pm 5 \mu\text{M}$  (mean  $\pm$  sem,  $n = 4$  experiments), was determined when data were fitted with a Hill equation (Fig 2.3). Importantly, the apparent affinity of ATP for the purified soluble ATeam3.10 sensor was approximately 20-fold higher ( $K_{\text{app}} = 0.52 \pm 0.02 \mu\text{M}$ , mean  $\pm$  sem,  $n = 14$  experiments) (Fig 2.4) compared to the “on-cell” response (Fig 2.3). Taken together, the difference between the  $K_{\text{app}}$  values for ATP between ecAT3.10 expressed on living cells and purified AT3.10 in vitro may reflect changes in the binding properties for ecAT3.10 imparted by surface-tethering of the sensor. There has been a concern in the literature that glycosylation of ATeam can inactivate and alter the sensor’s properties (Liemburg-Apers et al., 2011; Morciano et al., 2017), but similar to other studies (Vishnu et al., 2014) we did not find evidence that glycosylation affects sensor function. Despite the change in affinity, the sensitivity range overlapped with the reported physiological range of extracellular ATP from basal nanomolar to peak micromolar concentrations (Douglas Fields, 2011; Y. Zhang, Phillips, Li, & Yeung, 2008).

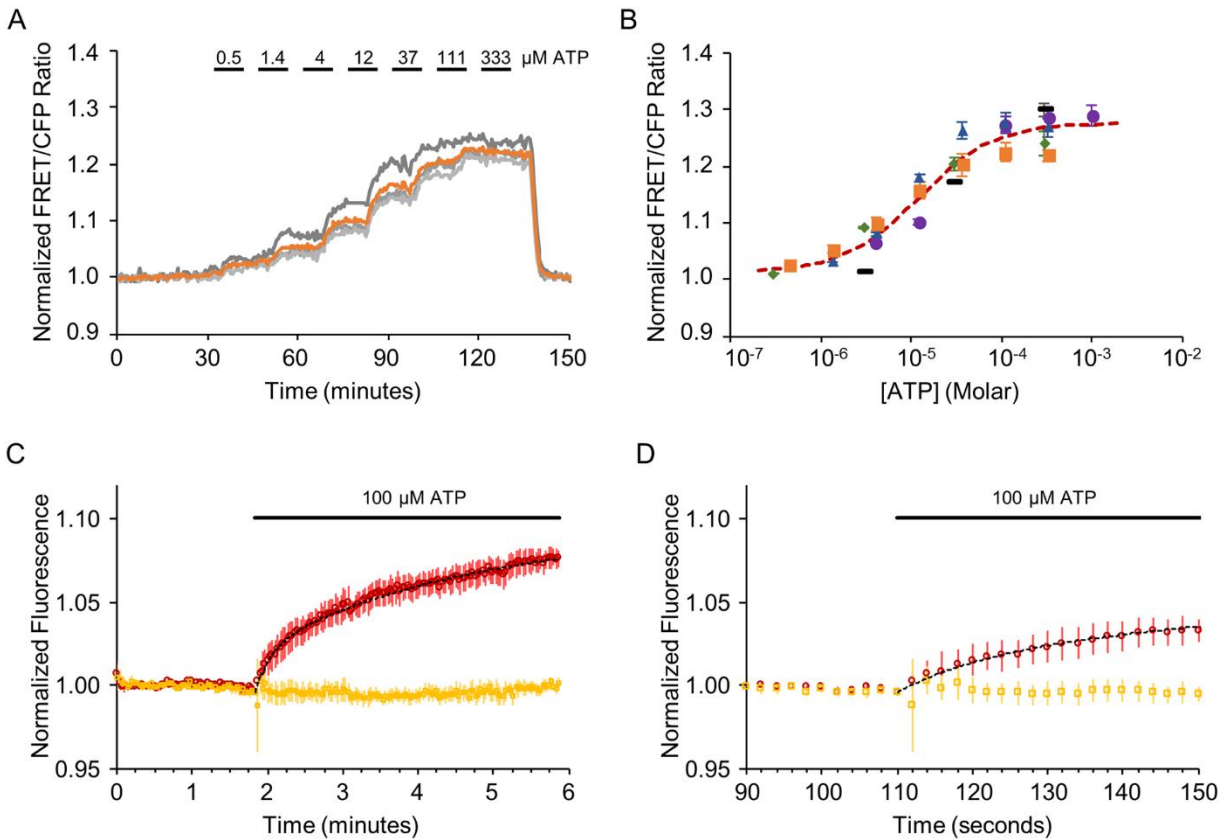


Figure 2.3. Characterization of ATP affinity and response kinetics

ecATeam3.10 exhibits a concentration-dependent change in FRET/CFP ratio signal. Live Neuro2A cells expressing ecAT3.10 were imaged at room temperature under continuous perfusion, during which increasing concentrations of extracellular ATP were washed in a stepwise fashion. (A) A representative time course from one experiment with four cells. Each grey trace represents the response from an individual cell in which the regions of interest were drawn around the membrane. The orange trace is the mean response. (B) Summary of ATP dose-response data from five independent experiments, each represented its own symbols. The orange squares represent data from (A), and the dashed red curve is fit to the mean of all experiments. In four of the five experiments, sufficient data was available for independent fitting to a Hill equation (mean  $\pm$  sem,  $n = 4$  experiments:  $K = 12 \pm 5 \mu\text{M}$ ,  $\text{Ratio}_{\text{max}}/\text{Ratio}_{\text{min}} = 1.23 \pm 0.01$ ,  $n = 1.4 \pm 0.2$ ). A global fit of data from all five experiments was also performed for comparison. (fitting mean  $\pm$  sem,  $n = 5$  experiments:  $K = 11 \pm 2 \mu\text{M}$ ,  $\text{Ratio}_{\text{max}}/\text{Ratio}_{\text{min}} = 1.28 \pm 0.01$ ,  $n = 0.9 \pm 0.1$ ). (C-D) ecAT3.10 responds to an increase in extracellular ATP within seconds. (C) Cells were imaged during fast perfusion wash in of  $100 \mu\text{M}$  ATP, and the sensor exhibited an increase in FRET within seconds ( $n = 27$  cells, 3 experiments; two-exponential fit:  $\tau_{\text{fast}} = 13 \pm 1 \text{ sec}$ ,  $\tau_{\text{slow}} = 172 \pm 18 \text{ sec}$ ). (D) An expanded view of the initial response shown in (C). Red, FRET fluorescence channel intensity. Yellow, YFP fluorescence channel intensity. Dotted black curve, two-exponential fit. *Data collected and analyzed by Jason Conley*

We also characterized the kinetics with which the ecAT3.10 sensor responds to extracellular ATP. Neuro2A cells expressing ecAT3.10 were imaged at room temperature with continuous perfusion at a rate of 5 mL/min in a laminar flow fast perfusion chamber. In order to increase the acquisition speed, only the FRET and YFP fluorescence intensity channels were collected at 2 second intervals, which did not require any filter changes. The ecAT3.10 sensor responded within several seconds upon wash in of 100  $\mu$ M ATP, and on average the response was best fit to a two exponential function with a fast time constant,  $\tau = 13 \pm 1$  sec, and a slow time constant,  $\tau = 172 \pm 18$  sec ( $n = 27$  cells, 3 experiments) (Fig 2.3). Thus, the sensor can detect micromolar changes in extracellular ATP concentrations within seconds.

#### **2.4.2 ecAT3.10 reports extracellular ATP turnover by ectonucleotidase activity**

We next demonstrated that ecAT3.10 can be used to detect the clearance of extracellular ATP via ectonucleotidase activity in cell cultures. During the measurement of the ATP affinity of ecAT3.10, continuous bath perfusion conditions were employed in order to continuously replenish ATP and control the extracellular ATP concentration. Physiologically, however, ectonucleotidases contribute to purinergic signaling dynamics by clearing extracellular ATP by hydrolysis (Lorenz, Pinto, & Seifert, 2007; Robson et al., 2006), thereby generating ADP, AMP, and adenosine, which can act independently as purinergic signals. In order to test ecAT3.10's ability to detect endogenous ectonucleotidase activity (Lorenz et al., 2007), we performed experiments in which a single addition of exogenous ATP was made to cultured Neuro2A cells expressing ecAT3.10 in an imaging dish under static bath conditions without solution exchange. We initially used Neuro2A cells because they express the ectonucleotidase NTPDase1 (CD39) (Gronwald et al., 1988).

Our observations indicate that endogenous ectonucleotidases exhibit substantial activity to maintain low basal extracellular ATP levels around cultured cells. We first tested the addition of 10  $\mu$ M ATP to ecAT3.10-expressing Neuro2A cells under static bath conditions. The concentration was chosen to mimic moderate to high physiological concentrations and because it demonstrated approximately half-maximal responses in the continuous perfusion experiments (Fig 2.3). Surprisingly, under static bath conditions no significant increase in the sensor ratio signal was detected (Fig 2.4), which is in stark contrast to bath perfusion experiments (Fig 2.3). However, pre-treatment with the ectonucleotidase inhibitor ARL67156 (Lévesque, Lavoie, Lecka,

Bigonnesse, & Sévigny, 2007) reconstituted the average peak response (vehicle,  $1.02 \pm 0.01$  versus  $100 \mu\text{M}$  ARL67156,  $1.10 \pm 0.02$ , mean  $\pm$  sem,  $n = 6$  experiments from 2 independent investigators,  $p = 0.009$ , t-test), and therefore the loss of signal change in the absence of ARL67156 is not caused by a loss of responsivity of the sensor itself. Potentiation of the response by ARL67156 indicates that high ectonucleotidase activity turns over extracellular ATP at a significant rate, at least at the cell surface. Importantly,  $100 \mu\text{M}$  ARL67156 had no effect on the ability of purified soluble ATeam3.10 to detect ATP in vitro. The dose-response and  $K_{app}$  values for ATP in the presence and absence of ARL67156 were not significantly different ( $0.52 \pm 0.02 \mu\text{M}$ ,  $n = 14$  versus  $0.46 \pm 0.07 \mu\text{M}$ ,  $n = 5$ ,  $p = 0.34$ , t-test) (Fig 2.4). Furthermore, the sensor ratio signal remained elevated until exogenous apyrase ( $3\text{U/mL}$ , high ATPase activity) was added to degrade the ATP (Fig 2.4). Apyrase itself does not affect the ability of ecAT3.10 to detect ATP, and the decrease is not due to loss of sensor by internalization because the membrane-localized ratio signal is insensitive to sensor concentration. The apyrase addition caused a decrease in ecAT3.10 signal, demonstrating that the sensor remained responsive and was specific to ATP (Fig 2.4).

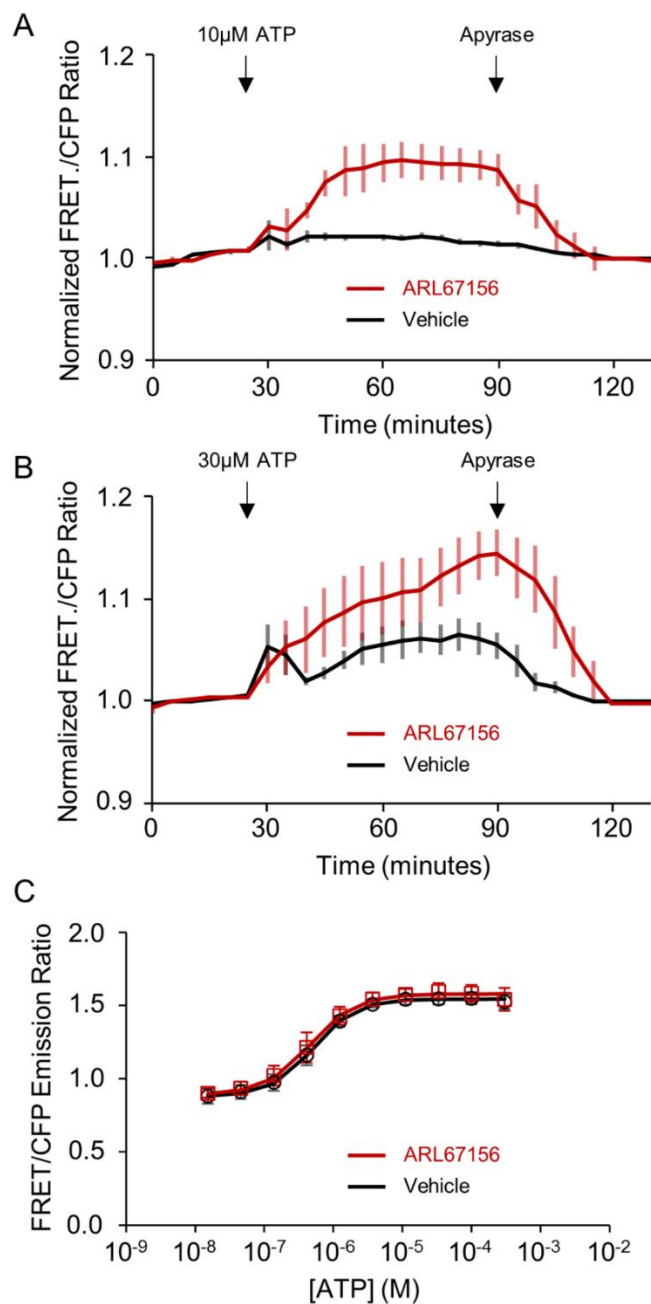


Figure 2.4. ecATeam3.10 detects ATP hydrolysis by ectonucleotidases.

Live Neuro2A cells expressing ecAT3.10 were imaged under non-perfusion, static bath conditions. (A) The addition of 10  $\mu\text{M}$  ATP did not elicit a response (black) unless the cells were pre-treated with the ectonucleotidase inhibitor ARL67156 at 100  $\mu\text{M}$  (red). Apyrase addition degrades extracellular ATP confirming a reversible ATP-specific sensor response. (B) Ectonucleotidase inhibition by ARL67156 pre-treatment also potentiated responses when 30  $\mu\text{M}$  ATP was added. Vehicle, black. ARL67156, red. (A) and (B),  $n = 6$ , 2 independent investigators. (C) ARL67156 does not directly affect the ATeam3.10 sensor response to ATP. *Data collected and analyzed by Jason Conley, Saranya Radhakrishnan and Steve Valentino*

We next tested whether ectonucleotidase activity could clear surface ATP levels after the addition of a higher bulk concentration of extracellular ATP. Upon addition of 30  $\mu\text{M}$  ATP, an initial increase in the sensor ratio signal was detected, and vehicle addition did not elicit a response (Fig 2.4). However, the sensor response to ATP was transient. After reaching a peak, within minutes the ecAT3.10 ratio signal spontaneously decreased, which is consistent with the hydrolytic breakdown of ATP by endogenous ectonucleotidase activity (Fig 2.4). Pretreatment with the ectonucleotidase inhibitor ARL67156 abrogated the spontaneous decrease and potentiated the peak response (vehicle,  $1.07 \pm 0.02$  versus 100  $\mu\text{M}$  ARL67156,  $1.14 \pm 0.02$ , mean  $\pm$  sem,  $n = 6$  experiments from 2 independent investigators,  $p = 0.02$ , t-test). The effect of ARL67156 supports the hypothesis that endogenous ectonucleotidases actively clear extracellular ATP, though hydrolytic activity was not able to completely suppress an increase in cell surface ATP when challenged with larger bulk ATP increases. In addition, the time-course of the response is complex under these static bath conditions because diffusion rate, clearance rate, and endogenous release (discussed below) rate all contribute to the overall dynamics. Overall, these data demonstrate that ecAT3.10 can be used to image and measure extracellular ATP clearance by endogenous ectonucleotidase activity on live cultured cells.

### **2.4.3 ecAT3.10 detects nucleotide-stimulated endogenous ATP release**

We next demonstrated that ecAT3.10 can be used to measure nucleotide-stimulated release of endogenous ATP from cells. It has previously been reported that P2X7 receptors can mediate ATP release from Neuro2A cells (Gutiérrez-Martín et al., 2011) , and it is well established that ATP (Anderson, Bergher, & Swanson, 2003; Bodin & Burnstock, 1996; Newman, 2001, 2003; Z. Zhang et al., 2007a) and ADP (Lu et al., 2015; Mansfield & Hughes, 2014) can stimulate the release of ATP from a variety of cultured cells. The ATeam sensor itself can detect changes in ATP within seconds (H Imamura et al., 2009), which is well-matched to detect nucleotide-stimulated ATP release. Nucleotide-stimulated ATP release has previously been reported to cause an initial increase in extracellular ATP within seconds that can continue to increase and remain elevated over minutes (Anderson et al., 2003; Bodin & Burnstock, 1996; Gutiérrez-Martín et al., 2011; Lu et al., 2015; Mansfield & Hughes, 2014; Newman, 2001, 2003; Z. Zhang et al., 2007b) , and in particular ATP-stimulated ATP release under static bath conditions has been observed to increase over tens of minutes (Bodin & Burnstock, 1996).

Here, we imaged ecAT3.10-expressing Neuro2A cells under static bath conditions in order to observe persistent increases in extracellular ATP. In these experiments, technical replicates were imaged in a multi-well plate at 5-minute intervals. We observed a pronounced biphasic response following the addition of 100  $\mu$ M ATP to ecAT3.10-expressing in Neuro2A cells (Fig 2.5) or HEK293 cells. On average, a secondary increase in the ecAT3.10 ratio signal followed the initial decrease that we attribute to ARL67156-sensitive ectonucleotidase activity. This observation led to the hypothesis that the secondary increase is caused by a purinergic receptor-mediated release of intracellular ATP from cells. For example, such a release could plausibly be stimulated by ATP itself (Gutiérrez-Martín et al., 2011), one of its hydrolysis products, or possibly an intermediary purinergic ligand released by the initial ATP stimulation (Gómez-Villafuertes, García-Huerta, Díaz-Hernández, & Miras-Portugal, 2015; Iglesias & Spray, 2012; Lakshmi & Joshi, 2006; Masgrau et al., 2009; Reigada et al., 2017; von Schack et al., 2011). Therefore, we tested exogenous addition of ADP, adenosine, UDP, and UTP in comparison to ATP, each at a bulk extracellular concentration of 100  $\mu$ M. The addition of ADP caused a robust increase in the ratio signal that was further potentiated by pretreatment with ARL67516 (Fig 2.5), whereas adenosine, UDP, and UTP did not elicit any response. Clearly, there are complex differences between the ATP-elicited and ADP-elicited dynamics that likely reflect a number of signaling events that are well beyond the scope of this study. We therefore focused our study of the nature of the ADP-stimulated response to determine if the response is caused directly by ADP binding to the sensor or if ADP stimulates an endogenous release of intracellular ATP.

Our subsequent experiments indicate that the ecAT3.10 response is specific to ATP and not caused by an effect of ADP directly on the sensor. First, as a low affinity ligand for the soluble ATeam3.10 sensor, ADP could directly bind the sensor to produce an increase in the ratio signal. In fact, 100  $\mu$ M ADP nearly saturates the purified soluble ATeam3.10 sensor, which suggests that ADP binding to ecAT3.10 could be responsible for the observed live-cell response from ecAT3.10-expressing Neuro2A cells (H Imamura et al., 2009) . However, the ATeam3.10 sensor is nearly 100-fold more selective for ATP compared to ADP (S7 Fig), and given our observation that the ATP response profile of surface-bound ecAT3.10 is drastically shifted relative to soluble ATeam3.10, we tested the response of ecAT3.10 to direct ADP binding with bath perfusion experiments (Fig 2.6).

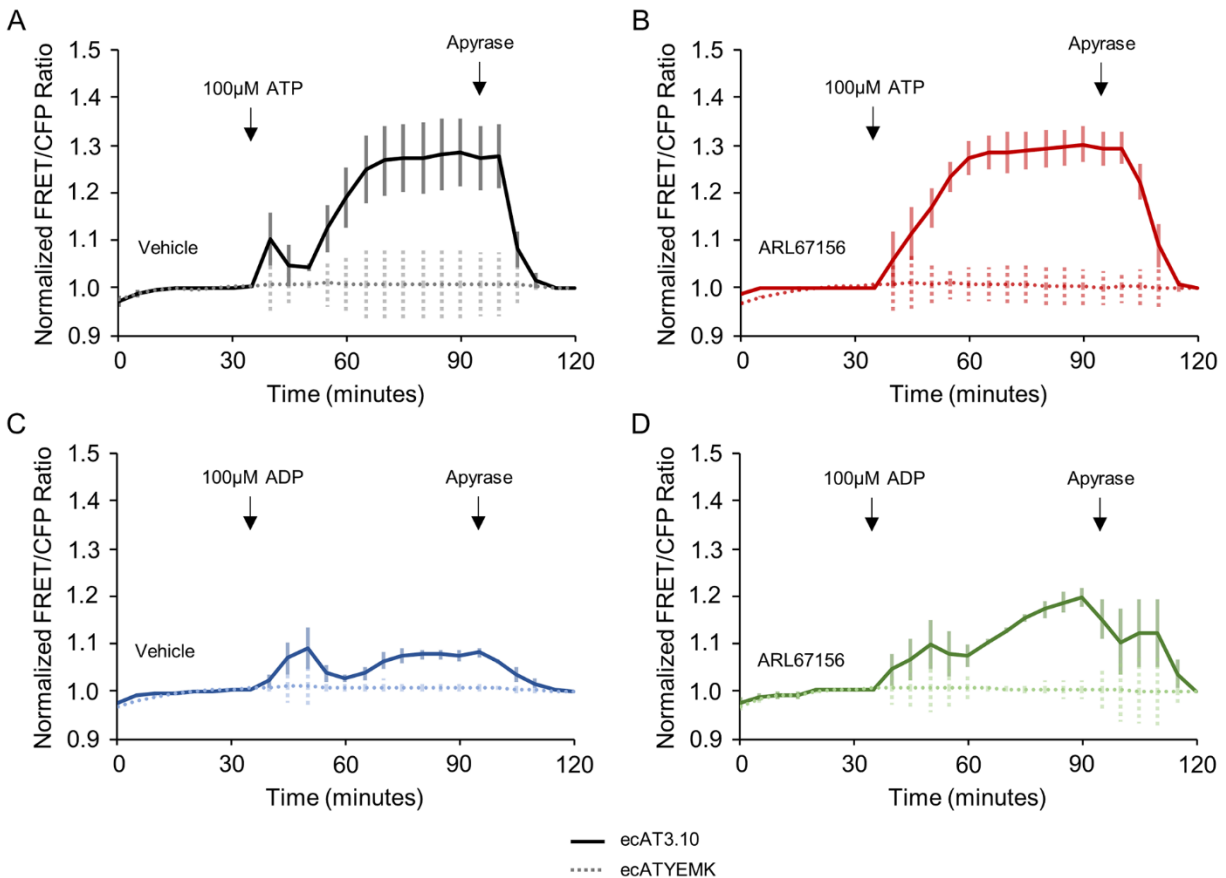


Figure 2.5. ecAT3.10 detects nucleotide-stimulated release of ATP from cells

(A) A biphasic response was apparent on average when 100  $\mu\text{M}$  ATP was added at time = 30 minutes to the static bath of ecAT3.10-expressing Neuro2A cells. The decrease in signal at time = 45 minutes is due to ARL67156-sensitive ectonucleotidase activity, and the subsequent increase in signal after time = 55 minutes reports a secondary release of endogenous ATP from cells. (B) Pretreatment with 100  $\mu\text{M}$  ARL67156 abrogates the transient decrease in ectonucleotidase activity. (C) Addition of 100  $\mu\text{M}$  ADP also stimulate a release of ATP from cells, which was potentiated by pretreatment with ARL67156 (D). Apyrase addition degrades extracellular ATP confirming a reversible ATP-specific sensor response. Solid lines show average responses from ecAT3.10, and dashed traces show average responses from the negative control ecATYEMK sensor ( $n = 3$ ). *Data collected and analyzed by Jason Conley, Saranya Radhakrishnan and Steve Valentino*

In contrast to the soluble sensor, ecAT3.10 showed a minimal fold increase in ratio signal upon wash-in of ADP (30  $\mu\text{M}$  ADP,  $1.009 \pm 0.002$ ; 100  $\mu\text{M}$  ADP,  $1.026 \pm 1.005$ ) compared to a subsequent wash-out of ADP and wash-in of ATP (30  $\mu\text{M}$  ATP,  $1.106 \pm 0.009$ ; 100  $\mu\text{M}$  ATP,  $1.14 \pm 0.01$ , mean  $\pm$  sem,  $n = 3$  experiments). Although the ecAT3.10 is not perfectly specific for ATP compared to ADP, it may be improved with future engineering. However, the current sensor is 5–

10 times more responsive to ATP, and thus, while a direct response to ADP binding may contribute a minor fraction of the signal, it does not account for the total magnitude of the response, supporting a stimulated release of ATP. Interestingly, these data are consistent with the approximate 20-fold affinity difference observed for ATP between ecAT3.10 and soluble ATeam3.10 (Fig 2.3). Second, we showed that the ADP-mediated increase in the sensor ratio signal was not due to a direct effect of the nucleotides on the individual fluorescent proteins in ecAT3.10. To test this, we used a low affinity ATeam variant, ATeam1.03YEMK (H Imamura et al., 2009), to generate the surface-targeted sensor, ecATYEMK. In contrast to ecAT3.10, this negative control construct ecATYEMK showed no response to either ATP or ADP (Fig 2.5), confirming that the response is not a non-specific effect on the individual CFP or YFP. Taken together, these data show that the increase in ecAT3.10 ratio signal cannot be solely attributed to direct ADP binding to the sensor, and they suggest that the increase is caused by an ADP-stimulated release of cellular ATP.

To confirm that the ecAT3.10 response is measuring an ADP-stimulated release of ATP from the Neuro2A cells, we measured extracellular ATP levels with an orthogonal biochemical assay, the widely accepted luciferase end-point assay. To carry out this experiment, cells were stimulated with 100  $\mu$ M ADP and the real-time ecAT3.10 response was measured by fluorescence microscopy (Fig 2.6). Simultaneously during imaging, samples of the static bath solution were taken at intervals, and the extracellular ATP levels were determined with a commercial luciferase-based ATP detection kit (Fig 2.6). As expected, the addition of ADP caused an increase in the extracellular ATP concentration that, as measured by the luciferase detection method, grossly mirrored the temporal pattern of the ecAT3.10 signal. Specifically, both the real-time ecAT3.10 ratio signal and the end-point luciferase measurements increased following the addition of ADP, and both decreased following the addition of apyrase ( $n = 4$  experiments) (Fig 2.6). We did observe differences in the detailed changes in extracellular concentration detected by ecAT3.10 versus the luciferase measurements, which reflect the differences between cell surface and bulk volume measurements. These observations confirm that ecAT3.10 can detect the ADP-stimulated release of endogenous ATP from Neuro2A cells.

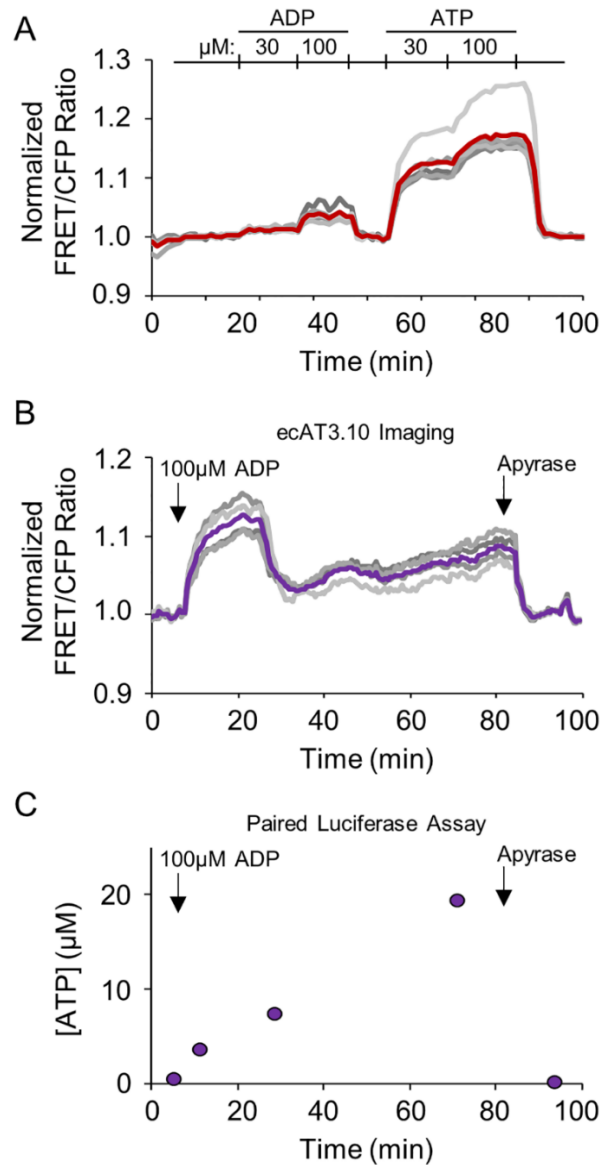


Figure 2.6. ecATeam3.10 detects ADP-stimulated release of endogenous ATP

(A) ecAT3.10-expressing Neuro2A cells were imaged under continuous perfusion conditions to demonstrate that ecAT3.10 has greater sensitivity to ATP compared to ADP. (B) Under static bath conditions, paired measurements by ecAT3.10 real-time imaging and endpoint luciferase assays demonstrate that ADP stimulates ATP release. In (A) and (B) grey traces are individual cells, and the bold trace is the cell mean. Arrows in (B) and (C) indicate the addition of ADP and apyrase, sequentially. In (C), time points represent samples from the bath solution taken during the ecAT3.10 imaging experiment shown in (B). *Data collected and analyzed by Jason Conley*

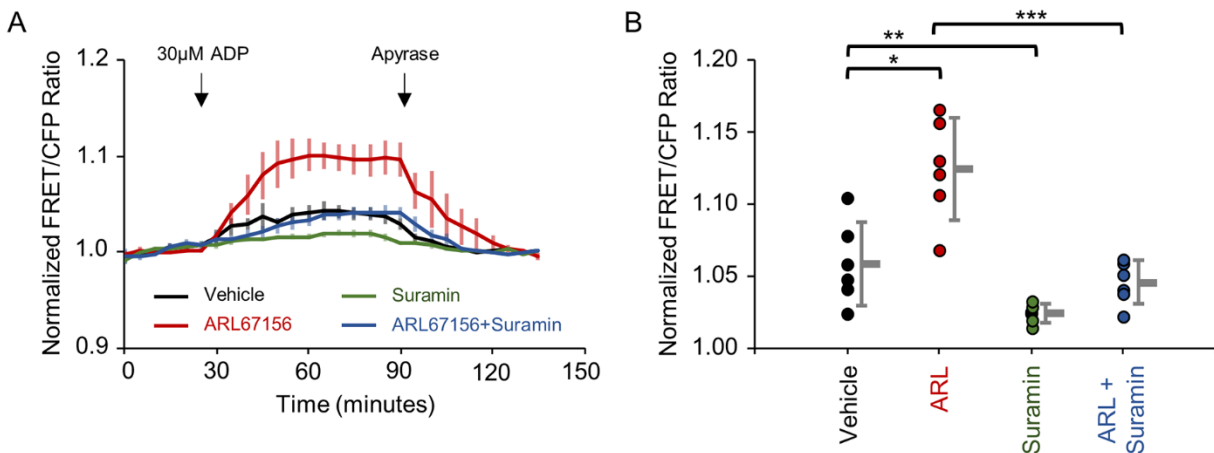


Figure 2.7. ADP-stimulated release of ATP release

(A) Average time course of ecAT3.10 ratio signal (baseline normalized,  $n = 6$  experiments) from Neuro2A cells that were imaged under static bath conditions.  $30 \mu\text{M}$  ADP was added to stimulate release of ATP. Pretreatment with  $100 \mu\text{M}$  ARL67156 (red) potentiated the response in comparison to vehicle treatment (black). Treatment with  $3.3 \mu\text{M}$  suramin (green) attenuated extracellular ATP levels compared to vehicle (black), and treatment with suramin in the presence of ARL67156 (blue) attenuated the release of ATP compared to ARL67156 alone (red). Apyrase addition degrades extracellular ATP confirming a reversible ATP-specific sensor response. (B) Summary of cell averaged peak responses for individual experiments. Peak responses: vehicle,  $1.06 \pm 0.01$ ; ARL67156,  $1.13 \pm 0.01$ ; suramin,  $1.027 \pm 0.002$ ; ARL67156 plus suramin,  $1.048 \pm 0.006$ , mean  $\pm$  sem. t-test,  $*p = 0.004$ ,  $**p = 0.02$ ,  $***p = 0.0004$ .  $n = 6$ , 2 independent investigators. *Data collected and analyzed by Jason Conley, Saranya Radhakrishnan and Steve Valentino.*

ADP-stimulated accumulation of extracellular ATP may be mediated by purinergic receptor signaling pathways, as several P2Y receptor isoforms are known to be modulated by ADP (Abbracchio et al., 2006). Therefore, a non-specific purinergic receptor antagonist, suramin, was tested for its effects on the ADP-stimulated release of ATP from Neuro2A cells (Abbracchio et al., 2006; Charlton et al., 1996; Coddou et al., 2011; Khakh & North, 2012). Specifically, the ecAT3.10 response to ADP ( $30 \mu\text{M}$ ) treatment was measured for Neuro2A cells that were pretreated with suramin ( $3.3 \mu\text{M}$ ), either in the presence or absence of the ectonucleotidase inhibitor, ARL67156 ( $100 \mu\text{M}$ ) (Fig 2.7). Consistent with ligand-stimulated ATP release from Neuro2A cells, pretreatment with ARL67156 potentiated the response to ADP which was reversed with subsequent apyrase treatment as expected (Fig 2.7). Furthermore, the ARL67156-potentiated ecAT3.10 response to ADP treatment was attenuated by suramin, suggesting that the ADP-stimulated release of ATP into the extracellular space was mediated by purinergic receptor

signaling components (Fig 2.7). Suramin non-specifically targets P2X and P2Y receptors, therefore we tested the P2Y inhibitor, pyridoxalphosphate-6-azophenyl-2',4'-disulfonic acid (PPADS). Suramin and PPADS attenuated release; however, we discovered that PPADS directly altered the sensor response (S8 Fig). Despite this, the confluence of evidence described above indicates that treatment of Neuro2A cells with ADP ultimately caused an accumulation of extracellular ATP that was detected by ecAT3.10, providing a proof-of-concept validation that ecAT3.10 was able to detect cell-mediated extracellular ATP dynamics.

## 2.5 Discussion

We have demonstrated that ecAT3.10 can be used to image and measure extracellular ATP dynamics in real-time, which is a significant advance because it provides a new tool to study purinergic signaling in live specimens. Extracellular ATP has been previously measured by a number of end-point biochemical and biophysical assays (Anderson et al., 2003; Bao et al., 2014; Beigi, Kobatake, Aizawa, & Dubyak, 1999; Bodin & Burnstock, 1996; Corriden & Insel, 2010a; Gourine et al., 2010; Khakh & North, 2012; Ledderose et al., 2014; Newman, 2001). Real-time monitoring of purinergic signaling has also been achieved using ATP sniffer cells (Brown & Dale, 2002; Hayashi, Hazama, Dutta, Sabirov, & Okada, 2004; Pangršič et al., 2007), enzyme-coupled optical fibers and electrodes (Gourine et al., 2010; Tan et al., 2017), and cell surface-tethered luciferase (Pellegatti, et al , 2005). These methods have estimated that basal ATP levels in cell culture and in tissue are as low as nanomolar concentrations, whereas peak release levels have been estimated to reach micromolar concentrations, representing a concentration range spanning several orders of magnitude (Bao et al., 2014; Beigi et al., 1999; Gourine et al., 2010; Khakh & North, 2012; Ledderose et al., 2014; Newman, 2001). Real-time measurements, including calibrated measurements from surface-tethered luciferase, are in agreement, though these measurements may have potentially underestimated surface ATP concentrations when not directly sampling at the cell surface (Bao et al., 2014; Choi & Barakat, 2010; Garcia et al., 2015; Ledderose et al., 2014). Surface-tethered luciferase could also underestimate surface levels because it requires access of a diffusible luciferin substrate and typically requires long integration times. To overcome this, a small organic fluorescent probe (Kurishita, Kohira, Ojida, & Hamachi, 2012) has been used to monitor surface ATP levels in real-time on immune cells (Bao et al., 2014; Ledderose et al., 2014), but it requires application of a lipidated probe. Overall, these methods variously suffer from

limitations due to spatiotemporal resolution, specificity, exogenous substrate access, or sample destruction, which limit their use in live specimens (Rajendran et al., 2016). A genetically encoded sensor, such as ecAT3.10, offers the capability to quantitatively visualize purinergic signaling with minimal perturbation after gene transfer. To this end, we have demonstrated that ecAT3.10 is able to reversibly report changes in extracellular ATP in a physiologically relevant concentration range.

Physiologically, clearance of extracellular ATP is constitutive, and we demonstrated that ecAT3.10 can detect ARL67156-sensitive ectonucleotidase activity that serves to maintain a low surface ATP concentration on cultured cells. It is therefore important to take these biological activities into account when deciphering the sensor responses. We measured the concentration-response relationship between ATP and ecAT3.10 under continuous perfusion conditions to maximally hold the bulk ATP concentration constant. However, the cell surface is likely a privileged compartment (Choi & Barakat, 2010; Garcia et al., 2015) where the observed ATP diffusion coefficient may be different from the bulk diffusion coefficient, and both biological clearance and release contribute to the net response (Bao et al., 2014; Bodin & Burnstock, 1996; Ledderose et al., 2014; Newman, 2001; Y. Zhang et al., 2008). For example, Neuro2A cells are known to express the ectonucleotidase CD39 (Gronwald et al., 1988), but ecAT3.10 was able to reveal population heterogeneity at the level of single-cell analysis, which may be caused by cell-to-cell variation in CD39 activity that dampens the response magnitude. It is also possible that ectonucleotidase turnover of local surface ATP generates an ATP concentration gradient that increases into the bulk bath volume, which serves as a reservoir of diffusing ATP—though future experiments, beyond the scope of this study, are needed to test this compartmentation explicitly. Importantly, despite the variability in the response magnitude, the sensitivity of the sensor to ATP was consistent, supporting that ecAT3.10 reports physiological ATP dynamics. Overall, ecAT3.10 was able to detect clearance of extracellular ATP, suggesting that ecAT3.10 may prove useful in quantitatively characterizing CD39 activity, for example, that is linked to immunogenicity of various cancer cell types (Bastid et al., 2015). Furthermore, the high ectonucleotidase activity that we observed in cultured cells matches well with the physiological need to prevent non-specific activation of purinergic receptors.

To this end, we also provided evidence that ecAT3.10 could detect a purinergic receptor-mediated endogenous release of ATP as a proof-of-principle. It has been previously reported that Neuro2A cells express purinergic receptors (Gómez-Villafuertes et al., 2015; Iglesias & Spray, 2012; Lakshmi & Joshi, 2006; Masgrau et al., 2009; Reigada et al., 2017; von Schack et al., 2011) and can be stimulated to release ATP (Gutiérrez-Martín et al., 2011). While a stimulated release event itself is expected to occur within seconds (Bowser & Khakh, 2007), it well established that extracellular ATP concentrations can remain elevated for several minutes, particularly under static bath conditions (Anderson et al., 2003; Bodin & Burnstock, 1996; Gutiérrez-Martín et al., 2011; Lu et al., 2015; Mansfield & Hughes, 2014; Newman, 2001, 2003; Z. Zhang et al., 2007a). Similar to these previous reports, we observed that ecAT3.10 detected a suramin-sensitive increase in extracellular ATP following ADP treatment. Under these static bath conditions, the increases occurred and persisted over several minutes, which is not attributed solely to the intrinsic kinetics of the sensor because the sensor itself can respond to changes in extracellular ATP levels within seconds. Instead, the persistent elevation in ATP likely reflects recurrent activation and release, which has been previously hypothesized (MacDonald, Yu, Buibas, & Silva, 2008). Interestingly, despite its apparent affinity,  $K_{app} = 12 \mu\text{M}$  ATP, the sensor showed a strong response to the stimulated release. Because the surface-tethered sensor does not require a diffusible substrate, the response correlates to the actual ATP dynamics at the cell surface. Hence, our observations suggest that surface ATP levels may indeed reach higher peak ATP concentrations than previously estimated. It will be interesting to use ecAT3.10 to study ATP release *in vivo* in the future because the extracellular volume constraints in intact tissue, in addition to differences between surface and bulk dynamics, are fundamental to the spatial and temporal components of purinergic signaling.

In summary, ecAT3.10 is a genetically-encoded and ratiometric fluorescent sensor of extracellular ATP that represents an important first-step in the creation of a new set of tools available for studying purinergic signaling in live specimens with single-cell resolution. Fluorescent protein-based sensors have emerged as powerful molecular tools to quantitatively visualize analyte dynamics in real-time, with subcellular resolution, and with the potential for cell-specific expression *in vitro* and *in vivo*. The ecAT3.10 is a CFP-YFP based sensor that is compatible with red fluorescent sensors, for example, such as the calcium sensors (Akerboom et al., 2013; Dana et al., 2016; Inoue et al., 2014; Wu et al., 2014; Zhao et al., 2011) and pH sensors (Tantama et al.,

2011), that can be multiplexed to study signal transduction or improve quantitative calibration. Furthermore, the current work suggests that other available soluble ATP sensors can potentially be re-engineered as surface tethered sensors of extracellular ATP, though the current work also demonstrates the need for live-cell characterization. One of the potential challenges that calls for a broad toolset of sensors is the large concentration range of extracellular ATP in basal and stimulated conditions. For this reason, it will be important to engineer both ratiometric sensors (Thestrup et al., 2014) to study changes occurring over slower timescales as well as intensimetric sensors (T. W. Chen et al., 2013) to study faster events. By optimizing dynamic range, affinity ranges, and surface tether length, these sensors will ultimately enable purinergic researchers to study compartmentation of ATP dynamics in vivo in the future.

## **CHAPTER 3. DEVELOPMENT OF 2<sup>ND</sup> GENERATION RED-SHIFTED FLUORESCENT REDOX SENSOR**

### **3.1 Abstract**

Reactive oxygen species (ROS) are integral components of redox signaling in cells that mediate physiologically essential signaling across compartments and play a vital role in determining cell fate. Under pathological conditions, excessive presence of ROS can lead to oxidative stress that damages cellular components and leads to cellular dysfunction and death. To understand dynamic redox changes and identify the mechanisms that disrupt redox homeostasis, we need high-precision tools that can be used to define redox processes in live cells under physiological and pathophysiological conditions. Current redox sensitive dyes and fluorescent proteins enable the quantification of spatially distinct changes in ROS levels, but multicolor probes are needed for the accurate analysis of single-cell and compartment-specific redox dynamics that can be masked by population averaging. Genetically encoded fluorescent sensors that measure cellular redox status can be targeted to specific subcellular compartments to study the redox changes in intracellular compartments during live-cell imaging. To this end, our lab previously engineered a genetically encoded red-shifted redox-sensitive fluorescent protein sensor using a Förster resonance energy transfer (FRET) relay strategy. Here, we have developed a second-generation excitation ratiometric sensor called rogRFP2 with improved red emission for quantitative live-cell imaging. We generated a library of constructs and characterized the redox properties of the library to identify the most improved sensor. We went on to demonstrate that they can be used to targeted to cellular models to simultaneously measure cytosolic and mitochondrial ROS in living cells.

### **3.2 Introduction**

Reactive oxygen species (ROS) are central mediators of redox signaling within and across physiological compartments (Finkel, 2011; Schieber & Chandel, 2014). ROS act as secondary messengers and mediate this redox signaling to maintain a variety of cellular functions like controlling cell fate, growth and metabolism (Khacho et al., 2016; Vaahtera, Brosché, Wrzaczek, & Kangasjärvi, 2014). ROS also regulates neuronal signaling in development by altering synaptic function, neurogenesis, neurite growth, axonal guidance (Munnamalai & Suter, 2009). Some of

the commonly generated ROS in cells are superoxide anion ( $O_2^{\cdot-}$ ), hydroxyl radical (OH), and hydrogen peroxide ( $H_2O_2$ ), which are by-products of aerobic metabolism and are intrinsic to the signaling process in cells (Halliwell & Gutteridge, 2015). A well-known reversible redox signaling mechanism is the oxidation of cysteine residues in proteins that alter function by inducing allosteric changes in the protein (Dickinson & Chang, 2011; Winterbourn & Hampton, 2008).

To provide a healthy redox balance, cells have evolved antioxidant mechanisms, including antioxidant proteins (e.g. superoxide dismutases, catalases, peroxidases) and small molecules (e.g. glutathione, coenzyme Q10), that regulate intracellular ROS levels (Dey, Sidor, & O'Rourke, 2016). Together, ROS and antioxidants make up a redox network that maintains a redox homeostasis within cells. Cellular functions are also tightly regulated by the subcellular localization of these redox molecules, emphasizing the need for the spatial organization of redox regulation (Booth, Enyedi, Geiszt, Várnai, & Hajnóczky, 2016; Go & Jones, 2008a; Janssen-Heininger et al., 2008). Specifically, organelles like the mitochondria that have a metabolic burden generate high levels of ROS but also have their own discrete antioxidant mechanisms (M. P. Murphy, 2012; Shadel & Horvath, 2015). The interaction between different compartments and cross compartmental redox dynamics are highly coupled.

In addition to the physiological redox regulation, excessive presence of ROS can lead to pathological complications like oxidative stress that damages cellular components and causes dysfunction and cell death. Oxidative stress can be caused by an unbalanced increase in ROS production or impairment of antioxidant machinery (Espinosa-Diez et al., 2015). This stress response is commonly observed across several disorders like cancer, neurodegeneration and cardiovascular disorders making it critical to understand this fundamental process that can tip over from regulation to destruction (Heitzer, Schlinzig, Krohn, Meinertz, & Münzel, 2001; Panieri & Santoro, 2016; Xinkun Wang & Michaelis, 2010).

Genetically encoded redox sensitive fluorescent probes enhance our capability to quantitate and measure dynamic changes in redox activity in living cells and these can also be targeted to various subcellular compartments (Dooley et al., 2004; Gutscher et al., 2008; Hanson et al., 2004; Lohman & Remington, 2008; Meyer & Dick, 2010a; Wagener et al., 2016). The roGFP sensors developed

by Hanson et al. are prime examples of excitation ratiometric redox sensors that work robustly in live cells. These sensors were developed by modifying green fluorescent protein (GFP) and introducing two solvent-facing cysteines near the chromophore (Hanson et al., 2004). This results in the formation of a disulfide bond between the cysteines upon oxidation and changes the protonation state of the chromophore. This causes a shift in the excitation spectrum of the roGFP, causing an increase in 400 nm peak upon oxidation and a decrease in the 485 nm peak upon reduction. There are two versions of the roGFP sensors, the roGFP1, which was derived from wtGFP and the roGFP2, which was based on eGFP, and they both have the same cysteine modifications. roGFP2 has a higher signal yield as it is excited more efficiently at 488 nm than it is at 405 nm (Hanson et al., 2004). Ratiometric sensors such as the roGFP are valuable for live-cell imaging because they are self-normalizing and independent of expression level and sample excitation, therefore facilitating quantitative comparisons between individual compartments, cells, and experiments.

Furthermore, recent developments of red fluorescent redox sensors like the rxRFP and HyPerRed have made multicolor imaging possible (Ermakova et al., 2014; Fan & Ai, 2016; Fan et al., 2015; Piattoni et al., 2019; A. G. Shokhina et al., 2019; Arina G. Shokhina et al., 2019). However, the majority of these sensors report redox dynamics with changes in a single fluorescence intensity channel, and there remains a need to develop multicolor ratiometric redox sensors (Fan et al., 2017a). The spectral limitation restricts our ability to concurrently study ROS dynamics between different subcellular compartments. Previously, graduate students in our lab Stevie Norcross and Keelan Trull, developed a novel sensor design that uses a FRET relay to extend the emission profile of roGFP out to red wavelengths by attaching a red fluorescent protein (RFP) FRET acceptor without altering the desirable redox sensing properties of the roGFP itself (Norcross et al., 2017).

The first generation red-shifted redox sensor constructs were created by fusing RFPs mApple, mCherry, and mRuby2 to both the N- and C- terminus of roGFP1 and roGFP2. Our first-generation FRET-relay redox sensors were designed with an roGFP FRET donor connected to a red FRET acceptor using a seven amino acid linker. Unlike most FRET sensors that exhibit dynamic changes in FRET efficiency, in this design, the FRET from roGFP to RFP is constant, and the ratiometric

response originates from the roGFP donor. With the first-generation seven amino acid roGRFP2 linker we were able to achieve a 20% FRET efficiency without compromising the redox properties or the ratiometric response in the excitation spectrum, and we demonstrated the use of this sensor for dual-compartment imaging. In this study, we describe the design and development of an improved iteration of the red-shifted redox sensor with roGFP2 as the donor. After generating the sensor library, we characterize them to identify the top candidates with improved FRET efficiency and further validate them in solution. We also demonstrate that the redox properties of the parent roGFP donor are maintained in the second-generation sensor, which we now call “roGRFP2 “. The promising candidates were fused with a mitochondrial targeting sequence to enable the imaging of the mitochondrial redox dynamics simultaneously with the cytosol.

### **3.3 Materials and Methods**

#### **3.3.1 Materials**

Chemicals and cell culture media and supplements were purchased from Sigma, Formedium, and ThermoFisher Scientific. Molecular biology enzymes were purchased from New England Biolabs (NEB).

#### **3.3.2 Molecular Biology**

Plasmids with altered linker length were generated using Q5 mutagenesis of the L7 constructs expressed in the pRSETB bacterial expression vectors. The roGRFP2 and a0GG4g sequences were cloned into GW1 mammalian expression vector. They were cloned into GW1 vectors with COX8 repeat (4x) mitochondrial signal sequence for mitochondrial targeting and GW1 vector without a signal sequence for the cytosolic expression of the roGFP2 (Tantama et al., 2011).

#### **3.3.3 Protein Expression and Purification**

The sensor library was expressed in E. Coli strain BL-21 and cultured in Auto Induction Media (AIM) at 37°C for 12hrs and then at room temperature for 24-48hrs. Cells were then pelleted, resuspended in lysis buffer (25mM Sodium Phosphate Buffer (pH 7.8), 500mM NaCl, 10mM Imidazole, 5% Glycerol, 0.25mg/ml lysozyme, 0.1% Triton-X, 1mM PMSF, 5mM DTT) and lysed

by sonication. Lysate was then centrifuged at 30,000xg for 30min at 4°C, and passed through a 0.45 µm syringe. The sample was then run over a Ni column (GE Chelating Sepharose column charged with Ni<sup>2+</sup>). The column was then washed with a gradient of elution buffer (25 mM Sodium Phosphate Buffer [pH 7.8], 500 mM NaCl, 500 mM Imidazole, 5% Glycerol). The protein was eluted in elution, dialyzed in storage buffer (50mM MOPS, 750mM NaCl, 10% glycerol overnight at 4°C to remove excess imidazole and stored in the -80°C for use.

### 3.3.4 Steady-State Fluorescence Spectroscopy

To determine concentration, the protein was denatured using 1M NaOH and the chromophore absorbance was measured at 447 nM using an extinction coefficient of 44,000 M<sup>-1</sup>cm<sup>-1</sup> while accounting for the number of chromophores. The protein was diluted to a final concentration of 1 µM in 75 mM HEPES, 125 mM KCl, 1 mM EDTA, pH 7.0–7.3 for the spectroscopy and redox measurements.

In redox titration experiments, the solutions were degassed under vacuum and purged with argon gas, and protein solutions were equilibrated with 10 mM reduced DTT (1,4- dithiothreitol) or 10 mM oxidized DTT (trans-4,5-dihydroxy-1,2- dithiane) for 1 h before measurements (Dooley et al., 2004). Redox titrations carried out in solutions in which the total DTT concentration was held constant at 10 mM while the reduced DTT to oxidized DTT ratio was varied. Midpoint potentials were determined as previously described and by fitting titration data to a Boltzmann equation on Origin (Meyer & Dick, 2010). UV-vis and steady-state fluorescence spectroscopy was performed using a BioTek Synergy H4 microplate reader at room temperature.

To measure the dynamic range of the different constructs, the protein was diluted in 10mM reduced/oxidized DTT in distinct microcentrifuge tubes. For each sample, the excitation ratio (R) was calculated ( $F_{400nm}/F_{480nm}$ ). The excitation ratio for the sample diluted in 10mM reduced DTT was  $R_{reduced}$  and the ratio for sample diluted in 10mM oxidized DTT was  $R_{oxidized}$ . Dynamic range was calculated to be  $R_{Oxidized}/R_{Reduced}$ .

Two-photon photoluminescence measurements were performed by employing a home-built confocal PL microscope. The output of a high-repetition rate amplifier (Pharos Light Conversion,

400 kHz) was used to pump an optical parametric amplifier (OPA), which yielded the various excitation wavelengths used for the measurements. The excitation wavelengths ranged from 800 nm to 960 nm, in 20 nm increments. The laser beam was focused onto the sample using a 50X [(numerical aperture) NA=0.95] objective. The PL emission was collected with the same objective, optically filtered to remove residual pump light, dispersed with a monochromator (Andor Technology) and detected using a charge coupled device (CCD) (Andor Technology).

### **3.3.5 Time-Resolved Fluorescence Spectroscopy**

The protein was diluted to a final concentration of 1  $\mu$ M in 75 mM HEPES, 125 mM KCl, 1 mM EDTA, pH 7.3. Solutions were degassed under vacuum and purged with argon gas, and protein solutions were equilibrated with 10 mM oxidized DTT for 1 hour before measurements. Protein samples were placed in a 35 mm glass bottom dish (Cellvis, D35-20-1.5-N), and light was focused using a 20 $\times$  objective with a coverslip correction ring at 0.17 mm (Olympus LUCPlanFL, NA = 0.45). Fluorescence lifetimes of oxidized protein samples were measured on a custom- built microscope using a 447 nm pulsed diode laser (PicoQuant, LDH-P-C-450B) at a 10MHz repetition rate with an instrument response function full-width at half-maximum of 150 ps. Lifetimes were measured using a single photon avalanche diode (Pico-Quant, PDM series) and a single photon counting module (Pico-Quant) with a time resolution of  $\sim$  100 ps. roGFP donor emission was collected using a combination of 500 long-pass and 550 short-pass filters. Empirical lifetimes were measured from the photon decays, and FRET efficiency was calculated as  $1 - \tau_{\text{roGFP-RFP}}/\tau_{\text{roGFP}}$ . Fluorescein standard lifetimes were measure before each experiment and were in agreement with accepted values.

### **3.3.6 Cell Culture and Transfections**

Human embryonic kidney 293 (HEK293) cells were cultured in Dulbecco's modified eagle's medium with 4.5 g/L glucose, 10% cosmic calf serum, 3.7 g/L sodium bicarbonate, pH 7.0-7.4 and maintained at 37°C and 5% CO<sub>2</sub>. Cells were plated onto a 35mm glass bottomed culture dish at a density of  $2 \times 10^5$  cells, 24 hrs prior to transfection. Cells were transfected with calcium phosphate using 500ng of each construct. Cells were imaged 48 hours post transfection.

### **3.3.7 Live-Cell Imaging**

HEK293 cells were imaged in imaging solution containing 15 mM HEPES, 120 mM NaCl, 3 mM KCl, 3 mM NaHCO<sub>3</sub>, 1.25 mM NaH<sub>2</sub>PO<sub>4</sub>, 1 mM MgCl<sub>2</sub>, 2 mM CaCl<sub>2</sub>, and 10 mM glucose. Cells were equilibrated at room temperature for at least one hour before all imaging experiments. For widefield microscopy, cells were imaged in 35mm glass bottomed dishes at a 1-minute interval and treatments were added to a static bath with imaging solution. They were imaged on an Olympus IX83 fluorescence microscope with a Plan Apo VC 20X objective (0.75 NA), equipped with a Prior motorized stage and an Andor Zyla 4.2 sCMOS camera (6.5 μm pixel). The images were taken with a 2x2 pixel binning and exposure times ranging from 50-400 milliseconds. The LED light source was a Lumencor SpectraX light engine and the following filter pairs (Semrock or Chroma) were used: ex. 475/34nm, em. 525/50nm; ex. 395/25nm, em. 525/50nm, ex. 475/34nm, em. 632/60nm, ex. 395/25nm, em. 632/60nm, ex. 575/25nm, em. 632/60nm. DIC images were taken before and after each imaging experiment to verify cell health.

### **3.3.8 Data Analysis**

Images were analyzed using ImageJ. The fluorescent images were background subtracted above the mean background signal and then a threshold was set to three standard deviations over mean to eliminate background pixels. Ratio images were generated by dividing the 400 Ex image by the 490 Ex image for both the red and green emissions and the ratio signals were measured around the cell body.

### 3.4 Results and Discussion

#### 3.4.1 Sensor Design of 2<sup>nd</sup> generation roGFP2 sensor

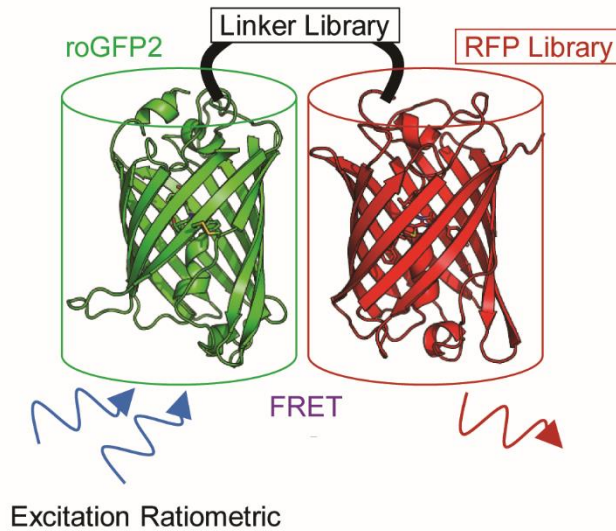


Figure 3.1. Diagram of the FRET relay from the roGFP donor to the RFP acceptor

Our first-generation FRET-relay redox sensors were designed with a combination of roGFPs and several RFPs which were fused using a seven amino acid linker (Figure 3.1). With this configuration, a 20% FRET efficiency was achieved and this sensor architecture provided a sufficient red fluorescent redox-dependent signal for dual-compartment imaging (Norcross et al., 2017). We sought to further improve the FRET between the two FPs by altering the linker length and selected specific FPs for the second-generation sensor library (Figure 3.2).

Fluorescent Protein	Ex. (nm)	Em. (nm)
roGFP2	400, 490	508
mApple	568	592
mRuby2	559	600
mCherry	587	610

Figure 3.2. Design of the roGFP2 sensor library

### 3.4.2 Generation of Sensor Library

We generated and screened a combinatorial library of different linker lengths and RFP FRET acceptors. Our initial proof-of-concept studies indicated that using roGFP2 as the redox-sensitive FRET donor achieved larger signal dynamic ranges compared to roGFP1 fusions, so we designed our second-generation library with roGFP2 as the donor. We combined the roGFP2 donor with three different RFPs, mRuby2, mApple, or mCherry, because they each exhibit different peak emission bands and in theory can still achieve high FRET efficiencies (Figure 3.2). Among the RFPs, mCherry has been used extensively in *in vivo* and *in vitro* studies of FRET pairs along with GFP (Bajar, Wang, Zhang, Lin, & Chu, 2016) as the emission profiles of GFP and mCherry have a huge spectral separation (Shaner et al., 2004). mApple was chosen for its brightness properties, and it has an intermediate spectral profile between mCherry and mRuby2 (Shaner et al., 2008). The emission of GFP overlaps substantially with the absorbance of mRuby2, which is bright and photostable RFP, and it has also been used in FRET pairs with Clover, a GFP derivative (Lam et al., 2012). We also varied the order of fusion, with the RFP fused to either the N- or C-terminus of roGFP2 via the linker. FRET efficiency largely depends on the distance and orientation between the donor and acceptor and on the spectral overlap between the FPs (Iqbal et al., 2008). After selecting the preferred roGFP and RFPs from previous studies, we proceeded to work with altering the linker length to reduce the distance between our donor roGFP and acceptor RFP. We varied the roGFP2-RFP linker by shortening the artificial peptide linker sequence as well as altering the native fluorescent protein termini. To alter the native termini, we tested deletions of up to eleven amino acids from flexible regions identified from X-ray crystal structures (Table 3.1). Site-directed mutagenesis was performed to create the different constructs, which were expressed in bacteria using the pRSetB vector.

Table 3.1. Linker variation for construct library

Construct	N-Terminal FP	Linker Region	C-Terminal FP
gL7c gL2c g11GG3c g11GG0c g4GG7c g4GG3c g4GG0c g0GG7c g0GG3c g0GG0c	roGFP2	GITLGMDELYKGGSGGRS <u>V</u> SKGEED GITLGMDELYKGG-----VSKGEED GITLGMDELYKGG-----EED GITLGMDELYKGG----- GITL-----GG-----VSKGEED GITL-----GG-----EED GITL-----GG----- -----GG-----VSKGEED -----GG-----EED -----GG-----	mCherry
cL7g cL2g c8GG0g c0GG4g c0GG0g	mCherry	GGMDELYKGGSGGRS <u>V</u> GGMDELYKGG-----V GGMDELYKGG----- -----GG-----V -----GG-----	roGFP2
gL7a gL2a g11GG3a g11GG0a g4GG7a g4GG3a g4GG0a g0GG7a g0GG3a g0GG0a	roGFP2	GITLGMDELYKGGSGGRS <u>V</u> SKGEEN GITLGMDELYKGG-----VSKGEEN GITLGMDELYKGG-----EEN GITLGMDELYKGG----- GITL-----GG-----VSKGEEN GITL-----GG-----EEN GITL-----GG----- -----GG-----VSKGEEN -----GG-----EEN -----GG-----	mApple
aL7g aL2g a8GG0g a0GG4g a0GG0g	mApple	GGMDELYKGGSGGRS <u>V</u> GGMDELYKGG-----V GGMDELYKGG----- -----GG-----V -----GG-----	roGFP2
gL7r gL2r g11GG2r g11GG0r g4GG6r g4GG2r g4GG0r g0GG6r g0GG2r g0GG0r	roGFP2	GITLGMDELYKGGSGGRS <u>M</u> VSKGEE GITLGMDELYKGG-----VSKGEE GITLGMDELYKGG-----EE GITLGMDELYKGG----- GITL-----GG-----VSKGEE GITL-----GG-----EE GITL-----GG----- -----GG-----VSKGEE -----GG-----EE -----GG-----	mRuby2
rL7g rL2g r12GG0g r4GG4g r4GG0g r0GG4g r0GG0g	mRuby2	AGLGGMDELYKGGSGGRS <u>V</u> AGLGGMDELYKGG-----V AGLGGMDELYKGG----- AGLG-----GG-----V AGLG-----GG----- -----GG-----V -----GG-----	roGFP2

### 3.4.3 Screening and Characterization of Sensor Library

In total, we were able to generate, express, and purify 28 novel constructs which we screened by solution studies of the purified proteins using time-resolved and steady-state spectroscopy. We performed an initial qualitative screening of our constructs by measuring their emission spectra (with both 405nm and 485nm) and excitation spectrum for the roGFP2 and RFP emissions. All of the fusion constructs exhibited a clear red fluorescence emission peak upon donor excitation at 405nm and 485nm. Despite high residual green fluorescence and a large emission peak at 525nm, the red emission peak was distinct as seen with the construct mApple-0GG4-roGFP2 abbreviated “a0GG4g” (Figure 3.3).

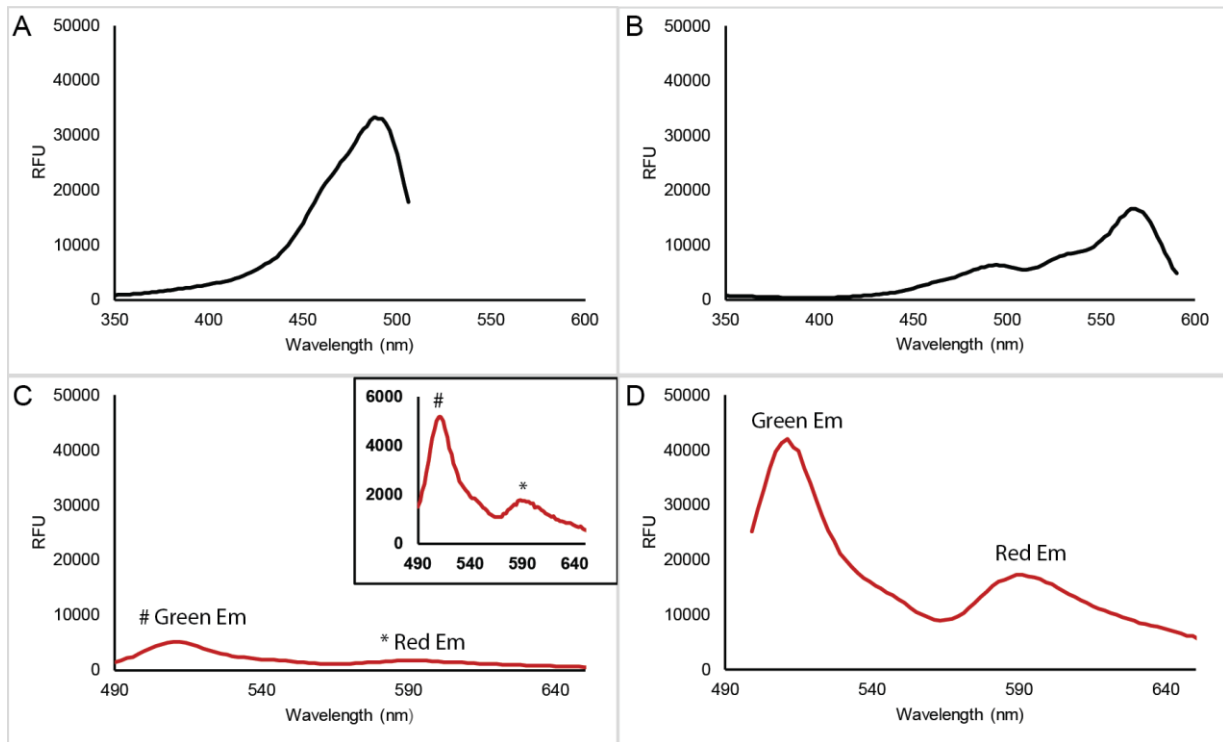


Figure 3.3. Steady-state spectroscopy screen of a0GG4g

(A) Excitation spectrum of roGFP2 with emission at 525nm (B) Excitation spectrum of roGFP2 with emission at 610nm (C) FRET emission spectrum with excitation at 405nm (scaled up to show the distinct roGFP2 emission peak at 525nm and the red FRET emission peak at 592nm) (D) FRET emission spectrum with excitation at 485nm which also shows the FRET emission peak along with the roGFP2 emission peak.

For the quantitative assessment of our constructs, we used time-resolved spectroscopy because the decrease in donor fluorescence lifetime is a robust metric for measuring FRET efficiency. As expected, all of the library constructs exhibited a decrease in donor lifetime relative to the parent roGFP2 control as well as an increase in the corresponding red emission upon donor excitation. We paired this with steady-state spectroscopy to measure the signal dynamic range (dynamic range =  $\text{ratio}_{\text{oxidized}}/\text{ratio}_{\text{reduced}}$ ), which we define as the magnitude of the ratiometric change in the excitation spectrum of the red emission channel upon going from the fully reduced to the fully oxidized state.

We assessed redox sensing and calculated the dynamic range by measuring the fluorescence excitation spectra in the presence of excess reduced or oxidized DTT. We observed a redox-dependent ratiometric change in the excitation spectrum of all constructs when collected donor green emission or FRET acceptor red emission. The excitation ratios ( $\text{Ratio} = F_{400\text{nm}}/F_{485\text{nm}}$ ) were calculated for the red emission channel in the oxidized and reduced states and used to calculate the dynamic range. All constructs exhibited reasonable dynamic ranges for use, but as expected, dynamic ranges were diminished relative to the parent roGFP2 control because of less than perfect FRET and spectral crosstalk. Representative figure of the construct a0GG4 is shown below (Figure 3.4). Despite the reduced dynamic ranges, we clearly retained the redox sensing and ratiometric properties of the donor roGFP.

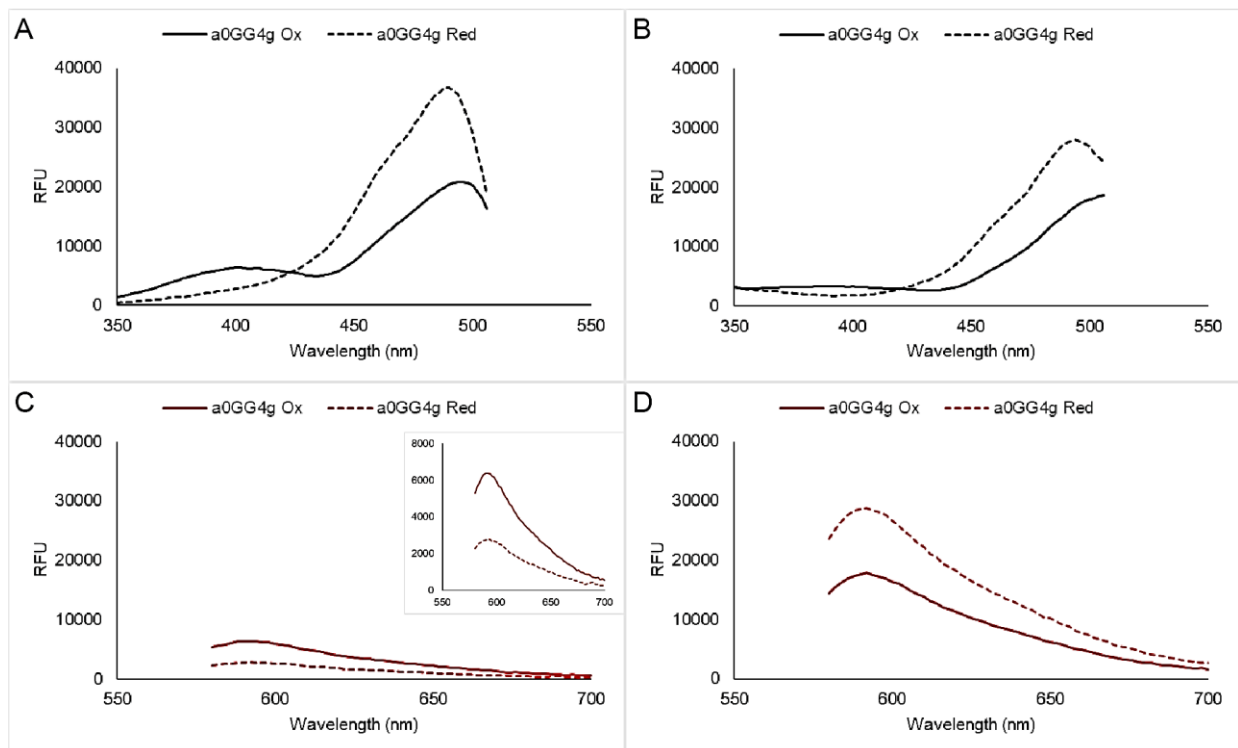


Figure 3.4. Redox titration and dynamic range measurement of a0GG4g

(A) Excitation spectrum while collecting emission at 525nm for the oxidized and reduced constructs (B) Excitation spectrum while collecting emission at 610 nm for the oxidized and reduced constructs (C) FRET emission spectrum with excitation at 405nm and the red FRET emission peak at 592nm; Oxidized a0GG4g construct has higher red emission than the reduced construct when excited at 405nm (D) FRET emission spectrum with excitation at 485nm and the FRET emission peak around 592nm; reduced construct has higher FRET emission when excited at 485nm than the oxidized construct. Dynamic range =  $\text{ratio}_{\text{oxidized}}/\text{ratio}_{\text{reduced}}$  with collected FRET emission

$$E = 1 - \frac{\tau_{DA}}{\tau_D}$$

$$\text{Ratio}_{\text{oxidized}} / \text{Ratio}_{\text{reduced}}$$



Figure 3.5. Linker and RFP acceptor library screen

FRET efficiency was calculated from the change in donor fluorescence lifetime relative to the roGFP2 control. Dynamic range was calculated as the fold difference of the  $F_{405}/F_{485}$  ratio measured in the presence of 10 mM DTT or 10 mM Oxidized DTT. N.D., not determined.

Most constructs also showed an improvement in FRET efficiency, but interestingly there were no clear patterns of dependency on linker length, choice of RFP acceptor, or the order in which the two proteins were fused (Figure 3.5). We selected the top two candidates with the highest FRET efficiency with a robust dynamic range, g0GG3a and a0GG4g and proceeded with further characterization of these constructs. The top performing library construct g0GG3a exhibited an improved FRET efficiency of 34% and dynamic range with a maximal 5-fold change in excitation ratio, and we renamed this variant “rogRFP2” as our second-generation sensor. This new rogRFP2

sensor contains roGFP2 with an 11 amino acid truncation of its C-terminus fused to a diglycine linker that bridges to mApple with a 9 amino acid truncation of its N-terminus. Solution characterization clearly shows a large 1 ns decrease in donor lifetime, which manifests as a significantly increased sensitized mApple red emission and suppressed roGFP2 green emission in the steady-state spectra (Figure 3.6.A, B). Furthermore, the midpoint potential remains unperturbed relative to the roGFP2 parent (Figure 3.6.C).

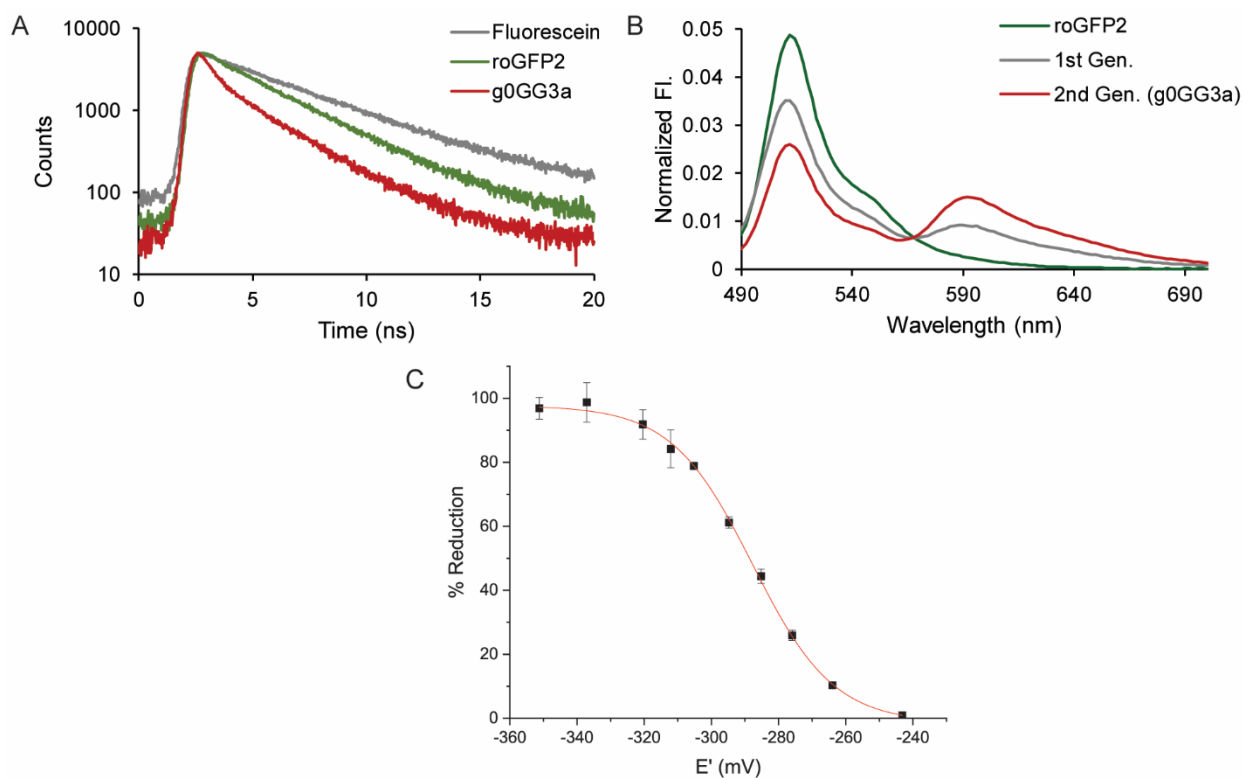


Figure 3.6. Characterization of the second generation roGRFP2 sensor

(A) Donor fluorescence lifetime of roGRFP2 (red) is significantly decreased compared to roGFP2 donor control (green). Fluorescein is shown for comparison (grey). (B) Fluorescence emission spectra of roGRFP2 (red) exhibits significantly improved red emission and suppressed green emission relative to the roGFP2 control (green) and first-generation sensor (grey). (C) The midpoint potential of roGRFP2 is  $-287.8 \pm 0.4$  mV (mean  $\pm$  s.e.m.,  $n=3$ ).

### 3.4.4 Proof-of-Concept studies in HEK293 cell line

With a FRET efficiency of around 34%, the second-generation FRET redox sensor, roGRFP2 generated a significant improvement in red fluorescence signal as compared to the first generation

despite the substantial residual fluorescence from the green donor. Previously, we found that our first-generation sensors could be targeted well to the mitochondria of HEK293 and Neuro2A cultured cell lines. Similarly, we hypothesized that the roGRFP2 can be targeted to specific subcellular locations and be used for dual color imaging of subcellular redox compartmentation due to the spatial separation between the sensors. To validate these sensors for this application, we cloned the constructs roGRFP2 and a0GG4g into mammalian expression vectors that could be targeted to the mitochondria or expressed in the cytosol.

Despite incomplete suppression of the donor green fluorescence, we validated that roGRFP2 could be efficiently targeted to the mitochondria of cultured cell lines by demonstrating this in HEK293 cells. Furthermore, even with less than perfect FRET efficiency, the improved red fluorescence from mitochondrially-targeted roGRFP2 was easily distinguished from the green fluorescence of co-transfected cytosolic roGFP2. The mito-roGRFP2 sensor was directed to the mitochondrial matrix using a cytochrome c oxidase subunit VIII (Cox8) signal sequence, which has previously been demonstrated as an effective mitochondrial targeting sequence (Filippin et al., 2005; Llopis et al., 1998). As an initial proof of concept for the use of the improved sensor in cell culture models, live cell ratiometric imaging was performed using widefield fluorescent microscopy. Red and green emissions were collected sequentially after a 400 and 490nm excitation. The red fluorescent protein was also excited at its excitation peak around 575nm, and the collected red emission was used to generate a mask that was used to isolate the mitochondrial signal during image analysis. This additionally helped us distinguish between the mitochondrial and cytosolic signals, enabling us to minimize the contribution of the residual green emission from the roGRFP2 sensor when quantifying the cytosolic roGFP2 signal.

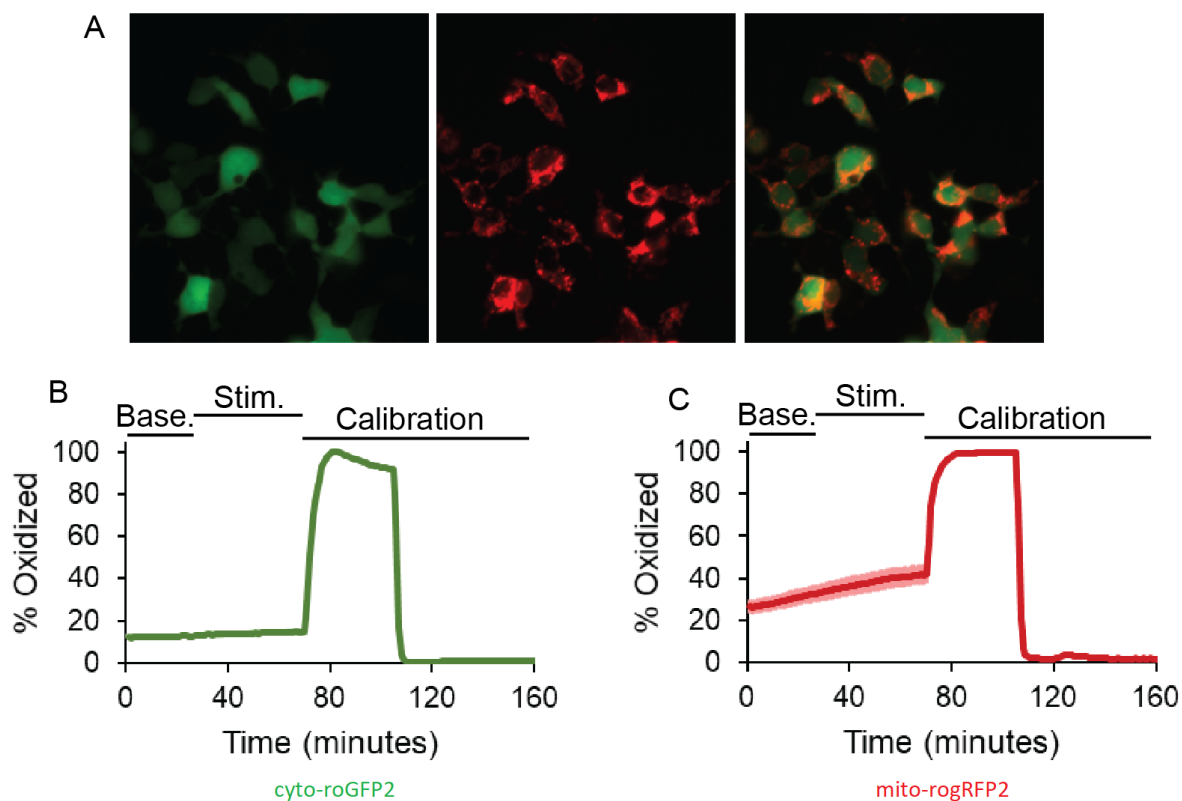


Figure 3.7. Proof of concept dual compartment imaging in HEK293 cells

(A) HEK293 cells co-expressing roGFP2 in the cytosol and roRFP2 in the mitochondria  
 (B,C) Live-cell dual color redox imaging of the HEK293 cells with a  $25\mu\text{M}$   $\text{H}_2\text{O}_2$  stimulation followed by a calibration with  $0.5\text{mM}$   $\text{H}_2\text{O}_2$  and  $2\text{mM}$  DTT.

During ratiometric imaging, we made baseline measurements of redox in the two compartments, followed by a short  $25\mu\text{M}$   $\text{H}_2\text{O}_2$  addition at 15mins which did not elicit a significant response from the compartments, followed by a sensor calibration. For the calibration,  $0.5\text{mM}$  of  $\text{H}_2\text{O}_2$  was added at 75mins to fully oxidize the sensor followed by a treatment of  $5\text{mM}$  DTT at 105mins to fully reduce the sensor. These values helped us determine the % oxidation of the two sensors.

### 3.4.5 Two-Photon Imaging

The green fluorescent roGFP-based sensors have been used successfully with two-photon microscopy, and therefore we tested whether the two-photon excitation profile is preserved in roRFP2. As predicted by the one-photon spectra, purified protein samples exhibited a ratiometric response upon oxidation, and for all tested two-photon excitation wavelengths, a strong red

fluorescence emission peak was observed at 600 nm despite incomplete suppression of the donor green emission peak (Figure 3.8).

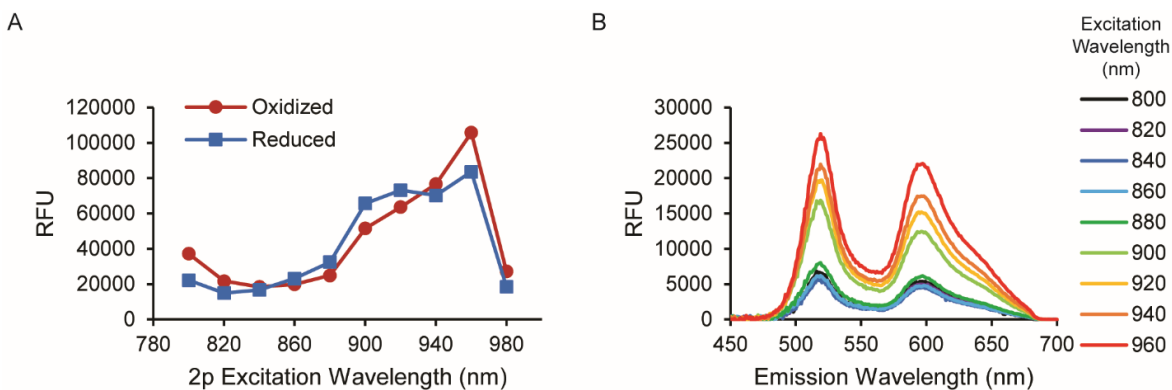


Figure 3.8. Two-photon cross sections of purified roGRFP2.

(A) Excitation and (B) emission spectra were collected with two-photon excitation. Purified protein was fully reduced with DTT or oxidized with oxidized DTT. (A) There is a ratiometric change at excitation wavelengths of 800 and 900 nm used for imaging. (B) The emission profile exhibits a strong red fluorescence peak at 600 nm. (*Prepared in collaboration with Jordan Snaider & Libai Huang*)

### 3.4.6 Grx1 and Orp1

roGFP2 interacts with glutaredoxins and preferentially equilibrates with glutathione redox potential (Meyer et al., 2007). Grx1-roGFP2 was designed to study the dynamics of thiol-redox buffer systems and allow for the faster measurement of glutathione redox potentials. The construct was generated by fusing the roGFP2 to glutaredoxin 1 (Grx1), which enhanced sensor kinetics for glutathione specificity, and this sensor was especially useful in reducing compartments such as the cytosol. The roGFP2-Orp1 sensor was generated by fusing a peroxidase Orp1 to roGFP2 to form an efficient redox relay that occurs through a thiol-disulfide exchange. The grx1-roGFP2 and roGFP2-Orp1 sensors have been used to map glutathione redox potentials and peroxide in the cytosol and mitochondria in both a developmental and aging model of drosophila. One of the potential future modifications of the roGRFP2 sensor will be to conjugate the Grx1 and Orp1 proteins to the sensor to ensure higher specificity of redox measurements. The roGRFP2 sensor was conjugated to Grx1, to create the Grx1-roGRFP2 construct and the a0GG4g sequence was

conjugated to Orp1 to create the a0GG4g-Orp1 construct. Both these were cloned into a prSetB vector for bacterial expression. In the future, we will characterize these new sensors for application.

### 3.5 Conclusion

Ratiometric live-cell imaging provides a powerful approach for quantitative redox biology, and we have engineered the second-generation red fluorescent sensor rogRFP2 for this purpose. Our FRET relay design has the advantages that it preserves the desirable redox sensing properties of the donor roGFP2, one of the most widely used genetically encoded fluorescent sensors as well as the ratiometric response that facilitates improved quantitation across compartments, cells, and experiments. In this work, we improved upon the first generation genetically encoded redox sensor to generate the rogRFP2 sensor, which exhibits a red fluorescent excitation-ratiometric readout. In the development of these second-generation sensors, we were able to increase the FRET efficiency and red emission by more than 50% compared to the first-generation sensors (Norcross et al., 2017). However, this second-generation sensor still exhibits incomplete donor suppression and residual green fluorescence that limits its use. Despite this shortcoming, future engineering efforts may be able to achieve even higher FRET efficiencies through modeling and rational design, and we were able to use the rogRFP2 sensor to perform dual compartment live-cell imaging in HEK293 cells. For the development of the 2<sup>nd</sup> generation redox sensors, we altered the linker length in an attempt to reduce the distance between the two FPs and improve FRET efficiencies. Further improvement of the sensor can be made using linker variations to try and shift the orientation of FPs. The Grx1 and Orp1 conjugated rogRFP2s are of particular interest for further studies of redox regulation in cellular and animal models. These constructs will be cloned into mammalian expression vectors and used for dual color imaging of glutathione or peroxide specific redox dynamics.

## **CHAPTER 4. NEURON ACTIVITY-DEPENDENT REDOX COMPARTMENTATION REVEALED WITH A SECOND GENERATION RED-SHIFTED RATIOMETRIC SENSOR**

### 4.1 Abstract

Oxidative stress is a common pathology that occurs in aging-related neurological disorders as well as brain injuries. For example, neuronal glutamate stimulation causes changes in intracellular reactive oxygen species (ROS) levels that occur downstream from mitochondrial calcium overload, and excitotoxic stimulation results in a redox cascade leading to oxidative stress. However, the precise details of how neuronal activity elicits redox changes in different cellular compartments have remained difficult to resolve. Current redox sensitive dyes and fluorescent proteins enable the quantification of spatially distinct changes in ROS levels, but multicolor probes are needed for the accurate analysis of single-cell and compartment-specific redox dynamics that can be masked by population averaging. Using the rogRFP2 sensor, activity-dependent redox changes were measured simultaneously in the cytosol and mitochondria of individual cultured neurons. An anticorrelation was observed in which glutamate stimulation caused oxidation in mitochondria accompanied by a concurrent reduction in the cytosol. This activity dependent redox compartmentation was confirmed to be a true redox behavior with an antioxidant rescue. In addition, this behavior was dependent on the activity of Complex I of the mitochondrial electron transport chain and could be modulated by the presence of co-cultured astrocytes. Furthermore, we also demonstrated that the red fluorescent rogRFP2 facilitates ratiometric redox imaging in drosophila retinas. Overall, the proof-of-concept studies reported here demonstrate that this new rogRFP2 redox sensor can be a powerful tool for understanding redox biology both in vitro and in vivo across model organisms.

### 4.2 Introduction

ROS are generated as metabolic by-products of cellular respiration but can also be generated by other exogenous sources such as radiation exposure or exposure to environmental toxins (Richardson, Quan, Sherer, Greenamyre, & Miller, 2005; Spitz, Azzam, Li, & Gius, 2004). ROS have important cellular functions in signaling, metabolism, regulating cell fate or morphology

(Halliwell & Gutteridge, 2015; Martindale & Holbrook, 2002). The impact of ROS in these roles can vary with cell type, differentiation state, environment, as well as the endogenous levels of antioxidants and reactive species (Jones et al., 2004). ROS usually exert their effects by modification of lipids and proteins, but ROS overload can cause DNA damage and modification, irreversible protein oxidation and lipid damage all of which can perpetuate cellular dysfunction and death (Go & Jones, 2008b). Oxidative stress, as discussed earlier, results from a disruption in cellular redox homeostasis, where there is excessive production of ROS or impairment of the cellular antioxidant machinery. ROS are generated during normal physiology and growth and also during activities such as exercise, and this type of oxidative stress can be beneficial as they lead to improvements in metabolism and induce cytoprotective pathways (Higdon, Diers, Oh, Landar, & Darley-USmar, 2012). Excessive oxidative stress, however, can irreparably damage macromolecules, eventually leading to cell death (Davies, 2016).

Oxidative stress is intrinsic to several aging related disorders like neurodegenerative disorders as well as cardiovascular disease and cancer (Heitzer et al., 2001; Panieri & Santoro, 2016). Oxidative stress also has several destructive downstream effects like cellular damage, oxidative DNA damage, and mitochondrial dysfunction. The brain, with its high metabolic demand and abundance of mitochondria is especially vulnerable to redox imbalance and oxidative stress (Attwell & Laughlin, 2001; Magistretti & Allaman, 2015). Neuronal membranes are lipid rich, and this, combined with their high oxygen consumption and relatively weaker antioxidant defenses due to reduced catalase activity and lower glutathione levels makes them susceptible to oxidative damage (Bell et al., 2015; Fernandez-Fernandez, Almeida, & Bolaños, 2012). Neuronal response and adaptation to oxidative stress is varied throughout the brain. Specific populations of neurons are selectively more vulnerable to oxidative stress, and because of this, age-related decline begins with these neurons in disorders such as Parkinson's disease and Alzheimer's disease (Xinkun Wang & Michaelis, 2010). Even though increased ROS levels might not directly trigger neurodegeneration, they are ancillary to other critical disturbances like mitochondrial dysfunction and glutamate excitotoxicity that propagate neuronal damage (Coyle & Puttfarcken, 1993).

Evidence of oxidative damage induced by excessive glutamate is also observed in epilepsy and ischemic stroke, and oxidative stress induced neuronal death has been rescued with the use of

antioxidants (Rama & Garcia Rodriguez, 2012; Rothstein et al., 1996). Extracellular levels of glutamate are regulated and maintained at low levels to avoid the excitotoxic effects of glutamate. In co-cultures of neurons and astrocytes, astrocytes express a neuroprotective effect (Bhatia et al., 2019; Shih et al., 2003). Some of the key functions of astrocytes include buffering extracellular glutamate levels, ROS elimination, and supplementation of neuronal cells (Bolaños, 2016; Rothman et al., 1999). In the brain, astrocytes are responsible for a majority of glutamate reuptake, and they sequester extracellular glutamate to keep the concentrations below 10 $\mu$ M.

Mitochondria play key and sometimes contradictory roles, helping to regulate metabolic burden by with the detoxification of neurotransmitters (Frigerio, Casimir, Carobbio, & Maechler, 2008) and utilization of metabolic substrates while also acting as a major source of ROS via the electron transport chain (Balaban, Nemoto, & Finkel, 2005). Therefore, much remains to be understood about redox relationships between neuronal activity and mitochondria. Some of the initial theories identified that chronic activation of the NMDA receptor caused and the influx of calcium resulting in mitochondrial accumulation of calcium, which generated ROS, thereby causing mitochondrial and cellular damage (Dugan et al., 1995; Reynolds & Hastings, 1995). It was later revealed in a study using cultured cerebellar granule neurons that an increase in superoxide was caused due to delayed calcium deregulation, antioxidant machinery failure, mitochondrial membrane collapse, and a rise in cytoplasmic calcium (Vesce, Jekabsons, Johnson-Cadwell, & Nicholls, 2005). This suggested that excitotoxicity when combined with bioenergetic crisis in the mitochondria, results in oxidative stress that leads to consequent neuronal damage (Nicholls, Johnson-Cadwell, Vesce, Jekabsons, & Yadava, 2007). In several aging related disorders, mitochondrial dysfunction is associated with other pathologies attributable to deficiencies in respiratory chain complexes. Among these, complex I is heavily implicated in PD and complex I inhibitors are used to recapitulate several pathological traits of the disease (J. W. Langston, 2017; Richardson et al., 2005; Schapira et al., 1990).

Our lab's long-term goal is to understand the roles of oxidative stress in PD pathogenesis, and this project moved us closer to this goal by establishing the use of our new rogRFP2 probe in excitable cells. We have been able to use our red-shifted redox sensor to uncover novel activity dependent redox phenomena in neuronal cultures and demonstrated the use of these sensors to look at the

effect of mitochondrial complex I disruption and neuroprotection offered by astrocytes on this redox phenomenon. Furthermore, this project established new collaborations that demonstrated the use of the roGFP2 probe for two-photon microscopy of rat brain slices and fly retinas.

### **4.3 Materials and Methods**

#### **4.3.1 Materials**

Chemicals and cell culture media and supplements were purchased from Sigma, Formedium, and ThermoFisher Scientific. Molecular biology enzymes were purchased from New England Biolabs (NEB).

#### **4.3.2 Molecular Biology**

The roGFP2 and aOGG4g sequences were cloned into GW1 mammalian expression vector. They were cloned into GW1 vectors with COX8 repeat (4x) mitochondrial signal sequence for mitochondrial targeting and GW1 vector without a signal sequence for the cytosolic expression of the roGFP2 (Tantama, Hung, & Yellen, 2011). Subsequently, they were cloned into FUGW vector for lentivirus production.

#### **4.3.3 Lentivirus production**

Lentivirus were produced and harvested from HEK293FT cells. HEK293FT cells were cultured in Dulbecco's modified Eagle's medium (DMEM) containing 4.5 g/L glucose, 3.7g/L sodium bicarbonate, 4 mM glutamine, 0.1 mM Non-essential Amino Acids (NEAA), 500 µg/mL Geneticin™ and supplemented with 10% cosmic calf serum. Cells were maintained in an incubator in a humidified incubator at 37°C with 5% CO<sub>2</sub>. Lentivirus was produced by delivering the transfer plasmids FUGW-roGFP2 and FUGW-mitoroGFP2 along with envelope and packaging plasmids, pCMV-VSV-G, pMDLg\_pRRE, pRSV-Rev into HEK293FT cells using calcium phosphate transfection method. Two days post transfection, the virus lysates were harvested in neuronal growth media and frozen.

#### **4.3.4 Cell Culture and Transfections**

Primary hippocampal neurons were isolated from P1 FVB mice and plated on nitric acid washed 18mm #1.5 glass coverslips or glass bottomed 35mm dishes (Cellvis) that were coated with 50 µg/ml poly-D-lysine (PDL). Neuronal cultures were maintained in Neurobasal-A medium supplemented with B-27, 5mM glucose, 0.25 mM Pyruvate, 0.5 mM GlutaMax, 1X Pen-Strep at 37°C and 5% CO<sub>2</sub> in a humidified incubator 30% feedings every 1-2 days. The cultured neurons were transfected with Calcium Phosphate on DIV 4-5 and imaged on DIV 6-8. Astrocytes were isolated from cortices of P1-P2 FVB mice and maintained in DMEM/F12 supplemented with 10% FBS until passage onto PDL coated coverslips. For neuron-astrocyte co-cultures, astrocytes were grown for 2-7 days on coverslips, and then neurons were plated on top of the feeder layer. All animal procedures were approved by and performed in accordance with guidelines by the Purdue Animal Care and Use Committee.

#### **4.3.5 Live-Cell Imaging**

Neurons were equilibrated for 1 hour prior to imaging in imaging solution consisting of 15mM HEPES, 120mM NaCl, 3mM KCl, 3mM NaHCO<sub>3</sub>, 1.25mM NaH<sub>2</sub>PO<sub>4</sub>, 5mM Glucose, 2mM CaCl<sub>2</sub>, 1mM MgCl<sub>2</sub>, 0.25mM Pyruvate, 0.5mM Glutamax, pH7.3 at 37°C and 5% CO<sub>2</sub> in a humidified incubator. For widefield microscopy, neurons were imaged at room temperature in 1-minute time intervals and treatments were added to a static bath with imaging solution. The neurons were imaged over 120mins with a 10uM glutamate addition at 20mins, 1mM Diamide at 40mins and 5mM DTT treatment at 85mins. DIC images were taken at the beginning and after the imaging paradigm to monitor neuron health. For the drug treatments, the neurons were pre-incubated as following- 100nM Rotenone for 1hr, 1mM N-Acetylcysteine for 24hrs, 500mM N-Acetylcysteine for 5 hrs and 5µM MitoTEMPO for 1 hr, prior to imaging. For imaging pH changes, neurons were incubated for 20mins with pH sensitive dye 0.5uM BCECF-AM62 and washed with media and imaging solution. The neurons were then imaged at baseline for 15mins, followed by a 10uM glutamate treatment for 20mins. Subsequently, a pH calibration was performed with buffers ranging from pH 6.5-7.8 in a high-potassium solution (15mM HEPES, 10mM glucose, 123mM KCl, 20mM NaCl, 2mM CaCl<sub>2</sub>, 1mM MgCl<sub>2</sub>) in the presence of 5 µM nigericin.

They were imaged on an Olympus IX83 fluorescence microscope with a Plan Apo VC 20X objective (0.75 NA), equipped with a Prior motorized stage and an Andor Zyla 4.2 sCMOS camera (6.5  $\mu\text{m}$  pixel). The images were taken with a 2x2 pixel binning and exposure times ranging from 50-400 milliseconds. The LED light source was a Lumencor SpectraX light engine and the following filter pairs (Semrock or Chroma) were used: ex. 475/34nm, em. 525/50nm; ex. 395/25nm, em. 525/50nm, ex. 475/34nm, em. 632/60nm, ex. 395/25nm, em. 632/60nm, ex. 575/25nm, em. 632/60nm. Confocal microscopy was performed on a confocal laser scanning microscope (Nikon A1R-MP, Purdue Life Sciences Imaging Facility) with a Plan Apo VC 60X oil DIC N2 objective (1.4 NA, pinhole 26.82  $\mu\text{m}$ ). Laser excitation at 488 nm or 561 nm was used with a 405nm/488nm/561nm/640nm multiband dichroic mirror and 525/50nm or 595/50nm emission filters. 512-by-512 pixel images were acquired using a Galvano scanner at 30 frames per second and collected on an A1-DU4 four detector unit with four photomultiplier tubes at a 0.41  $\mu\text{m}$ , 0.41  $\mu\text{m}$ , and 0.5  $\mu\text{m}$  (x,y,z) pixel size dimensions.

#### **4.3.6 Data Analysis**

Image stacks were analyzed with ImageJ as previously described. The fluorescent images were background subtracted above the mean background signal and then a threshold was set to three standard deviations over mean to eliminate background pixels. Ratio images were generated by dividing the 400 Ex image by the 490 Ex image for both the red and green emissions and the ratio signals were measured around the cell body and neurites. The fraction of oxidized sensor was calculated according to the equation  $Y_{\text{oxidized}} = (\text{Ratio} - \text{Ratio}_{\text{reduced}}) / [(F_{475,\text{oxidized}} / F_{395,\text{oxidized}}) \cdot (\text{Ratio}_{\text{oxidized}} - \text{Ratio}) + (\text{Ratio} - \text{Ratio}_{\text{reduced}})]$  as described in previous works. The change in oxidation over baseline was determined by comparing fold change of min/max change % oxidized after glutamate addition (T21-T39) over average % oxidized (T15-T19) before glutamate stimulation.

## **4.4 Results and Discussion**

### **4.4.1 Dual Compartment Redox Imaging in Hippocampal Neurons**

We first confirmed that the sensors could be used for dual compartment imaging in neurons to study the redox changes in the mitochondria and cytosol simultaneously. We transfected the

neurons with roGFP2 that expressed in the cytosol and mito-roGFP2 that expressed in the mitochondria. To confirm subcellular targeting and spatial localization of these sensors, we took confocal images at 60X using an oil objective. Confocal imaging of the neurons revealed robust targeting to of the roGFP2 sensor to the mitochondria and the emission signals were spatially localized to separate compartments (Figure 4.1).

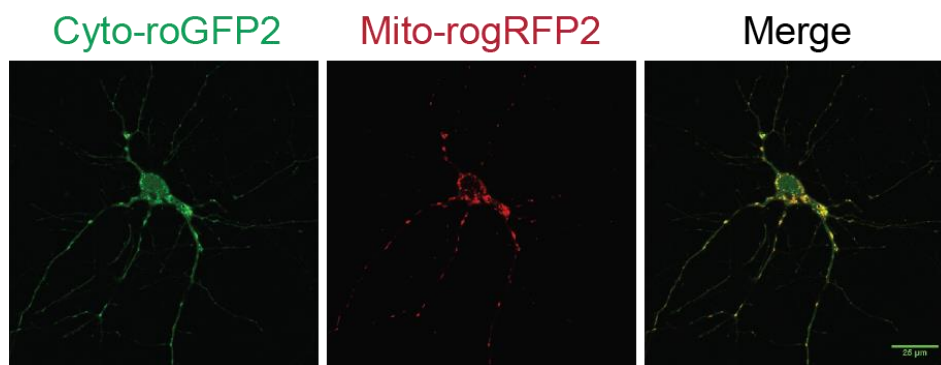


Figure 4.1. Compartment specific expression of redox sensors

Mitochondrial targeting of roGFP2 (red) is efficient when co-expressed with cytosolic roGFP2 (green) in primary mouse hippocampal neurons. Scale bar = 25  $\mu\text{m}$ .

#### 4.4.2 Assay Optimization

Extracellular levels of glutamate in the brain are regulated and maintained at low levels to avoid excitotoxic effects of glutamate (de Bundel et al., 2011; Herman & Jahr, 2007). In primary neuron cultures from rodent models, acute treatment with of excitotoxic levels of glutamate (100  $\mu\text{M}$ ) with glycine (10  $\mu\text{M}$ ) causes changes in ROS levels in different localized subcellular regions of neurons (Reynolds & Hastings, 1995). However, it is unclear if there are differences in redox responses between compartments of an individual cell, and to what extent acute redox changes occur, if at all, in response to with less extreme, sublethal glutamate stimulation that approaches more physiological ranges. We therefore used cultured primary mouse hippocampal neurons co-transfected with cytosolic roGFP2 (cyto-roGFP2) and mitochondrially-targeted roGFP2 (mito-roGFP2) to resolve these questions more clearly.

For our preliminary studies, the activity of the neurons was stimulated with varying concentrations of glutamate (5-25  $\mu\text{M}$ ) or potassium chloride (30-60 mM) (Edwards, Das, Molnar, & Hickman,

2010; Kushnareva, Wiley, Ward, Andreyev, & Murphy, 2005). Interestingly, glutamate stimulation caused opposing redox responses in the cytosol and mitochondria with varying degrees of change dependent on the concentration of glutamate (Figure 4.2. B,C). The neurons treated with 40mM KCl, however, only showed a reductive change in the cytosol and not the mitochondria (Figure 4.2.A).

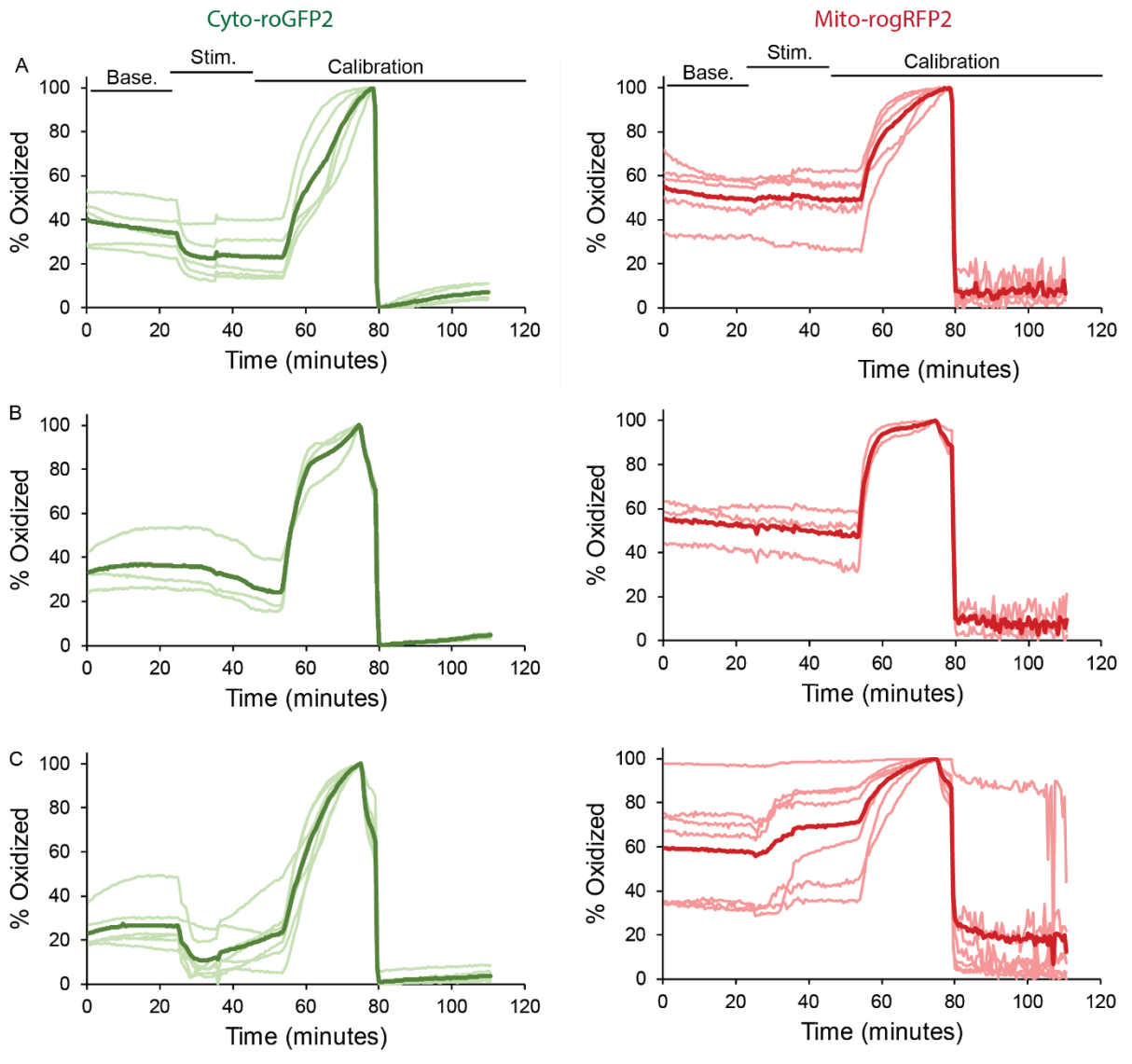


Figure 4.2. Stimulating neuronal activity using KCl and Glutamate

Neurons are stimulated from T20-T40 (A) 40mM KCl stimulation (n=5neurons), (B) 5µM glutamate stimulation (n=3 neurons) (C) 25µM glutamate stimulation (n=7 neurons)

Note that these experiments were conducted in static bath solutions with subsequent additions of different treatments, so the glutamate and KCl were in a solution for the entire duration of the experiment. At this level of stimulation, neurons maintained healthy morphology throughout the experiment, which included a sensor calibration phase. Neurons were imaged in an artificial cerebrospinal fluid imaging solution at room temperature, and after a baseline period glutamate was added to the bath (Tantama et al., 2013). Following glutamate stimulation, the sensors were calibrated by 0.5mM H<sub>2</sub>O<sub>2</sub> addition to fully oxidize the sensors followed by dithiothreitol (DTT) addition to fully reduce the sensors. However, we suspected that the H<sub>2</sub>O<sub>2</sub> addition was not able to fully oxidize the sensor in neurons, so we sought to optimize the calibration with a different oxidizing agent. To this end, we used Aldrithiol<sup>TM</sup>-2 (2,2'-Dipyridyl disulfide), diamide and a higher concentration of H<sub>2</sub>O<sub>2</sub>, all of which have been successfully used for the calibration of redox sensors in cultured cells and tissue.

The neurons were plated onto a 24 well glass bottom plate for easier imaging of multiple conditions simultaneously. They were imaged at 4min intervals, where the baseline was monitored for 28mins, followed by addition of 25μM glutamate for 20mins. The cells were then treated with either 100μM Aldrithiol (Figure 4.3.A), 1mM Diamide (Figure 4.3.B), 2mM H<sub>2</sub>O<sub>2</sub> (Figure 4.3.C) or 0.5 mM H<sub>2</sub>O<sub>2</sub> (Figure 4.3. D) followed by a treatment with 5mM DTT, which caused a complete reduction. Though both the Aldrithiol and diamide were able to oxidize the sensors, we experienced solubility issues with the Aldrithiol and decided to use diamide for all future experiments. All subsequent experiments were carried out using 10 μM glutamate stimulation as this resulted in the most consistent phenotype without causing significant neuronal damage

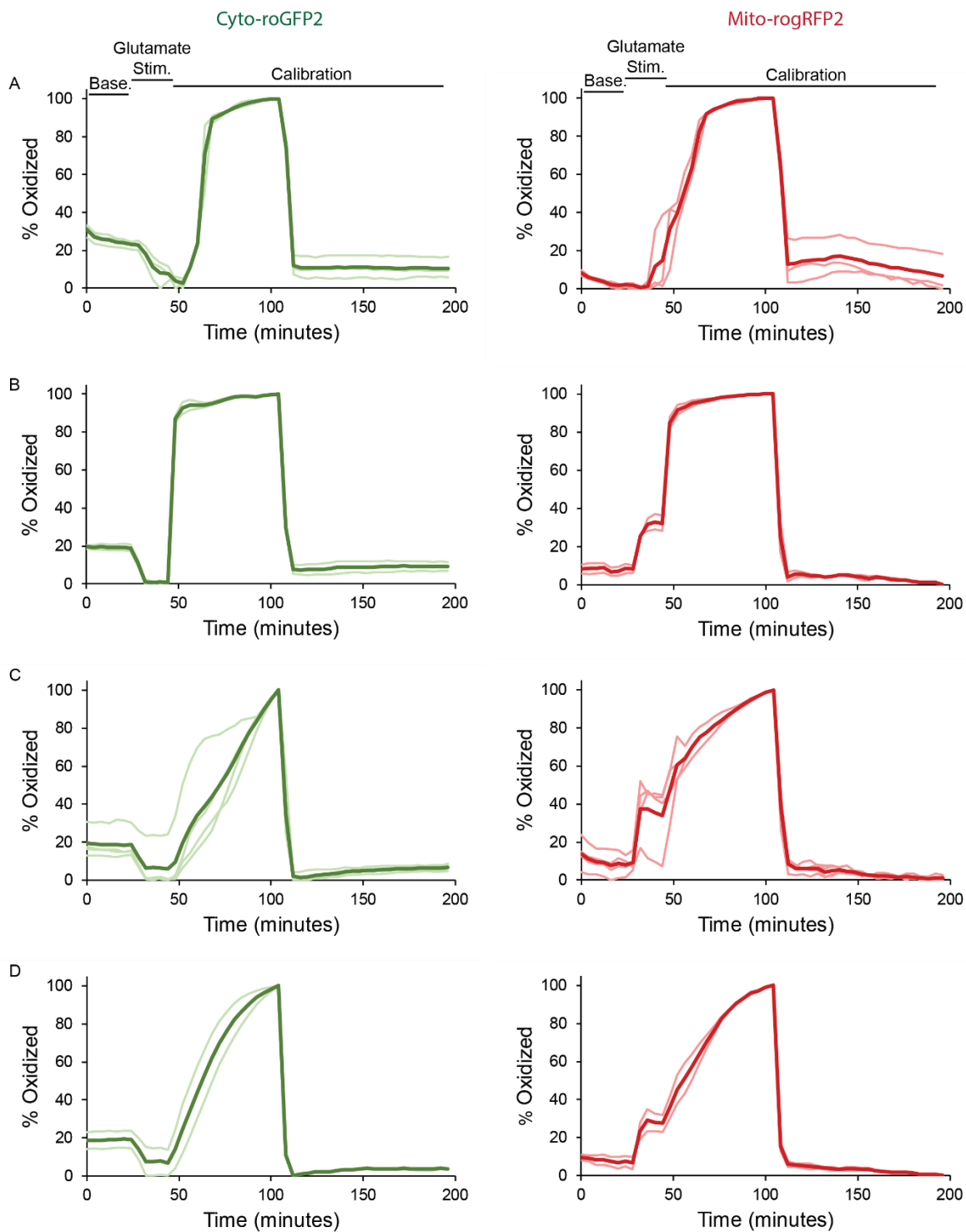


Figure 4.3. Optimization of oxidizing agent for calibration

(A) Neurons were treated with 100µM Aldrithiol in the calibration phase starting at T40, (B) 1mM Diamide was used in the calibration phase, (C) 0.5mM H<sub>2</sub>O<sub>2</sub> was used in the calibration phase, (D) 2mM H<sub>2</sub>O<sub>2</sub> was used in the calibration phase followed by 5mM DTT in (A), (B), (C) & (D)

### 4.4.3 Neuron Activity-Dependent Redox Dynamics

Interestingly, 10 $\mu$ M glutamate stimulation caused opposite redox responses in the cytosol and mitochondria as reported by the targeted sensors (Figure 4.4). Using the calibration on a cell-by-cell basis, ratio signals could be converted to the percent oxidation level of cyto-roGFP2 and mito-roGFP2 (Meyer & Dick, 2010a). At the population level, glutamate stimulation consistently caused an oxidation of the mitochondria (accompanied by a concurrent reduction of the cytosol).

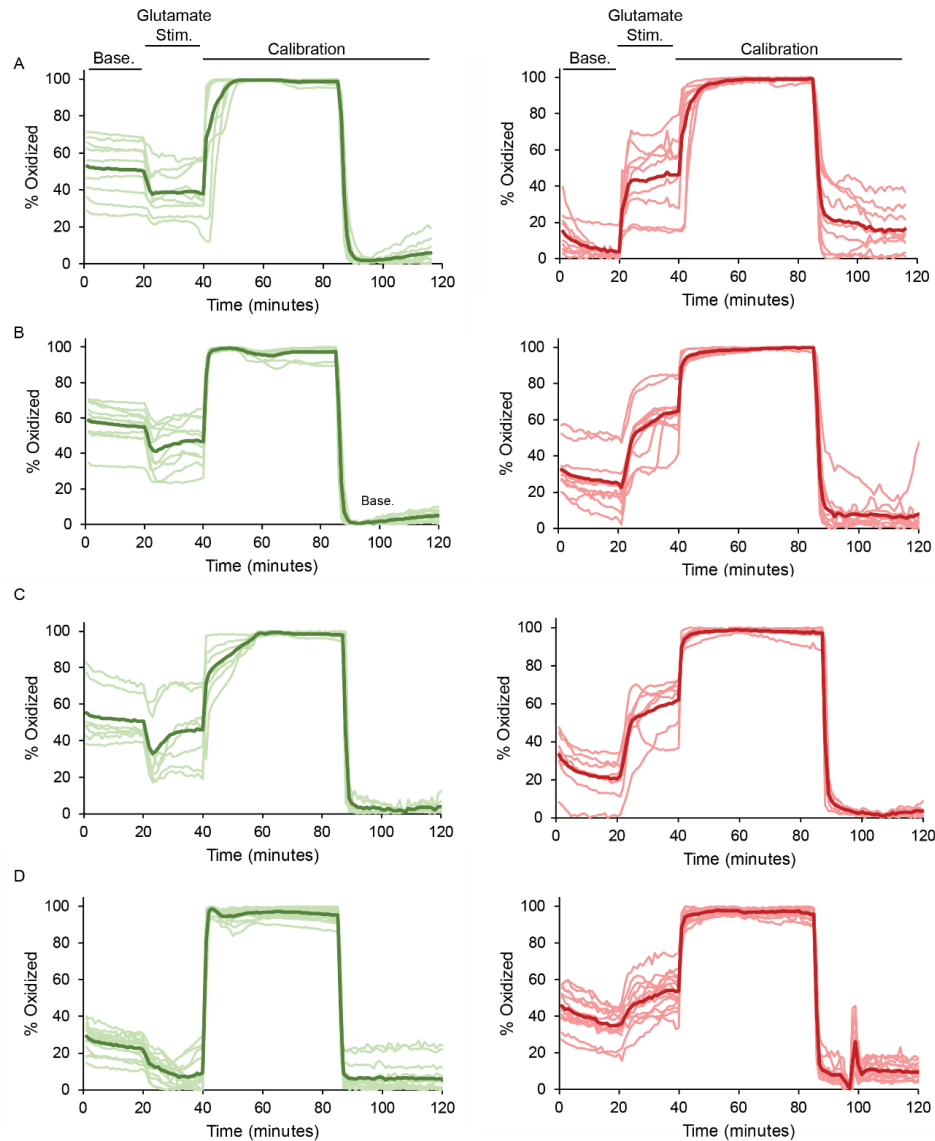


Figure 4.4. Neuron activity-dependent redox compartmentation

Experiments demonstrating changes in mitochondrial and cytosolic redox upon glutamate treatment from T20-T40, n=4 replicates with a total of 41 neurons

#### 4.4.4 pH dependence

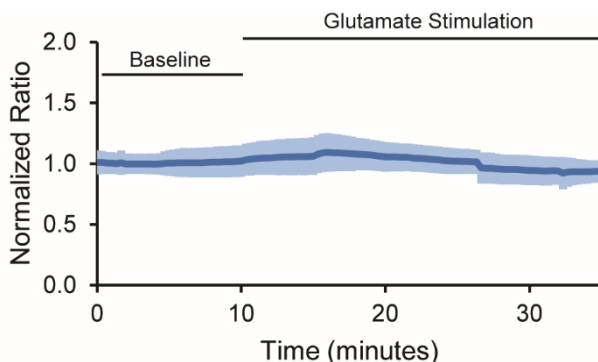


Figure 4.5. Measurement of pH changes using BCECF-AM

rogRFP2 activity-dependent response is not caused by pH changes. Glutamate does not stimulate a pH response.

We sought to confirm that the response to glutamate stimulation was a true redox response to the glutamate stimulation and not caused by pH changes. The neurons were loaded with pH-sensitive dye 0.5 $\mu$ M BCECF-AM and imaged to check for pH responses to glutamate stimulation. Post stimulation, the sensor was calibrated at pH 6.5-7.8 with a nigericin clamp (not shown above). The sensor response was not pH-dependent (Figure 4.5).

#### 4.4.5 Antioxidant rescue

We also validated that the sensor responses were specific to the cellular redox state. N-Acetyl cysteine (NAC) is a glutathione precursor and generally used as an antioxidant (Alboni et al., 2013; Wagener et al., 2016). We pretreated the neurons with 1mM NAC for 24hrs, and this attenuated the glutamate induced redox response in both the mitochondria and the cytosol. Additionally, we also tried a combination of 0.5mM NAC, and 5 $\mu$ M MitoTEMPO which is a mitochondria-targeted superoxide dismutase mimetic and this combination significantly attenuated the redox response in both the mitochondria and cytosol (Hou et al., 2012; Hung et al., 2018; Kolossov et al., 2015; H. Zhang et al., 2012).

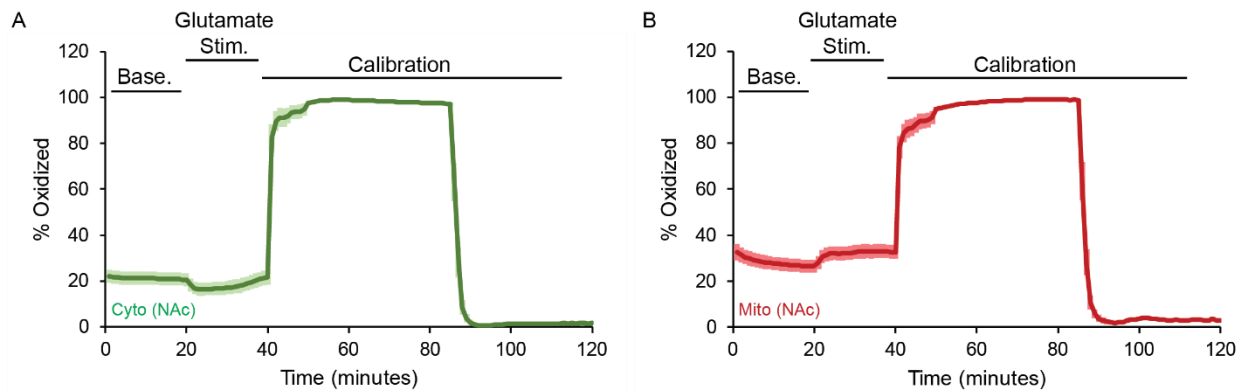


Figure 4.6. NAc antioxidant treatment

Neurons were treated with 1mM NAc for 24hrs and prior to imaging. (A) Cytosolic response of roGFP2 upon glutamate stimulation (B) Mitochondrial roGFP2 response upon stimulation.

Glutamate stimulation caused significant  $25\% \pm 4.6$  (Mean + 95% CI) increase in mito-roGFP2 oxidation relative to the baseline (n=4 experiments, 41 neurons;  $p=6 \times 10^{-12}$ , paired t-test) (Figure 4.7.D). In contrast, there was a significant  $-11\% \pm 1.8$  (Mean + 95% CI) reduction of cyto-roGFP2 relative to its baseline (n= 4 experiments, 41 neurons;  $p=8 \times 10^{-3}$ , paired t-test) (Figure 4.7.A).

When neurons were treated with a cocktail of antioxidants containing N-acetylcysteine and Mito-TEMPO, glutamate stimulation caused a much smaller  $3.9\% \pm 1.5$  (Mean + 95% CI) oxidation of mito-roGFP2 relative to baseline (n=3 experiments, 65 neurons;  $p= 0.05$ , paired t-test) (Figure 4.7.E), and the  $-1.8\% \pm 1.2$  (Mean + 95% CI) change in cyto-roGFP2 was not significant (n=3 experiments, 65 neurons;  $p= 0.4$ , paired t-test) (Figure 4.7.B).

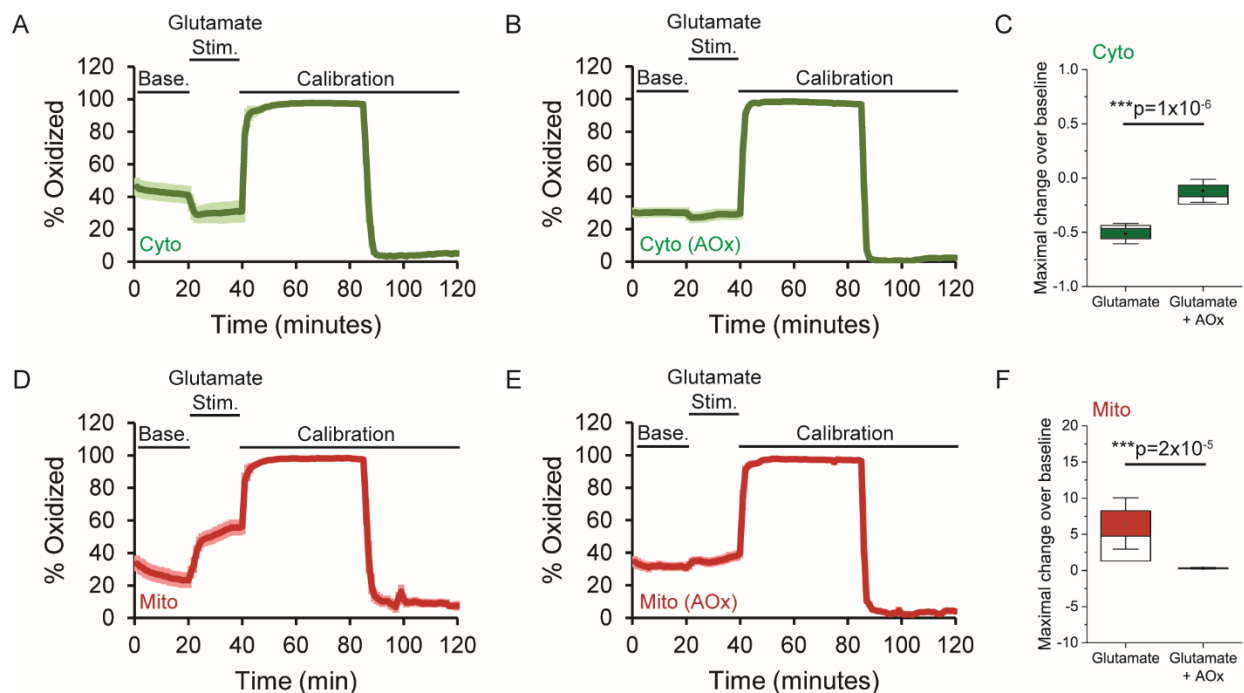


Figure 4.7. Neuron activity-dependent redox compartmentation and antioxidant rescue.

Cultured mouse primary hippocampal neurons were stimulated with 10  $\mu$ M glutamate followed by treatments with diamide and DTT to calibrate the (A-C) green fluorescent cytosolic roGFP2 and (D-F) red fluorescent mitochondrial roGRFP2. Glutamate stimulation caused (A) cytosolic reduction concurrent with (C) mitochondrial oxidation (mean  $\pm$  95% C.I.). Antioxidant treatment (“AOx”) with N-acetylcysteine and Mito-TEMPO blocked the (B, C) cytosolic and (E, F) mitochondrial redox responses.

#### 4.4.6 Single-Cell Analysis of Redox Compartmentation

Our population-level analysis revealed a novel phenomenon in which neuronal activity induces mitochondrial oxidation and cytosolic reduction on average. However, population averaging masks the heterogeneity of individual cell behaviors that may be physiologically important. For example, the mean population responses measured in Figure 4.4 cannot distinguish whether mitochondrial oxidation and cytosolic reduction occur within individual neurons or between different populations of neurons.

To better understand the origins of the population behavior, we further scrutinized single-cell responses and found that the anticorrelated cytosolic and mitochondrial redox responses observed at the population level are a reflection of anticorrelated responses within the individual neurons.

For example, Figure 4.8 illustrates the single neuron responses from one of the four independent experiments summarized earlier (Figure 4.4.B). The exact time course trajectories of individual neurons were heterogeneous and in some cases were multiphasic in nature (Figure 4.8.C), but in general, the response of individual neurons showed recapitulated the trend seen in the population average (Figure 4.8.D, E).

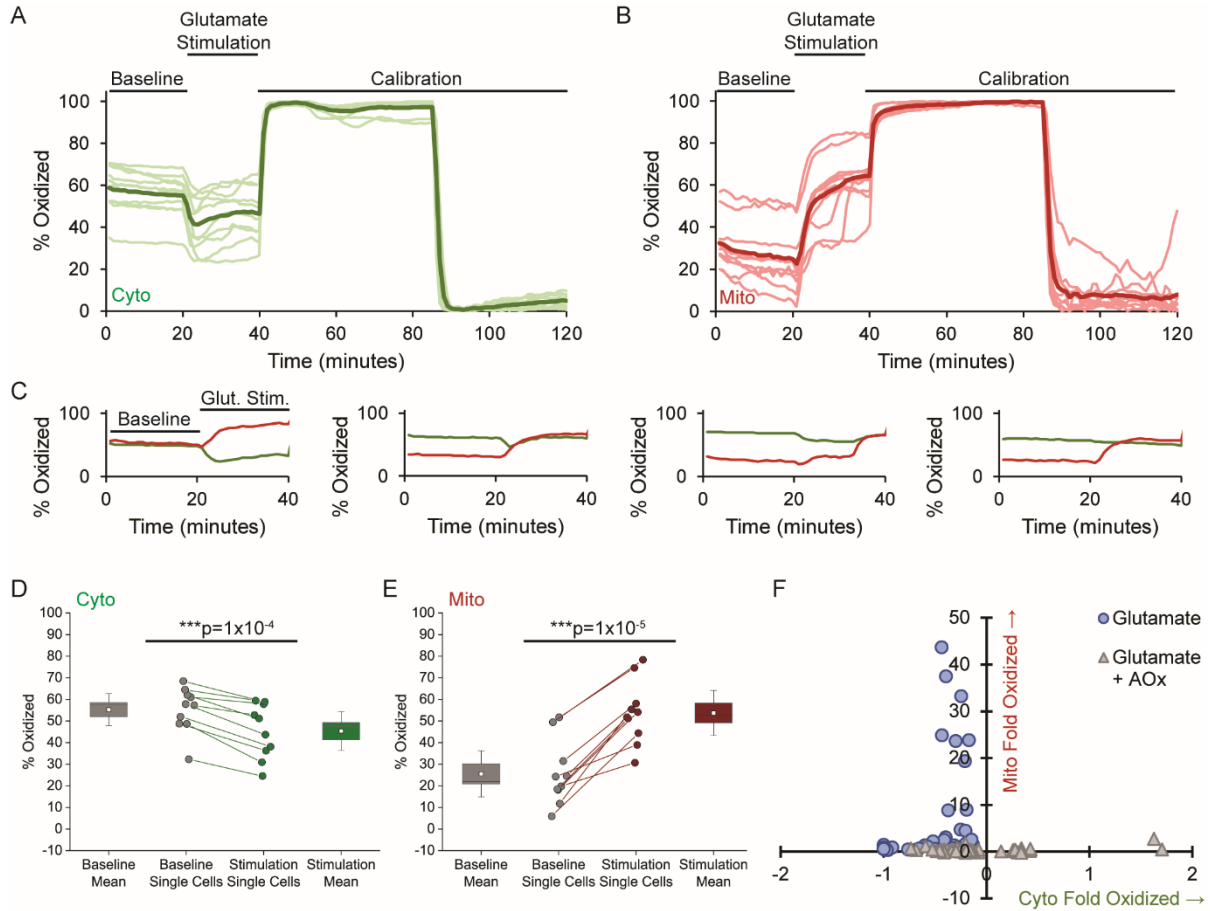


Figure 4.8. Single-cell analysis of activity-dependent redox compartmentation

Results are shown for a representative experiment. The population averaged redox responses (dark shaded lines) in the (A) cytosol (green) and (B) mitochondria (red) reflect the behavior of individual neurons (light shaded lines). (C) Individual neurons exhibit anticorrelated compartment-specific responses despite single-cell heterogeneity. Glutamate stimulation caused a significant (D) reduction in the cytosol paired with (E) oxidation in the mitochondria. (F) Maximal fold change in mito-roGFP2 oxidation versus cyto-roGFP2 oxidation for all neurons (positive, oxidation; negative, reduction).

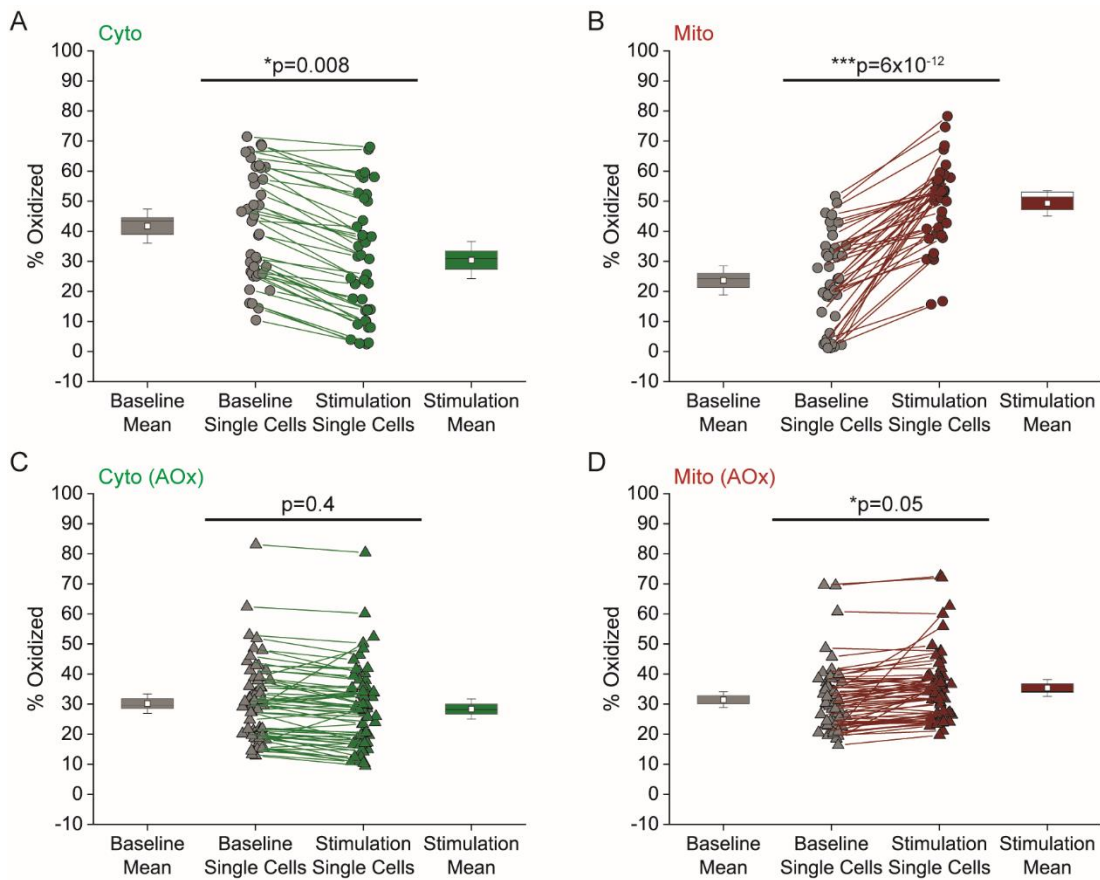


Figure 4.9. Antioxidants block the redox response in neurons

Single-cell analysis demonstrates that treatment with the antioxidants Mito-TEMPO and N-acetylcysteine (“AOx”) blocks glutamate stimulation of compartment-specific redox changes. Glutamate causes cytosolic reduction (A) that is attenuated in the presence of AOx (B). Glutamate causes mitochondrial oxidation (C) that is attenuated in the presence of AOx (D).

Glutamate stimulation caused significant  $28\% \pm 10$  (Mean + 95% CI) increase in mito-roGFP2 oxidation relative to the baseline ( $n=10$  neurons;  $p=1 \times 10^{-5}$ , paired t-test) for this representative experiment. In contrast, there was a significant  $-10\% \pm 4.8$  (Mean + 95% CI) reduction of cyto-roGFP2 relative to its baseline ( $n=10$  neurons;  $p=1 \times 10^{-4}$ , paired t-test) (Figure 4.8.D, E). We can visualize this trend with a two-dimensional plot in which the fold change in cyto-roGFP2 and mito-roGFP2 serve as coordinates for an individual neuron (Figure 4.8.F). With glutamate stimulation alone, all cells fall in the upper left quadrant, exhibiting mitochondrial oxidation paired with cytosolic reduction relative to baseline. Glutamate stimulation caused significant  $28\% \pm 10$  (Mean + 95% CI) increase in mito-roGFP2 oxidation relative to the baseline ( $n=10$  neurons from a single experiment;  $p=1 \times 10^{-5}$ , paired t-test). In contrast, there was a significant  $-10\% \pm 4.8$  (Mean

+ 95% CI) reduction of cyto-roGFP2 relative to its baseline (n=10 neurons from a single experiment;  $p=1 \times 10^{-4}$ , paired t-test) (Figure 4.8.D, E).

Thus, the new red fluorescent roGFP2 sensor has enabled us to observe previously unappreciated neuron activity-dependent redox compartmentation that arises as a stereotyped trend amongst the heterogeneity of single cell behavior. We next sought to demonstrate that this system provides a powerful assay platform to further dissect molecular and cellular aspects of redox homeostasis.

#### **4.4.7 Rotenone Treatment**

Rotenone is a selective inhibitor of complex I of the mitochondrial respiratory chain and it is also a pesticide that is used as a model for environmental toxins associated with Parkinson's disease (N. Li et al., 2003; Sherer et al., 2003; Testa, Sherer, & Greenamyre, 2005; Yadava & Nicholls, 2007). One of the main sources of cellular ROS is from the electron transport chain, and therefore we hypothesized that rotenone inhibition of Complex I would modulate the compartment-specific neuron activity-dependent redox responses we observed. In fact, rotenone treatment caused a drastic change in phenotype such that glutamate stimulation no longer caused a significant redox response in either the cytosol or mitochondria (Figure 4.10).

In neurons treated with 100 nM Rotenone (n=4 experiments, 51 neurons), glutamate stimulation caused a  $2.0\% \pm 1.9$  (Mean + 95% CI;  $p=0.44$ , paired t-test) increase in mito-roGFP2 oxidation relative to the baseline and a  $3.8\% \pm 1.4$  (Mean + 95% CI;  $p=0.25$ , paired t-test) reduction of cyto-roGFP2 relative to its baseline (Figure 4.10), but neither of these were statistically significant. However, the cytosolic response of rotenone-treated neurons exhibited a trend towards glutamate-stimulated oxidation (Figure 4.10.A), which contrasts with the reduction observed in untreated neurons. This trend is reflected in the mito-roGFP2 versus cyto-roGFP2 plot (Figure 4.10.E) in which the distribution single-cell responses of rotenone-treated neurons is shifted to the right compared to untreated neurons. Notably, the neurons in these imaging experiments maintained healthy morphology, and both the cyto-roGFP2 and mito-roGFP2 sensors responded appropriately to the calibration protocol.

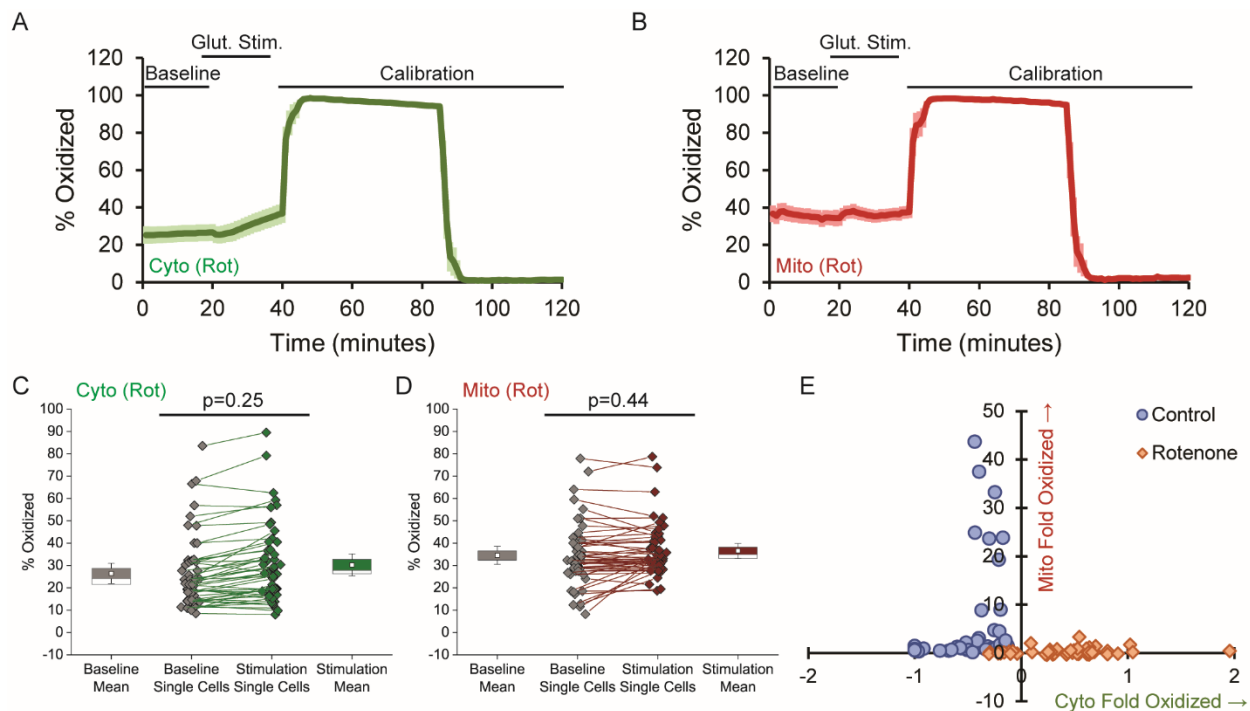


Figure 4.10. Rotenone attenuates activity-dependent redox responses in both compartments

Neurons treated with 100 nM rotenone did not exhibit significant (A, C) cytosolic or (B,D) mitochondrial redox responses (mean  $\pm$  95% C.I.) with glutamate stimulation; however, the cytosolic responses of individual neurons exhibited a trend towards oxidation (A,C,E).

The effect of rotenone suggests the activity of mitochondrial Complex I is crucial in shaping the activity-dependent redox response of neurons. Furthermore, the reversal of phenotype in the face of inhibition may suggest that the cytosolic response is dependent on the mitochondrial response. In the future, determining how these phenotypes evolve at different timescales will provide greater insight into the mechanisms underlying the intracellular redox coupling we have observed, and in this work we have established that the rogRFP2 sensor provides a tractable system for pharmacological studies in the future.

#### 4.4.8 Neuron-Astrocyte Co-Culture

Redox homeostasis in the brain involves both intracellular and intercellular mechanisms, and in particular astrocytes provide redox support to neurons in many ways. For example, astrocytes play a crucial role in buffering neuronal oxidative stress under excitotoxic conditions by sequestering excess glutamate, astrocytes activate antioxidant pathways in neurons, and astrocytes exhibit a

neuroprotective effect in the face of oxidative challenges (Bylicky, Mueller, & Day, 2018; Dringen, Pfeiffer, & Hamprecht, 1999; Kraft, 2004; Shih et al., 2003; Wilson, 1997). We therefore asked how the presence of astrocytes would affect the acute redox response of neurons in co-culture.

Interestingly, the presence of astrocytes significantly attenuated the magnitude of mitochondrial oxidation upon glutamate stimulation compared to neuron monocultures, but the cytosol still experienced a reduction compared to baseline (Figure 4.11). In neurons cultured on an astrocyte feeder layer, glutamate stimulation caused a  $5.6\% \pm 6$  (Mean + 95% CI) increase in mito-roGFP2 oxidation relative to the baseline (n=3 experiments, 37 neurons; p=0.10, paired t-test) which was not statistically significant. In contrast, there was a significant  $-9.26\% \pm 1.4$  (Mean + 95% CI) reduction of cyto-roGFP2 relative to its baseline (n= 3 experiments, 37 neurons; p= $5 \times 10^{-5}$ , paired t-test) (Figure 4.11.C, D), which is comparable in magnitude to the cytosolic response of neurons in monoculture. Notably, these neurons exhibited similar morphology to neuron monocultures, and the cyto-roGFP2 and mito-roGFP2 sensors responded equivalently to calibration. These results are consistent with previous literature on antioxidant roles of glia, and our system reveals an important new facet to the subcellular nature of how astrocytes modulate neuronal redox biology in a way that is now experimentally accessible in future studies.

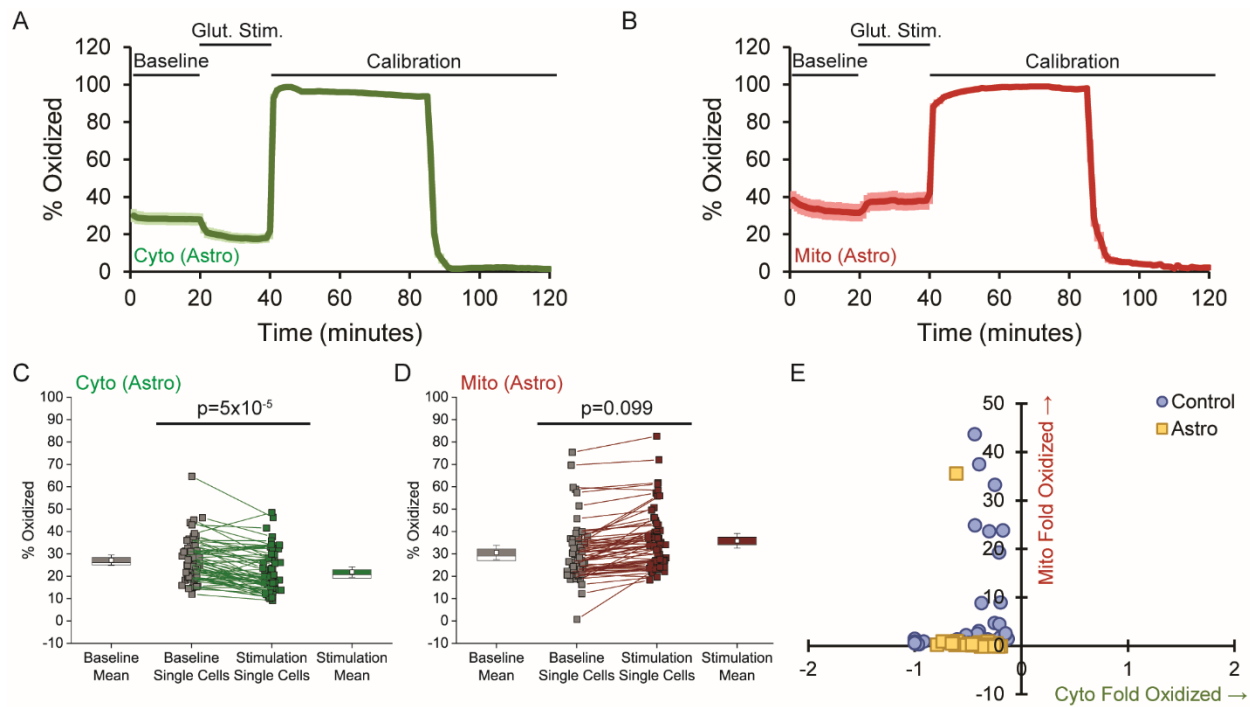


Figure 4.11. Astrocytes attenuate mitochondrial oxidative stress in neurons

The presence of co-cultured astrocytes does not affect the (A,C) cytosolic reduction observed after glutamate stimulation, but (B,D,E) mitochondrial oxidation was significantly attenuated.

Thus far, we have demonstrated that the roGFP2 redox sensor is an effective new tool for multiplexed ratiometric imaging using cultured primary neurons. Separately, we also wanted to demonstrate proofs-of-concept that the roGFP2 sensor could be used with thick samples from both vertebrate and invertebrate model organisms.

#### 4.4.9 Fly Retina Imaging

The green fluorescent roGFP-based sensors have been used successfully with two-photon microscopy for tissue and whole animal redox imaging (Albrecht, Barata, Großhans, Teleman, & Dick, 2011b). The roGFP based sensors have been used for in vivo imaging of fly larvae where they used a combination of Grx1 and Orp1 redox sensors to study the distribution of glutathione and hydrogen peroxide in specific subcellular compartments like mitochondria and cytosol (Albrecht et al., 2011b). We also sought to determine if the new roGFP2 sensor could be used for redox imaging in *Drosophila* in collaboration with the Weake lab. Although the roGFP-based

sensors have been used for in vivo imaging of fly larvae, they have limited use for imaging the eye because autofluorescence in the green emission band strongly interferes with sensor signals, particularly with 400 nm one-photon excitation (Figure 4.12). To test whether the red emission from rogRFP2 circumvents this problem, we generated transgenic flies expressing rogRFP2 in the cytosol of the photoreceptor cells, and one-photon confocal microscopy was used for ratiometric imaging of freshly dissected adult eyes.

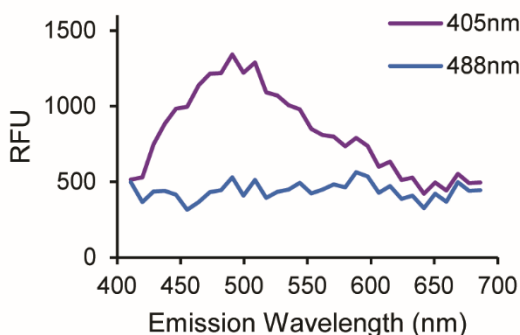


Figure 4.12. Fly retina autofluorescence interferes with green fluorescence imaging

Retinas from wildtype young ( $\leq 5$  days) male white-eyed  $w^{1118}$  flies were freshly dissected into PBS, and images were collected at various emission wavelengths using either 405 nm or 488 nm excitation. (Experiments performed by Dr. Hana Hall and Dr. Vikki Weake, Analysis by Saranya Radhakrishnan)

Red fluorescence from the rogRFP2 sensor was easily detectable, and as expected the ratio signal was much larger in magnitude for diamide exposure compared to full reduction with DTT ( $p=9 \times 10^{-4}$ ,  $n=6$ ) (Figure 4.13). Thus, the rogRFP2 sensor is a versatile tool that can be used in fly samples of various formats.

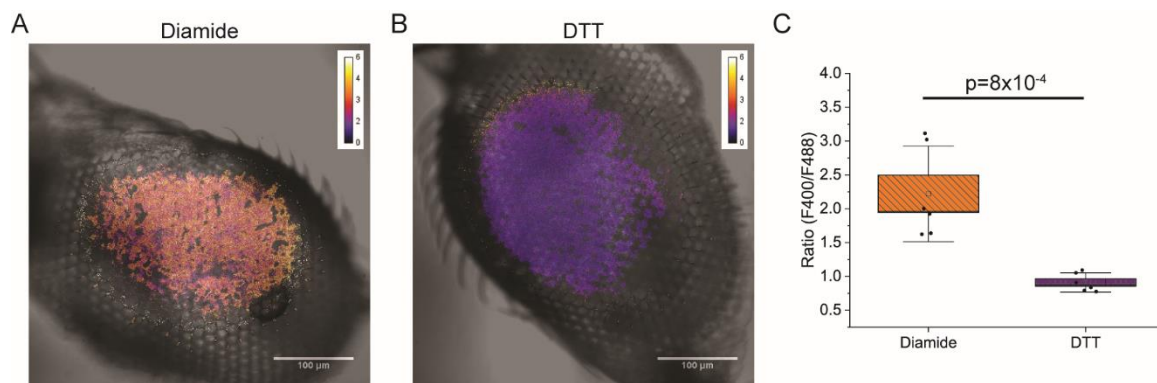


Figure 4.13. Ratiometric imaging in *Drosophila* retina

Eyes from adult transgenic flies expressing rogRFP2 in photoreceptor cells were dissected and imaged using one-photon confocal microscopy. Ratio images overlaid on DIC images show responses to (A) diamide and (B) DTT. (C) Eyes exposed to diamide are significantly more oxidized than those exposed to DTT. (Experiments performed by Dr. Hana Hall and Dr. Vikki Weake, Analysis by Saranya Radhakrishnan)

#### 4.5 Conclusion

Ratiometric live-cell imaging provides a powerful approach for quantitative redox biology, and we engineered the second-generation red fluorescent sensor rogRFP2 for this purpose. Here, we demonstrated that rogRFP2 can be used for ratiometric imaging of a variety of model species and sample formats, including cultured primary mouse neurons and *in vivo* imaging in adult drosophila eyes, making it a versatile tool.

To this end, the red fluorescent rogRFP2 sensor facilitated multiplexed ratio imaging of cultured primary mouse neurons and revealed unique activity-dependent redox responses that were compartmentalized between mitochondria and cytosol. We observed that glutamate stimulation caused a cytosolic reduction concurrent with mitochondrial oxidation at the single-cell level, which has not been previously observed to the best of our knowledge. Both rotenone treatment and co-culture with astrocytes modulated the redox response as expected, and inhibition by the mitochondrial toxin rotenone suggests that the cytosolic reduction is dependent on the mitochondrial oxidation. In particular, blockade by rotenone indicates the activity of mitochondrial Complex I is a major contributor to the activity-dependent redox compartmentation, which agrees with the plethora of evidence suggesting that the electron transport chain is a major source of ROS production, likely caused by calcium overload and increased mitochondrial respiration in the face

of increased neuronal activity. However, our observation of a cytosolic reduction indicates that ROS generated in mitochondria are not simply propagated to the cytosolic compartment even though glutamate excitotoxicity is broadly associated with neuronal oxidative stress and damage. The cytosolic reduction we observed for the first time here may contribute to a protective response, and our new sensor will enable us to study this level of subcellular redox homeostasis in greater mechanistic detail in the future.

## **CHAPTER 5. EXPLORING THE RELATIONSHIP BETWEEN LRRK2 AND OXIDATIVE STRESS IN PARKINSON'S DISEASE**

### **5.1 Abstract**

Oxidative damage has been implicated as a major cause of the neurodegeneration in both idiopathic and familial Parkinson's Disease (PD). Oxidative stress is usually caused when there is an imbalance between cell-buffering antioxidant mechanisms and the production of reactive free radicals, thereby causing an increase in the presence and activity of reactive oxygen species (ROS). Mutations in leucine-rich repeat kinase 2 gene (LRRK2) are among the most common genetic causes of PD, transmitted in an autosomal-dominant mode of inheritance and share pathological similarities to idiopathic PD. Recent research has shed light on its role in defective mitochondrial clearance, mitophagy defects and oxidative stress. We possess the capability of performing dual color ratiometric redox imaging and have observed redox compartmentation in neurons using this imaging system. Using these available toolsets for intracellular imaging of redox, our long-term goal is to visualize redox changes induced by LRRK2 and LRRK2 variants in different cellular compartments and if LRRK2 can affect this activity dependent redox compartmentation. Here, we aimed to test and establish an appropriate cellular model system for studying the LRRK2 mutants and to this end, we tested LRRK2 overexpression models in HEK293 cells, SH-SY5Y cells and hippocampal neurons. During testing, we also sought to optimize redox challenges that can induce LRRK2 dependent ROS increases in the cytosol or mitochondria. We observed LRRK2 dependent changes in redox responses in HEK293 cells and primary hippocampal neurons supporting the hypothesis that LRRK2 has cell autonomous, intrinsic effects on ROS.

### **5.2 Introduction**

Cellular and molecular mechanisms linked to oxidative stress have also been implicated in neurodegeneration and many aging-related disorders (Sohal & Orr, 2012). Parkinson's disease is a progressive neurodegenerative disorder characterized by the appearance of Lewy bodies and the selective loss of dopaminergic (DA) neurons in the substantia nigra. Oxidative damage and the resultant neurodegeneration have been observed in both idiopathic and genetic PD, specifically due to the increased susceptibility of DA neurons to oxidative stress. The high calcium burden

caused by the pacemaker-like firing of dopaminergic neurons of the substantia nigra has been associated with production of increase reactive oxygen species (ROS) (Guzman et al., 2010; D. James Surmeier, Guzman, Sanchez-Padilla, & Goldberg, 2010). The oxidative stress seen in PD, seems to be a cumulative effect of several aberrant processes in the neuron and exacerbated by genetic susceptibility to the disease. Deletion of DJ1 compromises mitochondrial oxidant defenses, increased oxidant stress, and compromised mitochondrial uncoupling in dopaminergic neurons in the substantia nigra (Guzman et al., 2010). Oligomeric  $\alpha$ -synuclein, the primary component of the lewy body pathology seen in PD also presents an oxidative stress component (Dryanovski et al., 2013; Leigh J. Hsu et al., 2000). Interestingly, studies show that mitochondrial dysfunction can induce  $\alpha$ -syn oligomerization via ROS increase-driven protein oxidation and that oligomeric  $\alpha$ -syn can cause mitochondrial deficits and oxidative stress (L J Hsu et al., 2000).

Mutations in leucine-rich repeat kinase 2 gene (LRRK2) are among the most prevalent genetic causes of PD, transmitted in an autosomal-dominant mode of inheritance and share pathological similarities to idiopathic PD (Zimprich et al., 2004). LRRK2 mutations account for 4% of familial PD and 1% sporadic PD in all populations and have a higher occurrence of up to 40% in certain populations (Klein & Westenberger, 2012b). Of these mutations, the G2019S mutation is the most prevalent and has high penetrance. The G2019S mutation is a gain of function mutation found in the kinase domain of the protein and is associated with oxidative stress and neurotoxicity (Lee et al., 2015; West et al., 2005). In postmortem PD patients and animal models with LRRK2-G2019S mutation, a high level of oxidative stress was observed in the striatum and substantia nigra (Angeles et al., 2011; Lee et al., 2015). One of the primary causes of oxidative burden in neurodegenerative disorders is mitochondrial dysfunction and defects in mitochondrial dynamics. The association of LRRK2 to mitochondrial dysfunction has recently gained traction with increasing reports of LRRK2 function in mitochondrial fragmentation and mitophagy, which could be an important contributing factor to oxidative stress in PD (Hsieh et al., 2016; Xinglong Wang et al., 2012a). In SH-SY5Y cells, the upregulation of kinase activity in the G2019S mutant caused mitochondrial uncoupling, leading to increased oxygen consumption and reduced membrane potential (Papkovskaia et al., 2012). Overexpression of LRRK2-WT in this cell type resulted in mitochondrial fragmentation, which was exacerbated in the LRRK2 G2019S and LRRK2 R1441C mutants (Xinglong Wang et al., 2012b). In HEK293T cells expressing wild type LRRK2 (LRRK2-

WT), Dynamin related protein 1 was observed to have increased association with mitochondria, which was further elevated in the LRRK2 G2019S mutant and was abolished in the cells expressing the kinase dead mutant (LRRK2-3XKD) (Niu et al., 2012). Additionally, LRRK2 (G2019S) overexpressing cells had increased ROS levels measured by the redox dye carboxy-H2DCFDA, whereas the LRRK2 3XKD mutant did not have increased ROS levels (Niu et al., 2012). Interestingly another study suggested that LRRK2-WT could have a neuroprotective role and has been shown to attenuate cell death induced by hydrogen peroxide treatment in both SH-SY5Y and HEK293 cells (Liou, Leak, Li, & Zigmond, 2008). The G2019S mutant has been shown to inhibit endogenous peroxidases by the increased phosphorylation of PRDX3, a peroxiredoxin that scavenges H<sub>2</sub>O<sub>2</sub> in the mitochondria (Angeles et al., 2011).

Despite evidence suggesting the physical association of LRRK2 to mitochondria membranes (Biskup et al., 2006), this association appears to be transient or context specific. In a study conducted in PD patient derived iPSC neurons, it was observed that LRRK2 G2019S mutation affects clearance of dysfunctional mitochondria by forming a complex with an outer mitochondrial membrane protein Miro and delaying the initiation of mitophagy. This protein facilitates mitochondrial transport by tethering the mitochondria to the microtubules and miro bound to LRRK2 enables the transport of damaged mitochondria, which are subsequently removed by mitophagy (Hsieh et al., 2016). It is vital to identify if the oxidative stress observed in PD was caused exclusively by the accumulation of damaged mitochondria caused by LRRK2 mutants or if the defects in mitophagy are also coupled with an increase in susceptibility to mitochondrial damage causing an overall increase of oxidative burden.

It is also unclear if LRRK2 mutants affect mitochondrial function, making it more vulnerable to environmental stressors like toxins or if the mutants impede the cell's ability to deal with mitochondrial damage or both (H. Liu et al., 2017). There is also much to be understood about how its relationship with ROS and how it alters vulnerability to redox changes. A study that looked at the interplay of genetics, prolonged environmental toxicity and aging in LRRK2 R1441G knock-in mice, found that cortical and mesencephalic neurons were more susceptible to low dose rotenone induced cell death than the wild type control mice (H. Liu et al., 2017). The toxin rotenone is known to inhibit mitochondrial complex I and produce increased mitochondrial ROS (N. Li et al.,

2003). In another study that looked into LRRK2 knockout and knock-in HEK293 cell lines, it was observed that rotenone induced ROS production caused activation of LRRK2 and phosphorylation of LRRK2 substrates (Burton et al., 2018). HEK293 cells were treated with 0-5 $\mu$ M H<sub>2</sub>O<sub>2</sub> to test if LRRK2 can be directly activated by ROS and this resulted in the phosphorylation of the LRRK2 substrate Rab10 (Steger et al., 2016). These results highlight the need to explore the molecular mechanism by which LRRK2 activity can be stimulated by ROS and how this relates to the other downstream effects of LRRK2 on oxidative stress.

Genetically encoded redox sensitive fluorescent probes enhance our capability to quantitate and measure dynamic changes in redox activity in living cells and these can also be targeted to various subcellular compartments. These tools can be harnessed to study the redox process under pathological conditions like oxidative stress in PD. In this chapter, we wanted to establish *in vitro* model systems amenable to sensor imaging approaches. After focusing on improving our toolset to enable simultaneous measurements in multiple cellular compartments and observing activity-dependent redox compartmentation in neurons, we wanted to use that experimental paradigm to see if mutations in LRRK2 can affect this redox phenomenon. But before answering this question, we also wanted to determine if LRRK2 has intrinsic, cell autonomous effects on redox compartmentation and if does, are we able to observe LRRK2 dependent redox changes in HEK293 and SH-SY5Y cells.

## 5.3 Results

### 5.3.1 LRRK2 mutants in HEK293 cells

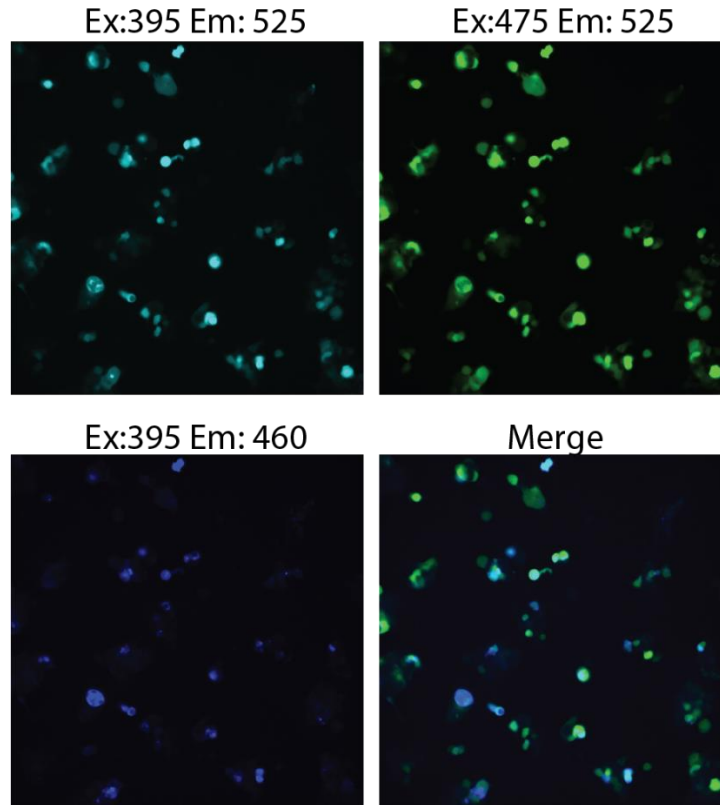


Figure 5.1. LRRK2 mutants and Grx1roGFP2 in HEK293 cells

We were interested in looking at the effects of these LRRK2 mutations on cellular ROS, specifically that originating from the mitochondria and the cytosol. We wanted to observe if the LRRK2 mutations had a cell autonomous effect, intrinsic effects independent of cell type on ROS in HEK293 cells. This cell line has been previously used to study LRRK2 mutations and their effect on mitochondrial dynamics and redox response. Additionally, the human embryonic kidney fibroblast cell line has been extensively used for mammalian cell culture experiments due to their ease of use and high transfection efficiency for transient transfections.

The LRRK2 mutants were cloned into a mammalian expression vector GW1, tagged with tag-BFP. GW1-LRRK2-tagBFP constructs were created for the Wild-type (WT) and Y1699C (mutation in

COR domain), R1441C (ROC/GTPase domain), 3XKD (Kinase-Dead), G2019S (Kinase domain) mutants. The LRRK2 mutant constructs were co-expressed with the Grx1-ROGFP2 and mitoGrx1-ROGFP2 genetically redox probes into HEK293 cells. The mito-Grx1, which has a mitochondrial targeting sequence, was used to specifically measure redox changes in the mitochondria and the Grx1-ROGFP was used to quantitate cytosolic redox changes.

We sought to expose the cells to an artificial redox change and measure their cytosolic and mitochondrial recovery. We had robust mitochondrial targeting in the Grx1-ROGFP and colocalized expression of the tagBFP on some cells. The cells were imaged at baseline and then treated with 0.5mM Hydrogen Peroxide and with 2mM DTT for the sensor calibration. The Grx1-ROGFP2 sensor is an excitation ratiometric sensor, so sensor response was quantitated as a ratio of emission upon excitation at 475/395. The response to H<sub>2</sub>O<sub>2</sub> was immediate and caused a drop in the ratio response, but recovery from the oxidized state after the addition of DTT differed based on the compartment being measured. Mitochondrial recovery from oxidative stress was slower than the cytosolic as expected due to mitochondrial metabolic adaptation that causes resistance to sudden changes in oxidation.

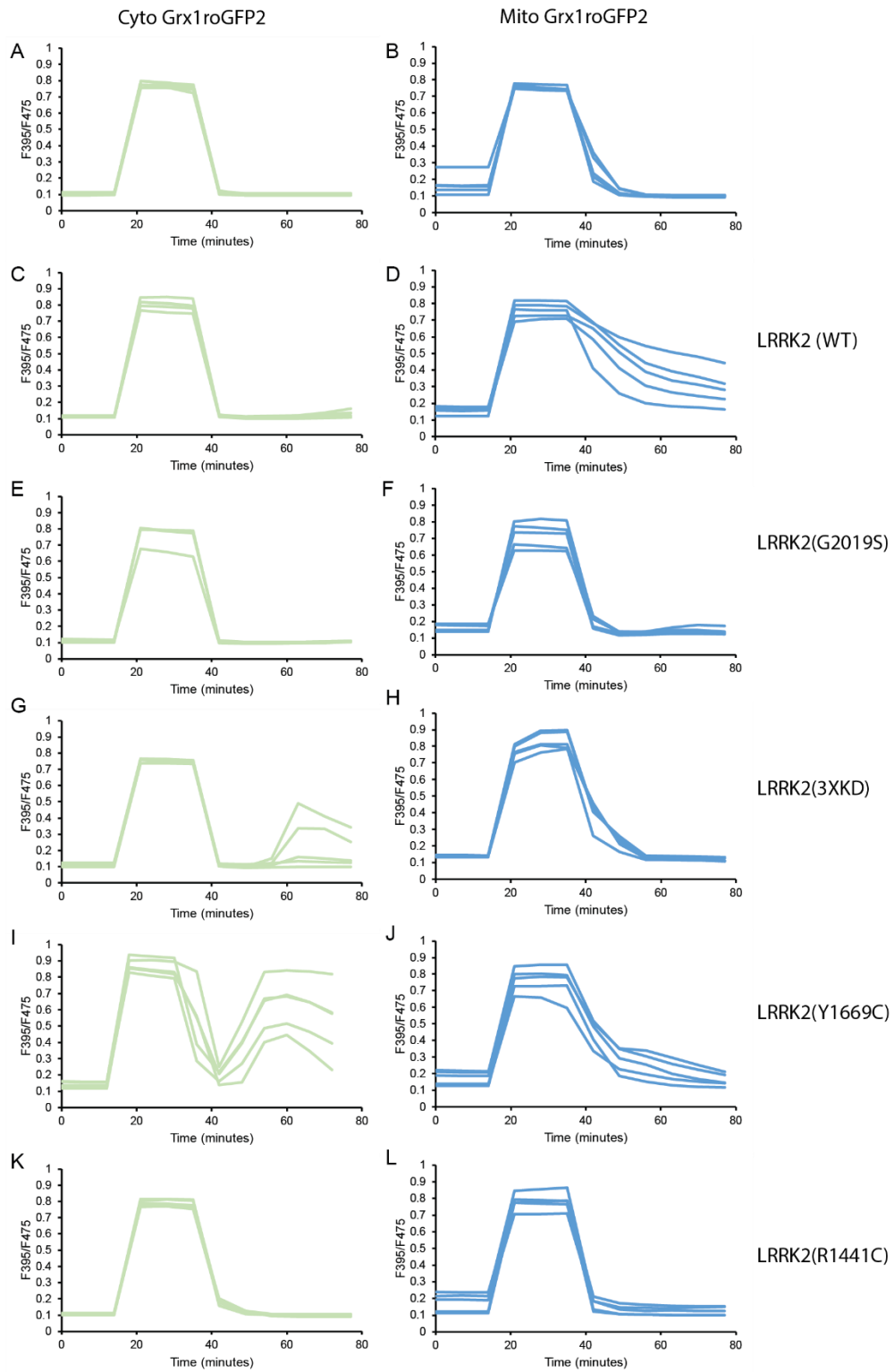
An interesting outcome to be noted was that the variant of the LRRK2 construct that was co-expressed appeared to influence the recovery from peroxide oxidation and in some cases caused a secondary phase of oxidation after reducing back to basal levels (Figure 5.2). The LRRK2 WT showed a much-delayed recovery from the oxidation treatment in the mitochondria, after the DTT addition (Figure 5.2.D). This effect was not observed in mitochondria of the LRRK2-3XKD mutant. However, the LRRK2-3XKD mutant showed a secondary phase of oxidation in the cytosol, which was not observed in any of the other LRRK2 mutants (Figure 5.2.G). This warranted further investigation, and we went onto test the application of a small oxidative challenge of 25 $\mu$ M H<sub>2</sub>O<sub>2</sub> followed by a calibration with 0.5mM H<sub>2</sub>O<sub>2</sub> and 2mM DTT on the LRRK2 WT and LRRK2 3XKD mutants. The redox challenge elicited a small response in the cytosol (Figure 5.2.A) and an even smaller response in the mitochondria (Figure 5.2.B) in the cells that did not express any LRRK2. However, in the cells expressing the LRRK2 WT construct, the redox change elicited an extremely large but transient oxidative response, which matched the sensor response to 0.5mM H<sub>2</sub>O<sub>2</sub>, which is typically sufficient to completely oxidize the sensor (Figure 5.2.C). A similar response was

observed in the mitochondrial targeted sensor as well (Figure 5.2.D). In the cells expressing LRRK2 3XKD mutants, the sensor stayed oxidized after the initial redox stimulation and was only reduced with the addition of 2mM DTT, both in the cytosol and mitochondria (Figure 5.2 E, F)

#### Figure 5.2. Grx1-roGFP2 response in LRRK2 mutants

Most of the cells expressing the LRRK2 mutants, had similar cytosolic responses as compared to the cells that were not transfected with LRRK2. The LRRK2 kinase domain mutant interestingly showed a secondary phase of oxidation after the DTT treatment. In the mitochondria, however, there appeared to be a delay in the recovery from peroxide oxidation even after the DTT addition in the LRRK2 WT overexpression model.

Figure 5.2 continued



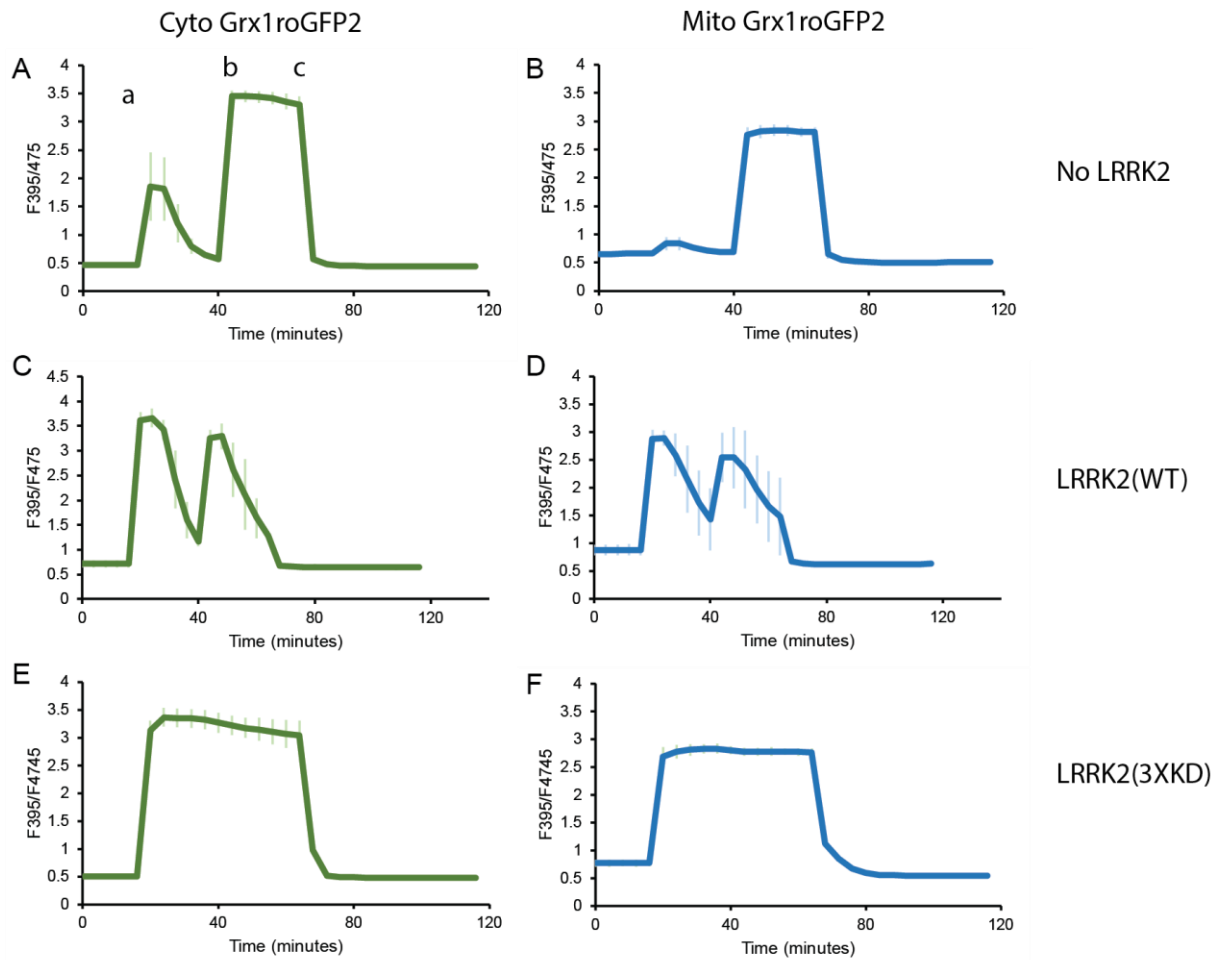


Figure 5.3. Redox challenge in LRRK2 mutants

The timing of additions were: a-Addition of 25 $\mu$ M H<sub>2</sub>O<sub>2</sub> at T16, b-addition of 0.5mM H<sub>2</sub>O<sub>2</sub> at T40, c- addition of 2mM DTT at T64 The presence of LRRK2(WT) and LRRK2 (3XKD) appears to affect the response to a redox challenge. n= 4 cells for all conditions

Despite the variability in some of the responses, we observed that are potentially some intrinsic effects of LRRK2 on redox homeostasis and that kinase activity is dispensable for redox effect on HEK293 cells. However, these experiments proved quite challenging and the effort of optimizing the model and collecting quality data was significant. Therefore, we decided to focus our energy on SH-SY5Y cells as it a more relevant model to study PD.

### 5.3.2 SH-SY5Y model

The SH-SY5Y model is widely used for PD studies and its ability to undergo terminal neuronal differentiation gives us the potential to conduct activity dependent redox studies. The SH-SY5Y cell line derived as a sub-line of neuroblastoma cell line SK-N-SH, is one of the most frequently used cell lines in PD research. The use of this cell line has a lot of advantages, as it is of human origin, has catecholaminergic neuronal properties and terminal neuronal differentiation can be induced (Kovalevich & Langford, 2013). The most commonly employed method of forced differentiation is with the addition of retinoic acid (RA) in concentrations ranging from 5 $\mu$ M to 100 $\mu$ M (Kovalevich & Langford, 2013). A maintenance in low serum media during differentiation also helps improve the results of differentiation. Though it has been confirmed that there is an increase in neuronal markers upon RA treatment, there is conflicting evidence to the reports of DAergic markers in the differentiated cells (Cheung et al., 2009; Lopes et al., 2010). Phenotypic characterization of RA differentiation on SH-SY5Y cells revealed the induction of a terminal neuron with DAergic like character in some studies (Korecka et al., 2013) and a cholinergic phenotype in some others (Hashemi, et al 2003).

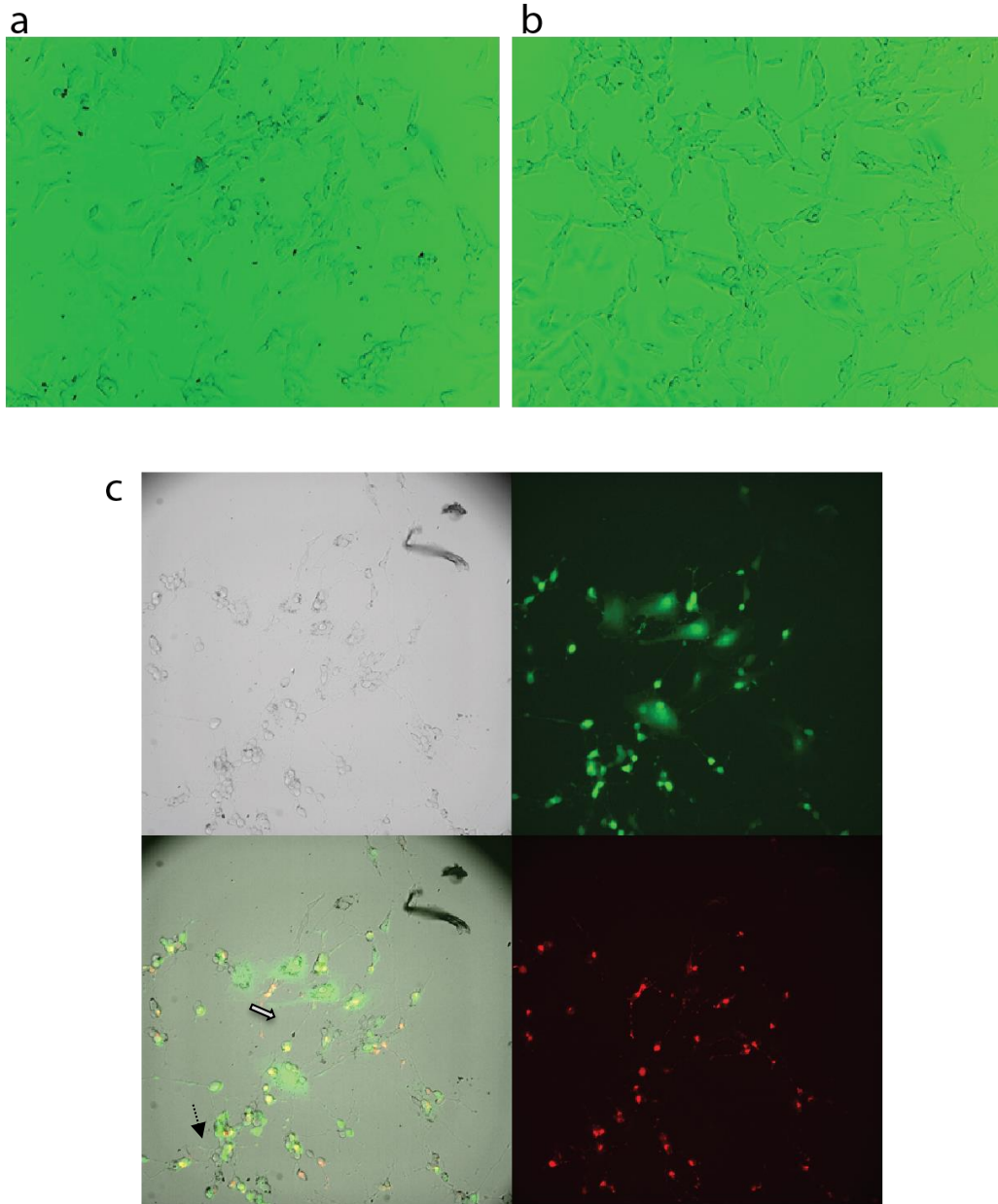


Figure 5.4. SH-SY5Y differentiation

a) Undifferentiated neurons at Day 0, b) Neurons differentiated in 1-2% serum media and 10µM RA, c) Neurons from b) induced with lentivirus expressing roGFP2 and mitorogRFP2 prior to differentiation. ‘N’ type cell (dotted arrow) and ‘S’ type (gray arrow) seen in picture

The differentiation protocol for the SH-SY5Y cell line was standardized after several trials and optimization of differentiation conditions. The cells were differentiated in 1-5% serum media containing 10-50µM retinoic acid over a period of 4-9 days. The cells were differentiated into ‘S’

type cells which are epithelial like and lack processes, and ‘N’ type cells that are neuronal-like with long neurites and a pyramidal shaped cell body (Figure 5.4).

One of the difficulties we faced while using this cell line was that it had poor transfection efficiencies, especially with the large LRRK2 constructs. We optimized the transfection protocol and found that we were able to achieve around 5% transfection efficiencies using calcium phosphate transfection. Alternately, we were able to successfully transduce the SH-SY5Y with lentiviral vectors and used this to express the cyto-roGFP2 and mito-roGFP2. The viral transduction was tested in combination with the differentiation; the cells were transduced prior to the start of the differentiation protocol and after terminal differentiation.

Previously, we were able to use the cyto-roGFP2 sensor and the mito-roGFP2 sensor to observe activity dependent redox changes in hippocampal neurons. We planned to use a similar dual color imaging paradigm to be able to observe if stimulation causes redox changes in the cytosol and mitochondria of SH-SY5Y cells. The transduced and terminally differentiated SH-SY5Y cells were then used for dual color redox imaging. We used different stimulations of glutamate, acetylcholine and KCl and none of these elicited a redox response in the differentiated SH-SY5Y cells (Figure 5.5). The signal from the mitochondrial roGFP2 was small and noisy due to the low expression of the sensor.

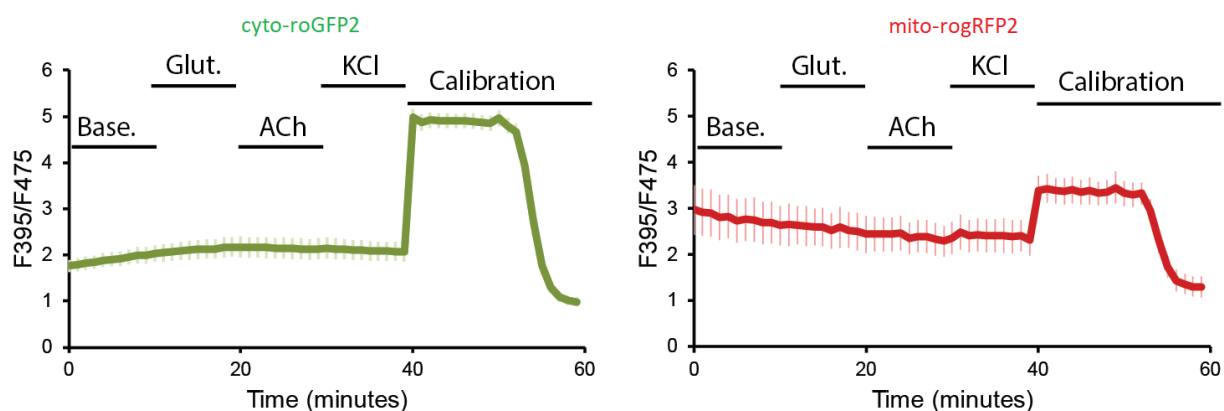


Figure 5.5. Stimulation of differentiated SH-SY5Y cells

Differentiated cells were treated with 100 $\mu$ M glutamate, 100  $\mu$ M acetylcholine and 80 mM KCl followed by a calibration with 1mM Diamide and 5mM DTT. No discernible redox changes were observed in the cytosol or the mitochondria.

It was unclear if the lack of redox response was because the differentiated neurons were not functional and therefore, could not be stimulated or if they can be stimulated, but the neuronal stimulation does not elicit a redox response in SH-SY5Y. There is previous evidence of terminally differentiated SH-SY5Y cells displaying both cholinergic and DAergic phenotypes, so we decided to test if these neuron-like cells were functional (Hashemi et al., 2003; Korecka et al., 2013). We used the Fluo4AM, which is a labeled calcium indicator that exhibits an increase in fluorescence at 488nm upon binding  $\text{Ca}^{2+}$ . We stimulated the neurons using successive applications of 100  $\mu\text{M}$  glutamate, 100 $\mu\text{M}$  acetylcholine, 80mM KCl. We observed calcium responses to acetylcholine and KCl but not to glutamate, indicating that these differentiated cells are functional and can be stimulated (Figure 5.6).

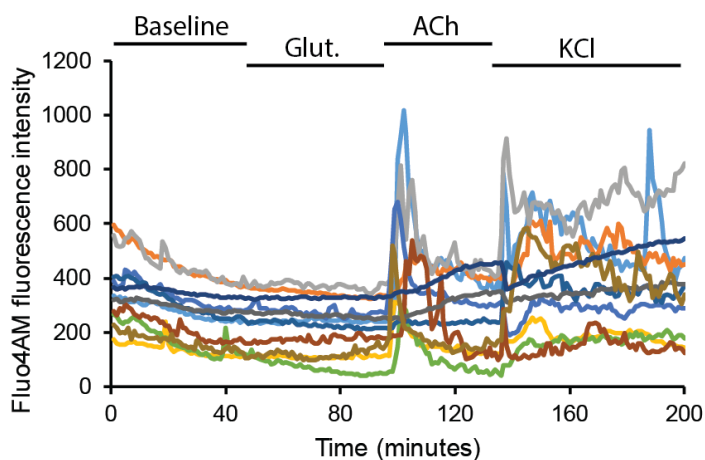


Figure 5.6. Calcium imaging of differentiated SH-SY5Y

Differentiated SH-SY5Y cells loaded with calcium indicator Fluo4AM, treated with 100  $\mu\text{M}$  glutamate, 100 $\mu\text{M}$  acetylcholine, 80mM KCl to elicit neuronal activity

Since the neuronal stimulations were not effective in eliciting a redox response, we wanted to observe if these cells are sensitive to low oxidative challenges that are similar to physiological levels. Additionally, we wanted to see if common sensitizers like rotenone that are associated with PD, can also affect the redox response in these cells. We moved on to trying low concentrations of peroxide on these differentiated cells. The peroxide challenge has been widely used in cellular models to induce oxidative stress, and we had limited success with it in the HEK293 cells. Other

groups have used chronic exposure to H<sub>2</sub>O<sub>2</sub> to study oxidative stress, but we were interested in seeing acute responses during live cell redox imaging.

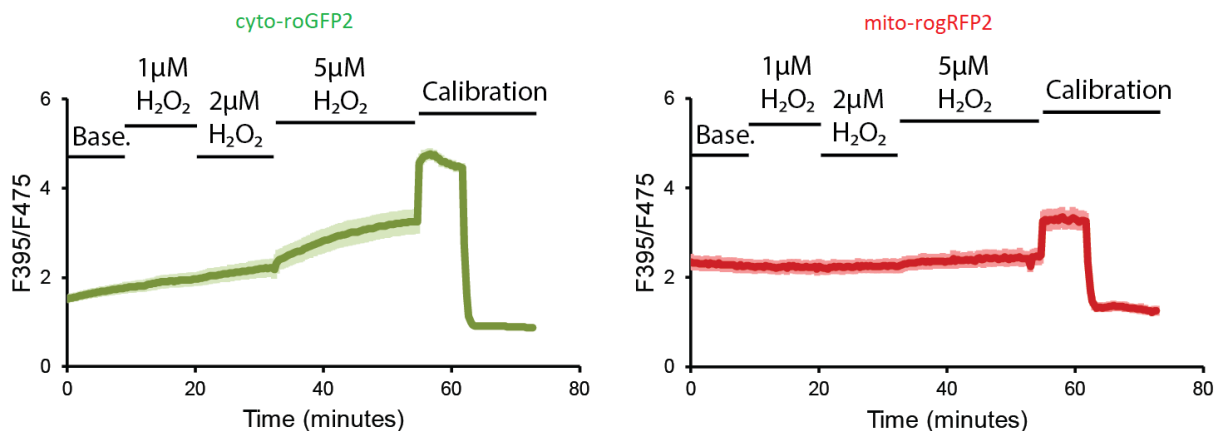


Figure 5.7. Hydrogen peroxide challenge on SH-SY5Y cells

1µM and 2µM H<sub>2</sub>O<sub>2</sub> showed minimal changes in cellular redox, but 5µM H<sub>2</sub>O<sub>2</sub> showed a robust response in the cytosol to the peroxide stimulation. MitorogRFP2 did not respond to the peroxide stimulation.

We attempted multiple strengths of peroxide stimulation on the SH-SY5Y cells, starting with 1 and 2µM H<sub>2</sub>O<sub>2</sub> that produced a negligible redox response in the cytosol and none in the mitochondria. The 5µM H<sub>2</sub>O<sub>2</sub> caused a significant increase in the cytosolic redox, and again, a significant redox response was not seen in the mitochondria. We decided to proceed with 5µM H<sub>2</sub>O<sub>2</sub> challenge for future experiments. The differentiated and transduced SH-SY5Y cells were now exposed to a singular redox challenge of 5µM H<sub>2</sub>O<sub>2</sub> (Figure 5.8), and this evoked a much smaller but steady response than earlier (Figure 5.7). The lower concentration redox challenges likely evoked a redox response that was ongoing when treated with a higher concentration of 5µM H<sub>2</sub>O<sub>2</sub>, which caused a steady increase in oxidation that was cut short by the oxidative diamide addition in the calibration. Again, the mitochondria signal was quite low and noisy, and there was no discernible redox response to the peroxide challenge. Rotenone is known to cause oxidative stress and induce cell death in SH-SY5Y cells. We wanted to look at the effect of a moderate rotenone pre-treatment on the redox response of SH-SY5Y cells. These cells expressed both the cyto-roGFP2 and mito-rogRFP2, but the signal in the mitochondria was too low to quantify. The pre-treatment of rotenone did not significantly alter the response to the peroxide challenge. We

will need to investigate this further after optimizing rotenone concentrations and with a higher concentration of peroxide.

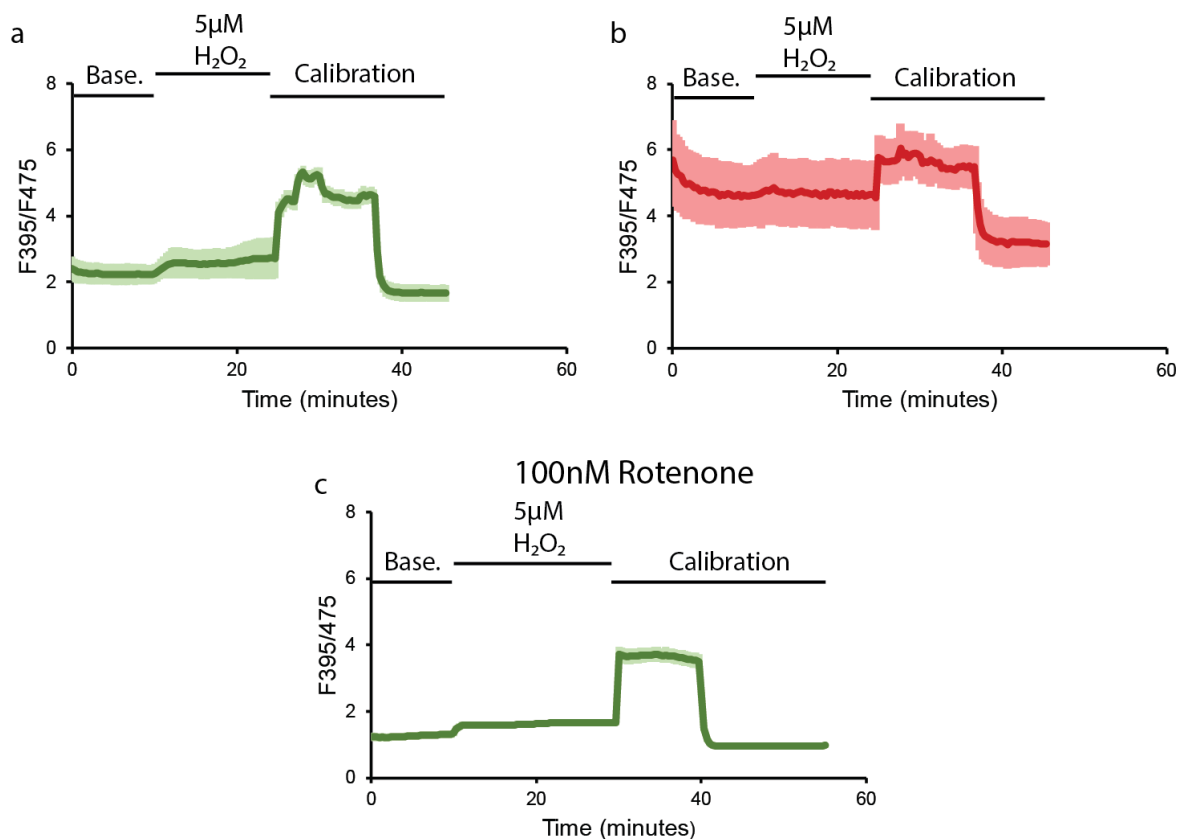


Figure 5.8. SH-SY5Y response to peroxide challenge and rotenone treatment

a) cytoroGFP2 b) mitrogrRFP2 c) cytoroGFP2 in cells pre-treated with 100nM Rotenone for 24hrs.

We established a redox imaging system with SH-SY5Y cells but decided that if we have to expend effort optimizing the stimulations, we wanted to go back to the primary neuronal model to ask our question if LRRK2 affects activity-dependent redox compartmentation.

### 5.3.3 Primary hippocampal neurons

In the previous chapter, we observed an interesting phenomenon of redox compartmentation in hippocampal neurons upon glutamate stimulation. We have established a hippocampal neuronal model in the lab and wanted to use it to study if LRRK2 has non-cell type specific, intrinsic effects

on redox response. In PD, the dopaminergic neurons of the midbrain are most affected and therefore, would be a more relevant model to study PD. However, the isolation of these cultures is more difficult and yields only a 5% enrichment of dopaminergic neurons. Previous research has observed that LRRK2 mutations impair synaptic plasticity in the mouse hippocampus (Sweet, Saunier-Rebori, Yue, & Blitzer, 2015) and regulates neurite outgrowth in rat hippocampal cultures (Heo, Kim, & Seol, 2010). However, the effect of LRRK2 on redox regulation in hippocampal neurons is unknown. Hence, we decided to do some preliminary testing in the hippocampal culture system. We sought to optimize a small redox challenge for the hippocampal neurons. Similar to experiments conducted in HEK293 and SH-SY5Y, we treated the hippocampal neurons with low doses of hydrogen peroxide, to observe a redox response in the two compartments.

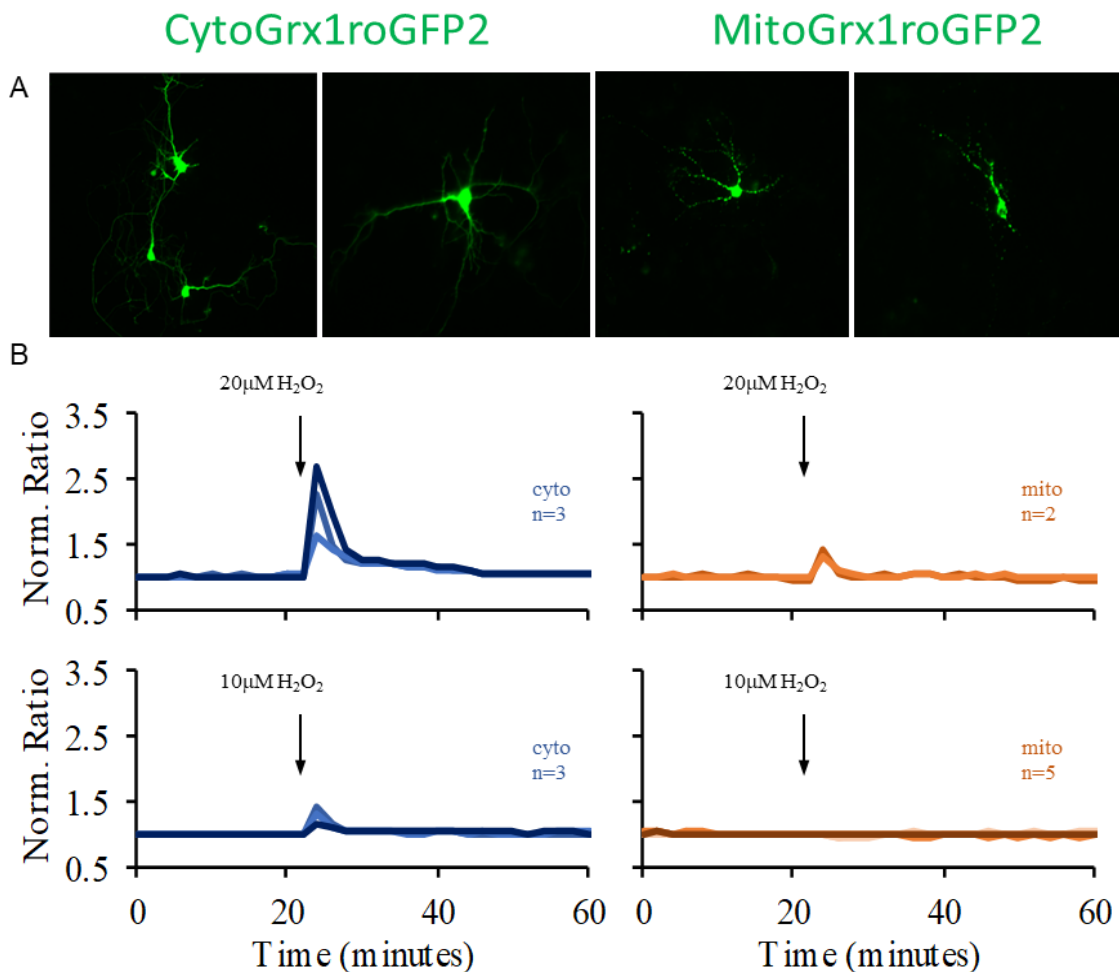


Figure 5.9. Redox responses in hippocampal neurons

Hippocampal neurons expressing either cyto- or mito-Grx1-roGFP2 were treated with 10 and 20 μM H<sub>2</sub>O<sub>2</sub> stimulations. The cytosol and mitochondria behaved differently

Primary hippocampal neurons transfected with cytosolic or mitochondrial targeted Grx1-roGFP2 were treated with a low oxidation challenge of 10 $\mu$ M and 20 $\mu$ M H<sub>2</sub>O<sub>2</sub>. The responses observed in the two compartments were distinct from each other, and the mitochondria appear to require a stronger redox stimulation to respond.

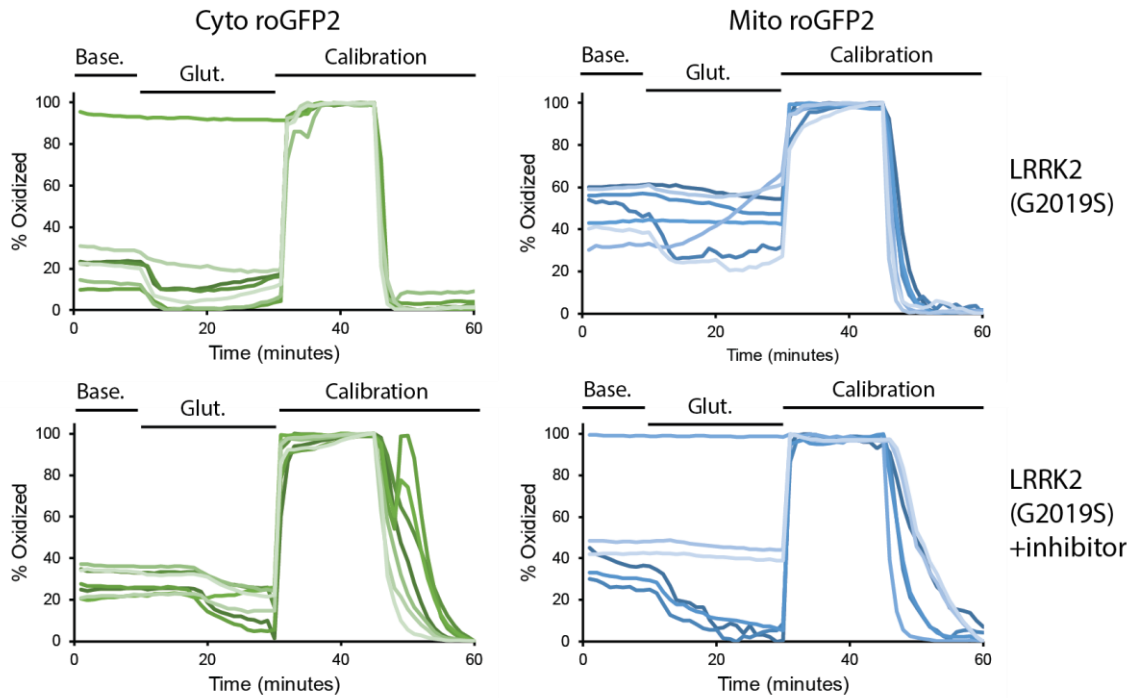


Figure 5.10 LRRK2 redox response to glutamate stimulation.

A set of constructs containing the LRRK2 mutants tagged with a bright red FP, mScarlet was generated by a post doc in the lab. We used this construct along with the cyto and mito roGFP2 sensors to observe if LRRK2 (G2019S) affected activity dependent redox in hippocampal neurons and if this effect could be rescued with a pre-incubation of LRRK2-IN-1, an inhibitor of LRRK2 kinase activity. In earlier studies, we had observed that glutamate stimulation caused an activity dependent mitochondrial oxidation and cytosolic reduction. With the LRRK2(G2019S) mutant, the cytosolic phenotype seems to remain unaffected. Interestingly, the mitochondrial response is quite varied, where some neurons show mitochondrial reduction, some do not respond, and one shows oxidation. The LRRK inhibitor appears to cause a more severe reduction in the mitochondria and a delayed cytosolic reduction. It is likely however, that the delay in the cytosolic response is not indicative of an inhibitor effect and more likely a mixing issue during

experimentation. This result is also consistent with the HEK293 data with the kinase dead mutant and suggests that kinase activity is dispensable for the effect on redox homeostasis, suggesting either GTPase or other signaling activity is involved.

#### **5.4 Conclusions and Future Directions**

Parkinson's studies have been undertaken in a variety of cellular models and tissues. Immortalized cell lines like the HEK293 and the SH-SY5Y are convenient starting points for overexpression models. We wanted to determine if LRRK2 has cell autonomous, intrinsic effects on redox changes that are not dependent on cell type. We began our studies in the HEK293 cell line for our initial assessment of redox and the effect of different LRRK2 mutants on redox and confirmed that LRRK2 mutants did appear to alter redox responses in HEK293 confirming our hypothesis that LRRK2 could potentially have intrinsic effects on redox, however, the experiments proved challenging and cumbersome.

We decided to switch to a more physiological model for Parkinson's. We decided to work with SH-SY5Y cells lines that have high endogenous levels of LRRK2 and can be differentiated into neuronal-like cells (Kovalevich & Langford, 2013; Smith et al., 2005). Additionally, the ability of the SH-SY5Y cells to undergo terminal neuronal differentiation, offered us the opportunity to study activity dependent redox changes. However, this cell line was difficult to work with and took extensive optimization of both the differentiation protocol and the transfection protocol. We wanted to express multicolor probes and the large LRRK2 expressing plasmids inside the cell, but most transfection methods resulted in very low transfection efficiencies. We moved onto primary neuronal culture models to study the LRRK2.

The hippocampal neuron model has already been used in the lab to study activity dependent redox changes and discovered unique redox compartmentation. We wanted to see if this process could be affected by the presence of LRRK2. Unfortunately, due to issues of bleed through from the tagBFP2 reporter on LRRK2, we decided to image one compartment at a time in cells expressing either the cytosolic roGFP2 or the mitochondrial roGFP2 and LRRK2(G2019S)-mScarlet. The preliminary results from these experiments were interesting and supported our observation in the HEK293 cells that the redox response is kinase independent meriting further investigation in the

future. One of the important takeaways with this project has been the ascending move towards more physiological models of PD. While cell lines can give us a plethora of information about redox, PD specific phenotypes are better observed in primary neuronal cultures, especially midbrain cultures and in tissue slices. We attempted to isolate midbrain cultures from P1 mice and stained them for tyrosine hydroxylase, which is a marker for dopaminergic neurons and Map2, which is a neuronal marker that is not subtype specific. In the future, we should move to using these redox probes to look at redox changes in midbrain neurons.

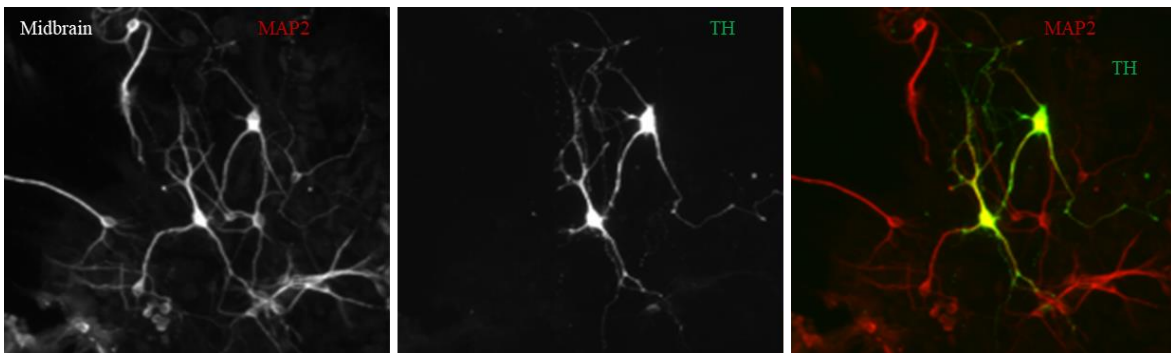


Figure 5.11. Dopaminergic neurons in midbrain culture.  
*Obtained in collaboration with Aswathy Chandran and the Rochet and Cannon labs.*

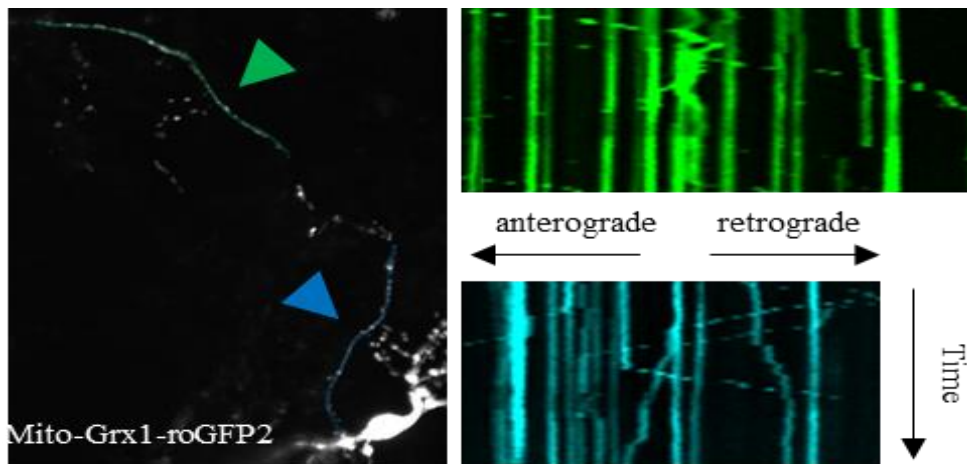


Figure 5.12 Tracking mitochondrial movement

Kymographs generated from primary mouse hippocampal neurons expressing mito-Grx1roGFP2 imaged at 20X magnification

Current literature presents evidence on the effect of LRRK2-G2019S on mitochondrial motility and the delayed arrest of damaged mitochondria (Hsieh et al., 2016). However, it is unclear if the delayed arrest propagates an increase in ROS originating from the damaged mitochondria. After expressing the mito-Grx1roGFP2 in hippocampal neurons, we demonstrated that we could use the roGFP2 fluorescence to also generate kymographs and track the changes in mitochondrial motility. For future studies, we could use a mitochondrial targeted redox sensor to track the changes in mitochondrial redox status, coupled with monitoring mitochondrial motility with different LRRK2 variants. Mitochondrial dynamics and fragmentation events should also be monitored and quantitated in different LRRK2 conditions.

In this study we established that we could use our sensor imaging approach with cellular models, and we were able to obtain some interesting preliminary results. In the future, it will be important to adopt cultured midbrain dopaminergic neurons or tissue slices to further investigate the effects of LRRK2 mutations on redox as well as other physiological changes seen in PD.

## **5.5 Materials and Methods**

### **5.5.1 Materials**

Chemicals and cell culture media and supplements were purchased from Sigma, Formedium, and ThermoFisher Scientific. Molecular biology enzymes were purchased from New England Biolabs (NEB).

### **5.5.2 Molecular Biology**

LRRK2-tagBFP2 constructs were cloned using Gibson cloning. The cloning was performed in multiple steps with the addition of tagBFP2 first followed by the cloning of the LRRK2 mutant sequences. Upon preparation of plasmid DNA, all sequences of the LRRK2 mutant constructs were confirmed by Sanger sequencing at Genewiz (South Plainfield, NJ).

### **5.5.3 Cell Culture and Transfections**

#### ***HEK293 cells***

Human embryonic kidney 293 (HEK293) cells were cultured in Dulbecco's modified eagle's medium (DMEM) with 4.5 g/L glucose, 10% cosmic calf serum, 3.7 g/L sodium bicarbonate, pH 7.0-7.4 and maintained at 37°C and 5% CO<sub>2</sub>. Cells were plated onto a 35mm glass bottomed culture dish at a density of 2x10<sup>5</sup> cells, 24 hrs prior to transfection. Cells were transfected with calcium phosphate using 500ng of each construct. Cells were imaged 48 hours post transfection.

#### ***SH-SY5Y cells***

SH-SY5Y cells were cultured in DMEM/F12 with 4.5 g/L glucose, 10% cosmic calf serum, 3.7 g/L sodium bicarbonate, 1mM sodium pyruvate, pH 7.0-7.4 and maintained at 37°C and 5% CO<sub>2</sub>. During the differentiation stages, the cells were maintained in low serum media 1-5% CCS for a period of 3-7 days. For the initial differentiation optimization, we started with serum concentrations of 2 and 5% and dropped it to 1 & 2 % respectively after giving the cells 24hrs to adapt to the low serum media. The cells were differentiated with 10µM retinoic acid but some conditions were tested with 50µM retinoic acid to induce a quick differentiation.

#### ***Cultured Primary Mouse Neurons***

Primary hippocampal neurons, cortical neurons and midbrain neurons were isolated from P1 FVB mice and plated on nitric acid washed 18mm #1.5 glass coverslips or glass bottomed 35mm dishes (Cellvis) that were coated with 50 µg/ml poly-D-lysine (PDL). Neuronal cultures were maintained in Neurobasal-A medium supplemented with B-27, 5mM glucose, 0.25 mM pyruvate, 0.5 mM GlutaMax, 1X Pen-Strep at 37°C and 5% CO<sub>2</sub> in a humidified incubator 30% feedings every 1-2 days. The cultured neurons were transfected with Calcium Phosphate on DIV 4-5 and imaged on DIV 6-8. All animal procedures were approved by and performed in accordance with guidelines by the Purdue Animal Care and Use Committee.

#### **5.5.4 Live-Cell Imaging**

Neurons and SH-SY5Y cells were equilibrated for 1 hour prior to imaging in imaging solution consisting of 15mM HEPES, 120mM NaCl, 3mM KCl, 3mM NaHCO<sub>3</sub>, 1.25mM NaH<sub>2</sub>PO<sub>4</sub>, 5mM Glucose, 2mM CaCl<sub>2</sub>, 1mM MgCl<sub>2</sub>, 0.25mM Pyruvate, 0.5mM Glutamax, pH7.3 at 37°C and 5% CO<sub>2</sub> in a humidified incubator. For widefield microscopy, the cells were imaged at room temperature in 1-minute time intervals and treatments were added to a static bath with imaging solution. DIC images were taken at the beginning and after the imaging paradigm to monitor neuron health. HEK293 cells were imaged in imaging solution containing 15 mM HEPES, 120 mM NaCl, 3 mM KCl, 3 mM NaHCO<sub>3</sub>, 1.25 mM NaH<sub>2</sub>PO<sub>4</sub>, 1 mM MgCl<sub>2</sub>, 2 mM CaCl<sub>2</sub>, and 10 mM glucose.

#### **5.5.5 Data Analysis**

Images were analyzed using ImageJ. Background subtraction was performed above the mean background signal and then a threshold was set to three standard deviations over mean to eliminate background pixels. Ratio images were generated by dividing the 400 Ex image by the 490 Ex image for both the red and green emissions and the ratio signals were measured around the cell body. The HEK293 cells expressing LRRK2 mutants were selected using the tagBFP2 signal and the hippocampal neurons with the LRRK2 mutants were selected using the mScarlet tag.

## CHAPTER 6. FUTURE PERSPECTIVES

### 6.1 Moving Towards In Situ and In Vivo Redox Imaging

Genetically encoded fluorescent probes have been extremely useful to study redox mechanisms under physiological conditions and the development of disease pathology in *in vitro* cellular models. To better understand how tissue microenvironments and intercellular interactions affect the production of ROS, we need to apply these tools to measure oxidative stress in intact tissues. Our understanding of redox signaling that affects pathophysiology has been enhanced with the availability of transgenic animal models expressing redox probes (Albrecht et al., 2011b; Swain et al., 2016; Wagener et al., 2016). This has been particularly useful in small animal models like zebrafish, fruit fly and nematodes (Braeckman, Smolders, Back, & De Henau, 2016; Breckwoldt, Wittmann, Misgeld, Kerschensteiner, & Grabher, 2015; Han et al., 2014; Timme-Laragy et al., 2013). The green fluorescent roGFP-based sensors have been used successfully with two-photon microscopy for tissue and whole animal redox imaging (Albrecht et al., 2011b; Z. Liu, Celotto, Romero, Wipf, & Palladino, 2012; Wolf, Nishimaki, Kamimura, & Ohta, 2014). However, there is still a need for red fluorescent redox sensors that can be used for one and two-photon quantitative redox imaging for *in vitro* and *in vivo* redox imaging.

In our work, we have developed and demonstrated the use of a red-shifted redox sensor in neuronal cultures and fly samples. Given the promising *in vitro* results, the roGRFP2 was also tested in collaboration with Brain MacVicar's research group at the University of British Columbia to determine to see if it is suitable for ratiometric redox imaging *in situ* using acute brain slices of roGRFP2 expressing rats. Acute brain slices were prepared for live two-photon microscopy of neurons in cortical layers II-IV, expressing the roGRFP2 construct under the hSyn promoter targeted to the cytosol. Ratiometric signals were recorded using two alternating channels with excitation wavelengths of 800 and 900 nm to quantify how neurons respond to bath applications of diamide and DTT. Transient bath application of diamide induced a robust increase in roGRFP2 ratios in the red fluorescence emission channel. The roGRFP2 is suitable for ratiometric redox imaging *in situ* using two-photon excitation, and this will enable the mechanisms of redox homeostasis to be studied in greater detail in the future.

One of the interesting observations during our redox compartmentation studies was the effect that astrocytes had on attenuating the neuronal redox response to glutamate stimulation. We can look at how astrocytes offer neuroprotection from oxidative stress and monitor redox communication between cell types. One of the major ways in which astrocytes have a neuroprotective effect is through the release of antioxidants like glutathione (Vargas, Johnson, Sirkis, Messing, & Johnson, 2008). Glutathione is exported in the astrocytes through the multidrug resistance-associated protein 1 (Mrp1) (Hirrlinger, Schulz, & Dringen, 2002). Inhibitors of Mrp1 like MK571 can be used to reduce glutathione secretion from astrocytes (Minich et al., 2006). This can help us further tease apart the mechanism by which astrocytes modulate activity dependent redox compartmentation. Alternately, we can also use the gap junction blocker Carbenoxolone which blocks coupling between astrocytes to see if it might make neurons more vulnerable to oxidative stress (Cheng et al., 2018; Zündorf, Kahlert, & Reiser, 2007). In addition, to explore if our glutamate induced cytosolic reduction is primarily a result of glutathione increases in the cytosol, we can use the GSH synthesis inhibitor buthionine sulfoximine to study if the response is altered (Dringen et al., 1999; T. W. Sedlak et al., 2019). Our rogRFP2 sensor gives us the ability to perform dual color imaging, where we can monitor redox changes in neurons and astrocytes simultaneously. To have a more precise understanding of the physiological response, we should study neuron-glia interactions in situ in brain slices to understand how astrocytes protect neurons from oxidative stress.

## **6.2 Models for Studying LRRK2**

LRRK2 variants cause dysfunction in a host of cellular processes like vesicular trafficking, lysosome-autophagy complex, protein translation, mitochondrial transport and mitophagy (Biskup et al., 2006; Cookson, 2016a; Dodson, Zhang, Jiang, Chen, & Guo, 2012; Ho et al., 2018; Hsieh et al., 2016). The G2019S variant is the most common pathogenic variant and has demonstrated a small but recognizable increase in in-vitro kinase activity and some of the mitochondrial and oxidative stress phenotypes seen in PD models can be attributed to the kinase activity of this mutant (Mortiboys, Johansen, Aasly, & Bandmann, 2010; Nguyen et al., 2011; Verma et al., 2017; West et al., 2005a). However, some of these phenotypes have also been observed in a kinase independent manner (Ramonet et al., 2011; Xinglong Wang et al., 2012a) so

it is important to understand the functions of LRRK2 that contribute to these effects and where the biochemical effects caused by these different mutations converge.

Animal models have been invaluable for LRRK2 and PD research. Transgenic models for LRRK2 mutants exist in *C. elegans*, *Drosophila*, and rodents (Dodson et al., 2012; Lee et al., 2015; Luth, Stavrovskaya, Bartels, Kristal, & Selkoe, 2014; Ramonet et al., 2011). Conditional expression of LRRK2 G2019S and WT, and BAC transgenic mice expressing LRRK2 G2019S, LRRK2 R1441C, and LRRK WT have all shown minimal evidence of neurodegeneration in DA neurons (X. Li et al., 2010; Y. Li et al., 2009; Melrose et al., 2010; Ramonet et al., 2011; Tsika et al., 2014). However, aging mice with knock in LRRK2 G2019S show evidence of mitochondrial abnormalities, consistent with mitochondrial fission in the striatum (Yue et al., 2015). Human BAC-LRRK2 G2019S rats did not show signs of neurodegeneration or develop significant deficits in motor or cognitive function with age, but they presented with increased oxidative stress in the SNpc and striatum (Lee et al., 2015). In LRRK2 G2019S KI mice, the striatum was more sensitive to rotenone, and the mutation enhanced rotenone-dependent alteration of mitochondrial homeostasis (Tozzi et al., 2018). Despite the fact that these rodent models do not recapitulate the key features of neurodegeneration seen in end-stage PD, they facilitate studies of environmental toxins and gene-environment interactions. In transgenic mice, the G2019S variant confers increased sensitivity to mitochondrial toxin rotenone (H. Liu et al., 2017), and this is also seen in induced dopaminergic neurons derived from LRRK2 mutant carriers. Moving on from cellular models of LRRK2 to transgenic models will help us gain a larger perspective on the redox changes happening in tissue, and our expanded redox probe toolset makes it easier for us to study redox changes in situ and in vivo. It also offers us the exciting opportunity to look at the effect of toxins like rotenone and paraquat and appreciate how they could potentially accelerate the effects of LRRK2 variants that result in the oxidative stress phenotype.

In viral-mediated animal models of LRRK2, robust DA neurodegeneration was observed. When the transgene was virally expressed in both neuronal and glial cells and was able to activate glial inflammation and concurrently elicit neurodegeneration unlike in other LRRK2 genetic models (Dusonchet et al., 2011; Tsika et al., 2015). This supports the theory that LRRK2 could have both cell-autonomous and non-cell autonomous processes that lead to neurodegeneration. Imploring the

non-cell autonomous mechanisms of LRRK2 would probably help us understand the development of this disease in humans. Using the dual cell imaging model that we proposed earlier, we can look at inflammatory pathways and investigate the role of glia in mediating neuronal oxidative stress and the degeneration of DA neurons.

Another highly relevant model for PD studies is the use of patient derived induced pluripotent stem cells (iPSCs) that can be used to derive neurons. The use of this model has become more tractable in recent times due to the development of better methods of differentiation. Dopaminergic neurons derived from LRRK2 iPSCs show increased vulnerability to cellular stress, reduced neurite length,  $\alpha$ -syn accumulation, and compromised mitochondrial function (Cooper et al., 2012; Nguyen et al., 2011; Reinhardt et al., 2013; Sanders et al., 2014). More recently, LRRK2 G2019S mutant induced defects in mitophagy and mitochondrial transport was observed in a model of iPSCs (Hsieh et al., 2016). An important advantage of this model is that it allowed us to look at LRRK2 pathology in human cells.

### **6.3 Sensor Design and Protein Engineering**

In our sensor library, the roGFP2 linker was shortened, but only a maximal 34% FRET efficiency was achieved. Theoretically, the spectral overlap between roGFP2 emission and the absorbance of the RFPs can support greater than 75% FRET efficiency. To gain better insight, we carried out conformational modeling for one roGFP2-mCherry candidate with a flexible linker using the FPMOD software developed by the Truong lab (Pham, Chiang, Li, Shum, & Truong, 2007). The modeling demonstrates that several conformations exhibit >95% FRET efficiency, and conformational averaging is the major limitation to achieving greater FRET efficiency. For our third-generation sensor, we will design conformationally locked architectures by using a coiled-coil motif or an intermediate bystander domain to enforce conformational restraints

One of the issues we ran into when using the LRRK2 constructs tagged with tagBFP2 was the bleed through into the GFP channels. Fluorescent proteins have a lot of overlap, and we are spectrally limited in our choices of tags for the LRRK2 when we have a dual compartment imaging system that already uses a red and green FP. With the tagBFP2, with lower expression in the cells, we could not positively identify the cells that truly had LRRK2, and with high expression we had

bleed through. One of the ways to proceed in the future would be to use a near IR fluorescent protein with the LRRK2 (Shcherbakova et al., 2016). Alternately, another way to move forward would be to use multicistronic vectors to express the LRRK2 sequence along with roGFP2 separated by an IRES or 2A sequence (Ibrahimi et al., 2009; Pelletier & Sonenberg, 1988).

To summarize, my thesis work has expanded our capabilities to study cellular redox using genetically encoded sensors. I have engineered the next generation red-shifted redox sensor, roGRFP2, which offers the opportunity for multiplexed live cell imaging and *in vivo* imaging of redox. With this sensor, we have been able to discover activity-dependent redox compartmentation in neuronal cultures. Through collaboration, we have been able to establish that the roGRFP2 sensor can be used in other animal models. Additionally, I have established cellular models for studying LRRK2, and this has created a platform for future work to explore the relationship between PD associated LRRK2 mutations and oxidative stress.

## REFERENCES

- Abbracchio, M. P., Burnstock, G., Boeynaems, J. M., Barnard, E. A., Boyer, J. L., Kennedy, C., Weisman, G. A. (2006). International Union of Pharmacology LVIII: Update on the P2Y G protein-coupled nucleotide receptors: From molecular mechanisms and pathophysiology to therapy. *Pharmacological Reviews*. <https://doi.org/10.1124/pr.58.3.3>
- Akerboom, J., Carreras Calderón, N., Tian, L., Wabnig, S., Prigge, M., Tolö, J., ... Looger, L. L. (2013). Genetically encoded calcium indicators for multi-color neural activity imaging and combination with optogenetics. *Frontiers in Molecular Neuroscience*, 6(March), 2. <https://doi.org/10.3389/fnmol.2013.00002>
- Alboni, S., Gibellini, L., Montanari, C., Benatti, C., Benatti, S., Tascetta, F., ... Pariante, C. M. (2013). N-acetyl-cysteine prevents toxic oxidative effects induced by IFN- $\alpha$  in human neurons. *International Journal of Neuropsychopharmacology*, 16(8), 1849–1865. <https://doi.org/10.1017/S1461145713000266>
- Albrecht, S. C., Barata, A. G., Großhans, J., Teleman, A. A., & Dick, T. P. (2011a). In vivo mapping of hydrogen peroxide and oxidized glutathione reveals chemical and regional specificity of redox homeostasis. *Cell Metabolism*. <https://doi.org/10.1016/j.cmet.2011.10.010>
- Albrecht, S. C., Sobotta, M. C., Bausewein, D., Aller, I., Hell, R., Dick, T. P., & Meyer, A. J. (2014). Redesign of genetically encoded biosensors for monitoring mitochondrial redox status in a broad range of model eukaryotes. *Journal of Biomolecular Screening*, 19(3), 379–386. <https://doi.org/10.1177/1087057113499634>
- Andersen, J. K. (2004). Oxidative stress in neurodegeneration: Cause or consequence? *Nature Reviews Neuroscience*, 10(7), S18. <https://doi.org/10.1038/nrn1434>
- Anderson, C. M., Bergher, J. P., & Swanson, R. A. (2003). ATP-induced ATP release from astrocytes. *Journal of Neurochemistry*. <https://doi.org/10.1111/j.1471-4159.2004.02204.x>
- Angeles, D. C., Gan, B. H., Onstead, L., Zhao, Y., Lim, K. L., Dachsel, J., ... Tan, E. K. (2011). Mutations in LRRK2 increase phosphorylation of peroxiredoxin 3 exacerbating oxidative stress-induced neuronal death. *Human Mutation*, 32(12), 1390–1397. <https://doi.org/10.1002/humu.21582>
- Aquilano, K., Baldelli, S., & Ciriolo, M. R. (2014). Glutathione: New roles in redox signalling for an old antioxidant. *Frontiers in Pharmacology*. <https://doi.org/10.3389/fphar.2014.00196>
- Araque, A., Carmignoto, G., Haydon, P. G., Oliek, S. H. R., Robitaille, R., & Volterra, A. (2014). Gliotransmitters travel in time and space. *Neuron*. <https://doi.org/10.1016/j.neuron.2014.02.007>
- Arundine, M., & Tymianski, M. (2004). Molecular mechanisms of glutamate-dependent

- neurodegeneration in ischemia and traumatic brain injury. *Cellular and Molecular Life Sciences*. <https://doi.org/10.1007/s00018-003-3319-x>
- Attwell, D., & Laughlin, S. B. (2001). An energy budget for signaling in the grey matter of the brain. *Journal of Cerebral Blood Flow and Metabolism*, *21*(10), 1133–1145. <https://doi.org/10.1097/00004647-200110000-00001>
- Ayala, A., Muñoz, M. F., & Argüelles, S. (2014). Lipid peroxidation: Production, metabolism, and signaling mechanisms of malondialdehyde and 4-hydroxy-2-nonenal. *Oxidative Medicine and Cellular Longevity*. <https://doi.org/10.1155/2014/360438>
- Bajar, B. T., Wang, E. S., Zhang, S., Lin, M. Z., & Chu, J. (2016). A guide to fluorescent protein FRET pairs. *Sensors (Switzerland)*, *16*(9), 1–24. <https://doi.org/10.3390/s16091488>
- Balaban, R. S., Nemoto, S., & Finkel, T. (2005). Mitochondria, oxidants, and aging. *Cell*, *120*(4), 483–495. <https://doi.org/10.1016/j.cell.2005.02.001>
- Bao, Y., Ledderose, C., Seier, T., Graf, A. F., Brix, B., Chong, E., & Junger, W. G. (2014). Mitochondria regulate Neutrophil activation by generating ATP for Autocrine Purinergic signaling. *Journal of Biological Chemistry*. <https://doi.org/10.1074/jbc.M114.572495>
- Barberà-Cremades, M., Baroja-Mazo, A., Gomez, A. I., Machado, F., Di Virgilio, F., & Pelegrín, P. (2012). P2X7 receptor-stimulation causes fever via PGE2 and IL-1 $\beta$  release. *The FASEB Journal*. <https://doi.org/10.1096/fj.12-205765>
- Bastid, J., Regairaz, A., Bonnefoy, N., Dejou, C., Giustiniani, J., Laheurte, C., ... Eliaou, J. F. (2015). Inhibition of CD39 enzymatic function at the surface of tumor cells alleviates their immunosuppressive activity. *Cancer Immunology Research*. <https://doi.org/10.1158/2326-6066.CIR-14-0018>
- Beigi, R., Kobatake, E., Aizawa, M., & Dubyak, G. R. (1999). Detection of local ATP release from activated platelets using cell surface-attached firefly luciferase. *American Journal of Physiology - Cell Physiology*. <https://doi.org/10.1152/ajpcell.1999.276.1.c267>
- Bell, K. F. S., Al-Mubarak, B., Martel, M. A., McKay, S., Wheelan, N., Hasel, P., ... Hardingham, G. E. (2015). Neuronal development is promoted by weakened intrinsic antioxidant defences due to epigenetic repression of Nrf2. *Nature Communications*. <https://doi.org/10.1038/ncomms8066>
- Belousov, V. V., Fradkov, A. F., Lukyanov, K. A., Staroverov, D. B., Shakhbazov, K. S., Terskikh, A. V., & Lukyanov, S. (2006a). Genetically encoded fluorescent indicator for intracellular hydrogen peroxide. *Nature Methods*, *3*(4), 281–286. <https://doi.org/10.1038/nmeth866>
- Belousov, V. V., Fradkov, A. F., Lukyanov, K. A., Staroverov, D. B., Shakhbazov, K. S., Terskikh, A. V., & Lukyanov, S. (2006b). Genetically encoded fluorescent indicator for intracellular hydrogen peroxide. *Nature Methods*. <https://doi.org/10.1038/nmeth866>
- Belousov, V. V., Fradkov, A. F., Lukyanov, K. A., Staroverov, D. B., Shakhbazov, K. S., Terskikh,

- A. V., & Lukyanov, S. (2014). Red fluorescent genetically encoded indicator for intracellular hydrogen peroxide. *Nature Methods*, 3(4), 281–286. <https://doi.org/10.1038/nmeth866>
- Bender, A., Desplats, P., Spencer, B., Rockenstein, E., Adame, A., Elstner, M., ... Masliah, E. (2013). TOM40 Mediates Mitochondrial Dysfunction Induced by  $\alpha$ -Synuclein Accumulation in Parkinson's Disease. *PLoS ONE*. <https://doi.org/10.1371/journal.pone.0062277>
- Berg, J., Hung, Y. P., & Yellen, G. (2009). A genetically encoded fluorescent reporter of ATP:ADP ratio. *Nature Methods*. <https://doi.org/10.1038/nmeth.1288>
- Bertler, Å., & Rosengren, E. (1959). Occurrence and distribution of dopamine in brain and other tissues. *Experientia*. <https://doi.org/10.1007/BF02157069>
- Betarbet, R., Sherer, T. B., MacKenzie, G., Garcia-Osuna, M., Panov, A. V., & Greenamyre, J. T. (2000). Chronic systemic pesticide exposure reproduces features of Parkinson's disease. *Nature Neuroscience*. <https://doi.org/10.1038/81834>
- Bhatia, T. N., Pant, D. B., Eckhoff, E. A., Gongaware, R. N., Do, T., Hutchison, D. F., ... Leak, R. K. (2019). Astrocytes do not forfeit their neuroprotective roles after surviving intense oxidative stress. *Frontiers in Molecular Neuroscience*, 12(April), 1–12. <https://doi.org/10.3389/fnmol.2019.00087>
- Birben, E., Murat, U., Md, S., Sackesen, C., Erzurum, S., & Kalayci, O. (2012). Oxidative Stress and Antioxidant Defense. *WAO Journal*, 5(January), 9–19. <https://doi.org/10.1097/WOX.0b013e3182439613>
- Biskup, S., Moore, D. J., Celsi, F., Higashi, S., West, A. B., Andrabi, S. A., ... Dawson, V. L. (2006). Localization of LRRK2 to membranous and vesicular structures in mammalian brain. *Annals of Neurology*. <https://doi.org/10.1002/ana.21019>
- Björnberg, O., Østergaard, H., & Winther, J. R. (2006). Mechanistic insight provided by glutaredoxin within a fusion to redox-sensitive yellow fluorescent protein. *Biochemistry*. <https://doi.org/10.1021/bi0522495>
- Bodin, P., & Burnstock, G. (1996). ATP-stimulated release of ATP by human endothelial cells. *Journal of Cardiovascular Pharmacology*. <https://doi.org/10.1097/00005344-199606000-00015>
- Bolaños, J. P. (2016). Bioenergetics and redox adaptations of astrocytes to neuronal activity. *Journal of Neurochemistry*, 139, 115–125. <https://doi.org/10.1111/jnc.13486>
- Booth, D. M., Enyedi, B., Geiszt, M., Várnai, P., & Hajnóczky, G. (2016). Redox Nanodomains Are Induced by and Control Calcium Signaling at the ER-Mitochondrial Interface. *Molecular Cell*, 63(2), 240–248. <https://doi.org/10.1016/j.molcel.2016.05.040>
- Bowser, D. N., & Khakh, B. S. (2007). Vesicular ATP is the predominant cause of intercellular

- calcium waves in astrocytes. *Journal of General Physiology*.  
<https://doi.org/10.1085/jgp.200709780>
- Braeckman, B. P., Smolders, A., Back, P., & De Henau, S. (2016). In Vivo Detection of Reactive Oxygen Species and Redox Status in *Caenorhabditis elegans*. *Antioxidants and Redox Signaling*. <https://doi.org/10.1089/ars.2016.6751>
- Breckwoldt, M. O., Wittmann, C., Misgeld, T., Kerschensteiner, M., & Grabher, C. (2015). Redox imaging using genetically encoded redox indicators in zebrafish and mice. *Biological Chemistry*. <https://doi.org/10.1515/hsz-2014-0294>
- Brown, P., & Dale, N. (2002). Spike-independent release of ATP from *Xenopus* spinal neurons evoked by activation of glutamate receptors. *Journal of Physiology*. <https://doi.org/10.1113/jphysiol.2001.013193>
- Burma, N. E., Bonin, R. P., Leduc-Pessah, H., Baimel, C., Cairncross, Z. F., Mousseau, M., ... Trang, T. (2017). Blocking microglial pannexin-1 channels alleviates morphine withdrawal in rodents. *Nature Medicine*. <https://doi.org/10.1038/nm.4281>
- Burnstock, G. (2006a). Historical review: ATP as a neurotransmitter. *Trends in Pharmacological Sciences*, 27(3 SPEC. ISS.), 166–176. <https://doi.org/10.1016/j.tips.2006.01.005>
- Burnstock, G. (2006b). Purinergic signalling. *British Journal of Pharmacology*. <https://doi.org/10.1038/sj.bjp.0706429>
- Burton, E. A., Lanz, T. A., Keeney, M. T., Greenamyre, J. T., Sanders, L. H., Zharikov, A., ... De Miranda, B. R. (2018). LRRK2 activation in idiopathic Parkinson's disease. *Science Translational Medicine*, 10(451), eaar5429. <https://doi.org/10.1126/scitranslmed.aar5429>
- Bylicky, M. A., Mueller, G. P., & Day, R. M. (2018). Mechanisms of Endogenous Neuroprotective Effects of Astrocytes in Brain Injury. *Oxidative Medicine and Cellular Longevity*, 2018, 1–16. <https://doi.org/10.1155/2018/6501031>
- Cadet, J., & Richard Wagner, J. (2013). DNA base damage by reactive oxygen species, oxidizing agents, and UV radiation. *Cold Spring Harbor Perspectives in Biology*. <https://doi.org/10.1101/cshperspect.a012559>
- Candas, D., & Li, J. J. (2014). MnSOD in oxidative stress response-potential regulation via mitochondrial protein influx. *Antioxidants and Redox Signaling*. <https://doi.org/10.1089/ars.2013.5305>
- Carlsson, A., Lindqvist, M., Magnusson, T., & Waldeck, B. (1958). On the presence of 3-hydroxytyramine in brain. *Science*. <https://doi.org/10.1126/science.127.3296.471>
- Cekic, C., & Linden, J. (2016). Purinergic regulation of the immune system. *Nature Reviews Immunology*. <https://doi.org/10.1038/nri.2016.4>
- Chang, M. C. Y., Pralle, A., Isacoff, E. Y., & Chang, C. J. (2004). A selective, cell-permeable

- optical probe for hydrogen peroxide in living cells. *Journal of the American Chemical Society*. <https://doi.org/10.1021/ja0441716>
- Charcot, J. M., Bourneville, & Brissaud, E. (1887). Oeuvres completes de J.M. Charcot: lecons sur les localisations dans les maladies du cerveau et de la moelle epiniere. *Bureaux Du Progres Medical*.
- Charlton, S. J., Brown, C. A., Weisman, G. A., Turner, J. T., Erb, L., & Boarder, M. R. (1996). PPADS and suramin as antagonists at cloned P2Y- and P2U-purinoceptors. *British Journal of Pharmacology*. <https://doi.org/10.1111/j.1476-5381.1996.tb15457.x>
- Chekeni, F. B., Elliott, M. R., Sandilos, J. K., Walk, S. F., Kinchen, J. M., Lazarowski, E. R., ... Ravichandran, K. S. (2010). Pannexin 1 channels mediate “find-me” signal release and membrane permeability during apoptosis. *Nature*. <https://doi.org/10.1038/nature09413>
- Chen, T. W., Wardill, T. J., Sun, Y., Pulver, S. R., Renninger, S. L., Baohan, A., ... Kim, D. S. (2013). Ultrasensitive fluorescent proteins for imaging neuronal activity. *Nature*. <https://doi.org/10.1038/nature12354>
- Chen, X., Zhong, Z., Xu, Z., Chen, L., & Wang, Y. (2010). 2',7'-Dichlorodihydrofluorescein as a fluorescent probe for reactive oxygen species measurement: Forty years of application and controversy. *Free Radical Research*, 44(6), 587–604. <https://doi.org/10.3109/10715761003709802>
- Chen, Y., Corriden, R., Inoue, Y., Yip, L., Hashiguchi, N., Zinkernagel, A., ... Junger, W. G. (2006). ATP release guides neutrophil chemotaxis via P2Y2 and A3 receptors. *Science*. <https://doi.org/10.1126/science.1132559>
- Cheng, Y., Hao, Y., You, J., Yin, X., Feng, L., Ma, D., ... Xin, M. (2018). Astrocytic gap junction inhibition by carbenoxolone enhances the protective effects of ischemic preconditioning following cerebral ischemia. *Journal of Neuroinflammation*, 15(1), 1–12. <https://doi.org/10.1186/s12974-018-1230-5>
- Cheung, Y. T., Lau, W. K. W., Yu, M. S., Lai, C. S. W., Yeung, S. C., So, K. F., & Chang, R. C. C. (2009). Effects of all-trans-retinoic acid on human SH-SY5Y neuroblastoma as in vitro model in neurotoxicity research. *NeuroToxicology*, 30(1), 127–135. <https://doi.org/10.1016/j.neuro.2008.11.001>
- Choi, H. W., & Barakat, A. I. (2010). Computational Modeling of ATP/ADP Concentration at the Vascular Surface. In *Computational Modeling in Biomechanics* (pp. 49–67). Dordrecht: Springer Netherlands. [https://doi.org/10.1007/978-90-481-3575-2\\_2](https://doi.org/10.1007/978-90-481-3575-2_2)
- Coddou, C., Yan, Z., Obsil, T., Pablo Huidobro-Toro, J., & Stojilkovic, S. S. (2011). Activation and regulation of purinergic P2X receptor channels. *Pharmacological Reviews*. <https://doi.org/10.1124/pr.110.003129>

- Coloma, M. J., Hastings, A., Wims, L. A., & Morrison, S. L. (1992). Novel vectors for the expression of antibody molecules using variable regions generated by polymerase chain reaction. *Journal of Immunological Methods*. [https://doi.org/10.1016/0022-1759\(92\)90092-8](https://doi.org/10.1016/0022-1759(92)90092-8)
- Cookson, M. R. (2016a). Cellular functions of LRRK2 implicate vesicular trafficking pathways in Parkinson's disease. *Biochemical Society Transactions*. <https://doi.org/10.1042/BST20160228>
- Cookson, M. R. (2016b). Structure, function, and leucine-rich repeat kinase 2: On the importance of reproducibility in understanding Parkinson's disease. *Proceedings of the National Academy of Sciences*, *113*(30), 8346–8348. <https://doi.org/10.1073/pnas.1609311113>
- Cooper, O., Seo, H., Andrabi, S., Guardia-Laguarta, C., Graziotto, J., Sundberg, M., ... Isacson, O. (2012). Pharmacological rescue of mitochondrial deficits in iPSC-derived neural cells from patients with familial Parkinson's disease. *Science Translational Medicine*. <https://doi.org/10.1126/scitranslmed.3003985>
- Corriden, R., & Insel, P. A. (2010a). Basal release of ATP: an autocrine-paracrine mechanism for cell regulation. *Science Signaling*, *3*(104), re1. <https://doi.org/10.1126/scisignal.3104re1>
- Corriden, R., & Insel, P. A. (2010b). Basal release of ATP: An autocrine-paracrine mechanism for cell regulation. *Science Signaling*. <https://doi.org/10.1126/scisignal.3104re1>
- Coyle, J. T., & Puttfarcken, P. (1993). Oxidative stress, glutamate, and neurodegenerative disorders. *Science*. <https://doi.org/10.1126/science.7901908>
- Dana, H., Mohar, B., Sun, Y., Narayan, S., Gordus, A., Hasseman, J. P., ... Kim, D. S. (2016). Sensitive red protein calcium indicators for imaging neural activity. *ELife*. <https://doi.org/10.7554/eLife.12727>
- Danquah, W., Catherine, M. S., Rissiek, B., Pinto, C., Arnau, S. P., Amadi, M., ... Friedrich, K. N. (2016). Nanobodies that block gating of the P2X7 ion channel ameliorate inflammation. *Science Translational Medicine*. <https://doi.org/10.1126/scitranslmed.aaf8463>
- Davalos, D., Grutzendler, J., Yang, G., Kim, J. V., Zuo, Y., Jung, S., ... Gan, W. B. (2005a). ATP mediates rapid microglial response to local brain injury in vivo. *Nature Neuroscience*. <https://doi.org/10.1038/nn1472>
- Davalos, D., Grutzendler, J., Yang, G., Kim, J. V., Zuo, Y., Jung, S., ... Gan, W.-B. (2005b). ATP mediates rapid microglial response to local brain injury in vivo. *Nature Neuroscience*, *8*(6), 752–758. <https://doi.org/10.1038/nn1472>
- Davies, M. J. (2016, April 1). Protein oxidation and peroxidation. *Biochemical Journal*. Portland Press Ltd. <https://doi.org/10.1042/BJ20151227>
- de Bundel, D., Schallier, A. S., Loyens, E., Fernando, R., Miyashita, H., van Liefferinge, J., ... Massie, A. (2011). Loss of system xc- does not induce oxidative stress but decreases extracellular glutamate in hippocampus and influences spatial working memory and limbic

- seizure susceptibility. *Journal of Neuroscience*. <https://doi.org/10.1523/JNEUROSCI.5465-10.2011>
- Deng, H., Le, W. D., Guo, Y., Hunter, C. B., Xie, W. J., Huang, M. S., & Jankovic, J. (2006). Genetic analysis of LRRK2 mutations in patients with Parkinson disease. *Journal of the Neurological Sciences*. <https://doi.org/10.1016/j.jns.2006.09.017>
- Devi, L., Raghavendran, V., Prabhu, B. M., Avadhani, N. G., & Anandatheerthavarada, H. K. (2008). Mitochondrial import and accumulation of  $\alpha$ -synuclein impair complex I in human dopaminergic neuronal cultures and Parkinson disease brain. *Journal of Biological Chemistry*. <https://doi.org/10.1074/jbc.M710012200>
- Dey, S., Sidor, A., & O'Rourke, B. (2016). Compartment-specific control of reactive oxygen species scavenging by antioxidant pathway enzymes. *Journal of Biological Chemistry*, 291(21), 11185–11197. <https://doi.org/10.1074/jbc.M116.726968>
- Dickinson, B. C., & Chang, C. J. (2011). Chemistry and biology of reactive oxygen species in signaling or stress responses. *Nature Chemical Biology*. <https://doi.org/10.1038/nchembio.607>
- Dodson, M. W., Zhang, T., Jiang, C., Chen, S., & Guo, M. (2012). Roles of the Drosophila LRRK2 homolog in Rab7-dependent lysosomal positioning. *Human Molecular Genetics*. <https://doi.org/10.1093/hmg/ddr573>
- Dooley, C. T., Dore, T. M., Hanson, G. T., Jackson, W. C., Remington, S. J., & Tsien, R. Y. (2004). Imaging dynamic redox changes in mammalian cells with green fluorescent protein indicators. *Journal of Biological Chemistry*. <https://doi.org/10.1074/jbc.M312847200>
- Douglas Fields, R. (2011). Imaging single photons and intrinsic optical signals for studies of vesicular and non-vesicular ATP release from axons. *Frontiers in Neuroanatomy*. <https://doi.org/10.3389/fnana.2011.00032>
- Dringen, R., Pfeiffer, B., & Hamprecht, B. (1999). Synthesis of the Antioxidant Glutathione in Neurons: Supply by Astrocytes of CysGly as Precursor for Neuronal Glutathione. *The Journal of Neuroscience*, 19(2), 562–569. <https://doi.org/10.1523/JNEUROSCI.19-02-00562.1999>
- Dryanovski, D. I., Guzman, J. N., Xie, Z., Galteri, D. J., Volpicelli-Daley, L. A., Lee, V. M. Y., ... James Surmeier, D. (2013). Calcium entry and  $\alpha$ -synuclein inclusions elevate dendritic mitochondrial oxidant stress in dopaminergic neurons. *Journal of Neuroscience*. <https://doi.org/10.1523/JNEUROSCI.5311-12.2013>
- Dugan, L. L., Sensi, S. L., Canzoniero, L. M. T., Handran, S. D., Rothman, S. M., Lin -, T. S., ... Choi, D. W. (1995). Mitochondrial production of reactive oxygen species in cortical neurons

- following exposure to N-methyl-D-aspartate. *Journal of Neuroscience*, 15(10), 6377–6388. <https://doi.org/10.1523/jneurosci.15-10-06377.1995>
- Dusonchet, J., Kochubey, O., Stafa, K., Young, S. M., Zufferey, R., Moore, D. J., ... Aebischer, P. (2011). A rat model of progressive nigral neurodegeneration induced by the Parkinson's disease-associated G2019S mutation in LRRK2. *Journal of Neuroscience*. <https://doi.org/10.1523/JNEUROSCI.5092-10.2011>
- Edwards, D., Das, M., Molnar, P., & Hickman, J. J. (2010). Addition of glutamate to serum-free culture promotes recovery of electrical activity in adult hippocampal neurons in vitro. *Journal of Neuroscience Methods*. <https://doi.org/10.1016/j.jneumeth.2010.04.030>
- Ellerby, L. M., & Bredesen, D. E. (2000, January 1). Measurement of cellular oxidation, reactive oxygen species, and antioxidant enzymes during apoptosis. *Methods in Enzymology*. Academic Press Inc. [https://doi.org/10.1016/s0076-6879\(00\)22040-5](https://doi.org/10.1016/s0076-6879(00)22040-5)
- Elliott, M. R., Chekeni, F. B., Trampont, P. C., Lazarowski, E. R., Kadl, A., Walk, S. F., ... Ravichandran, K. S. (2009). Nucleotides released by apoptotic cells act as a find-me signal to promote phagocytic clearance. *Nature*. <https://doi.org/10.1038/nature08296>
- Eltzschig, H. K., Sitkovsky, M. V., & Robson, S. C. (2012). Purinergic signaling during inflammation. *New England Journal of Medicine*. <https://doi.org/10.1056/NEJMra1205750>
- Ermakova, Y. G., Bilan, D. S., Matlashov, M. E., Mishina, N. M., Markvicheva, K. N., Subach, O. M., ... Belousov, V. V. (2014). Red fluorescent genetically encoded indicator for intracellular hydrogen peroxide. *Nature Communications*, 5. <https://doi.org/10.1038/ncomms6222>
- Espinosa-Diez, C., Miguel, V., Mennerich, D., Kietzmann, T., Sánchez-Pérez, P., Cadenas, S., & Lamas, S. (2015). Antioxidant responses and cellular adjustments to oxidative stress. *Redox Biology*. <https://doi.org/10.1016/j.redox.2015.07.008>
- Evans, M. D., Dizdaroglu, M., & Cooke, M. S. (2004). Oxidative DNA damage and disease: Induction, repair and significance. *Mutation Research - Reviews in Mutation Research*. <https://doi.org/10.1016/j.mrrev.2003.11.001>
- Ezeriņa, D., Morgan, B., & Dick, T. P. (2014). Imaging dynamic redox processes with genetically encoded probes. *Journal of Molecular and Cellular Cardiology*, 73, 43–49. <https://doi.org/10.1016/j.yjmcc.2013.12.023>
- Fan, Y., & Ai, H. W. (2016). Development of redox-sensitive red fluorescent proteins for imaging redox dynamics in cellular compartments. *Analytical and Bioanalytical Chemistry*, 408(11), 2901–2911. <https://doi.org/10.1007/s00216-015-9280-3>
- Fan, Y., Chen, Z., & Ai, H. W. (2015). Monitoring Redox dynamics in living cells with a redox-sensitive red fluorescent protein. *Analytical Chemistry*, 87(5), 2802–2810.

<https://doi.org/10.1021/ac5041988>

- Fan, Y., Makar, M., Wang, M. X., & Ai, H. W. (2017a). Monitoring thioredoxin redox with a genetically encoded red fluorescent biosensor. *Nature Chemical Biology*. <https://doi.org/10.1038/nchembio.2417>
- Fan, Y., Makar, M., Wang, M. X., & Ai, H. W. (2017b). Monitoring thioredoxin redox with a genetically encoded red fluorescent biosensor. *Nature Chemical Biology*, 13(9), 1045–1052. <https://doi.org/10.1038/nchembio.2417>
- Fernandez-Fernandez, S., Almeida, A., & Bolaños, J. P. (2012). Antioxidant and bioenergetic coupling between neurons and astrocytes. *Biochemical Journal*. <https://doi.org/10.1042/BJ20111943>
- Fernie, A. R., Carrari, F., & Sweetlove, L. J. (2004). Respiratory metabolism: Glycolysis, the TCA cycle and mitochondrial electron transport. *Current Opinion in Plant Biology*, 7(3), 254–261. <https://doi.org/10.1016/j.pbi.2004.03.007>
- Fields, R. D., & Burnstock, G. (2006). Purinergic signalling in neuron-glia interactions. *Nature Reviews Neuroscience*, 7(6), 423–436. <https://doi.org/10.1038/nrn1928>
- Filippin, L., Abad, M. C., Gastaldello, S., Magalhães, P. J., Sandonà, D., & Pozzan, T. (2005). Improved strategies for the delivery of GFP-based Ca<sup>2+</sup> sensors into the mitochondrial matrix. *Cell Calcium*. <https://doi.org/10.1016/j.ceca.2004.08.002>
- Finkel, T. (2011). Signal transduction by reactive oxygen species. *Journal of Cell Biology*. <https://doi.org/10.1083/jcb.201102095>
- Frigerio, F., Casimir, M., Carobbio, S., & Maechler, P. (2008). Tissue specificity of mitochondrial glutamate pathways and the control of metabolic homeostasis. *Biochimica et Biophysica Acta - Bioenergetics*, 1777(7–8), 965–972. <https://doi.org/10.1016/j.bbabi.2008.04.031>
- Gammon, K. (2014). Neurodegenerative disease: brain windfall. *Nature*. <https://doi.org/10.1038/nj7526-299a>
- Garcia, G. J. M., Picher, M., Zuo, P., Okada, S. F., Lazarowski, E. R., Button, B., ... Elston, T. C. (2015). Computational model for the regulation of extracellular ATP and adenosine in airway epithelia. *Subcellular Biochemistry*. [https://doi.org/10.1007/978-94-007-1217-1\\_3](https://doi.org/10.1007/978-94-007-1217-1_3)
- Ghiringhelli, F., Apetoh, L., Tesniere, A., Aymeric, L., Ma, Y., Ortiz, C., ... Zitvogel, L. (2009). Activation of the NLRP3 inflammasome in dendritic cells induces IL-1B-dependent adaptive immunity against tumors. *Nature Medicine*. <https://doi.org/10.1038/nm.2028>
- Glass, C. K., Saijo, K., Winner, B., Marchetto, M. C., & Gage, F. H. (2010). Mechanisms Underlying Inflammation in Neurodegeneration. *Cell*. <https://doi.org/10.1016/j.cell.2010.02.016>
- Gloeckner, C. J., Kinkl, N., Schumacher, A., Braun, R. J., O'Neill, E., Meitinger, T., ... Ueffing,

- M. (2006). The Parkinson disease causing LRRK2 mutation I2020T is associated with increased kinase activity. *Human Molecular Genetics*. <https://doi.org/10.1093/hmg/ddi439>
- Go, Y. M., & Jones, D. P. (2008a). Redox compartmentalization in eukaryotic cells. *Biochimica et Biophysica Acta - General Subjects*, 1780(11), 1273–1290. <https://doi.org/10.1016/j.bbagen.2008.01.011>
- Go, Y. M., & Jones, D. P. (2008b). Redox compartmentalization in eukaryotic cells. *Biochimica et Biophysica Acta - General Subjects*. <https://doi.org/10.1016/j.bbagen.2008.01.011>
- Goetz, C. G., Poewe, W., Rascol, O., & Sampaio, C. (2005). Evidence-based medical review update: Pharmacological and surgical treatments of Parkinson's disease: 2001 to 2004. *Movement Disorders*. <https://doi.org/10.1002/mds.20464>
- Goldberg, J. A., Guzman, J. N., Estep, C. M., Ilijic, E., Kondapalli, J., Sanchez-Padilla, J., & Surmeier, D. J. (2012). Calcium entry induces mitochondrial oxidant stress in vagal neurons at risk in Parkinson's disease. *Nature Neuroscience*. <https://doi.org/10.1038/nn.3209>
- Gómez-Villafuertes, R., García-Huerta, P., Díaz-Hernández, J. I., & Miras-Portugal, M. T. (2015). PI3K/Akt signaling pathway triggers P2X7 receptor expression as a pro-survival factor of neuroblastoma cells under limiting growth conditions. *Scientific Reports*, 5(November), 18417. <https://doi.org/10.1038/srep18417>
- Gourine, A. V., Kasymov, V., Marina, N., Tang, F., Figueiredo, M. F., Lane, S., ... Kasparov, S. (2010). Astrocytes control breathing through pH-dependent release of ATP. *Science*. <https://doi.org/10.1126/science.1190721>
- Groiss, S. J., Wojtecki, L., Sudmeyer, M., & Schnitzler, A. (2009). Deep brain stimulation in Parkinson-s disease. *Therapeutic Advances in Neurological Disorders*. <https://doi.org/10.1177/1756285609339382>
- Gronwald, R. G. K., Grant, F. J., Haldeman, B. A., Hart, C. E., O'Hara, P. J., Hagen, F. S., ... Murray, M. J. (1988). Cloning and expression of a cDNA coding for the human platelet-derived growth factor receptor: Evidence for more than one receptor class. *Proceedings of the National Academy of Sciences of the United States of America*. <https://doi.org/10.1073/pnas.85.10.3435>
- Gutiérrez-Martín, Y., Bustillo, D., Gómez-Villafuertes, R., Sánchez-Nogueiro, J., Torregrosa-Hetland, C., Binz, T., ... Artalejo, A. R. (2011). P2X7 receptors trigger ATP exocytosis and modify secretory vesicle dynamics in neuroblastoma cells. *Journal of Biological Chemistry*. <https://doi.org/10.1074/jbc.M110.139410>
- Gutscher, M., Pauleau, A.-L., Marty, L., Brach, T., Wabnitz, G. H., Samstag, Y., ... Dick, T. P. (2008). Real-time imaging of the intracellular glutathione redox potential. *Nature Methods*, 5(6), 553–559. <https://doi.org/10.1038/nmeth.1212>

- Gutscher, M., Sobotta, M. C., Wabnitz, G. H., Ballikaya, S., Meyer, A. J., Samstag, Y., & Dick, T. P. (2009). Proximity-based protein thiol oxidation by H<sub>2</sub>O<sub>2</sub>-scavenging peroxidases. *Journal of Biological Chemistry*. <https://doi.org/10.1074/jbc.M109.059246>
- Guzman, J. N., Sanchez-Padilla, J., Wokosin, D., Kondapalli, J., Ilijic, E., Schumacker, P. T., & Surmeier, D. J. (2010). Oxidant stress evoked by pacemaking in dopaminergic neurons is attenuated by DJ-1. *Nature*, *468*(7324), 696–700. <https://doi.org/10.1038/nature09536>
- Halliwell, B., & Gutteridge, J. M. C. (2015). *Free Radicals in Biology and Medicine*. *Free Radicals in Biology and Medicine*. <https://doi.org/10.1093/acprof:oso/9780198717478.001.0001>
- Halliwell, B., & Whiteman, M. (2004). Measuring reactive species and oxidative damage in vivo and in cell culture: How should you do it and what do the results mean? *British Journal of Pharmacology*. <https://doi.org/10.1038/sj.bjp.0705776>
- Han, P., Zhou, X. H., Chang, N., Xiao, C. L., Yan, S., Ren, H., ... Xiong, J. W. (2014). Hydrogen peroxide primes heart regeneration with a derepression mechanism. *Cell Research*. <https://doi.org/10.1038/cr.2014.108>
- Hanson, G. T., Aggeler, R., Oglesbee, D., Cannon, M., Capaldi, R. A., Tsien, R. Y., & Remington, S. J. (2004). Investigating Mitochondrial Redox Potential with Redox-sensitive Green Fluorescent Protein Indicators. *Journal of Biological Chemistry*, *279*(13), 13044–13053. <https://doi.org/10.1074/jbc.M312846200>
- Hao, L. Y., Giasson, B. I., & Bonini, N. M. (2010). DJ-1 is critical for mitochondrial function and rescues PINK1 loss of function. *Proceedings of the National Academy of Sciences of the United States of America*. <https://doi.org/10.1073/pnas.0911175107>
- Harischandra, D. S., Rokad, D., Neal, M. L., Ghaisas, S., Manne, S., Sarkar, S., ... Kanthasamy, A. G. (2019). Manganese promotes the aggregation and prion-like cell-to-cell exosomal transmission of  $\alpha$ -synuclein. *Science Signaling*. <https://doi.org/10.1126/scisignal.aau4543>
- Hashemi, S. H., Li, J. Y., Ahlman, H., & Dahlström, A. (2003). SSR2(a) receptor expression and adrenergic/cholinergic characteristics in differentiated SH-SY5Y cells. *Neurochemical Research*. <https://doi.org/10.1023/A:1022848718109>
- Hatcher-Martin, J. M., Gearing, M., Steenland, K., Levey, A. I., Miller, G. W., & Pennell, K. D. (2012). Association between polychlorinated biphenyls and Parkinson's disease neuropathology. *NeuroToxicology*. <https://doi.org/10.1016/j.neuro.2012.08.002>
- Hayashi, S., Hazama, A., Dutta, A. K., Sabirov, R. Z., & Okada, Y. (2004). Detecting ATP release by a biosensor method. *Science's STKE: Signal Transduction Knowledge Environment*. <https://doi.org/10.1126/stke.2582004p114>
- Haynes, S. E., Hollopeter, G., Yang, G., Kurpius, D., Dailey, M. E., Gan, W. B., & Julius, D. (2006). The P2Y<sub>12</sub> receptor regulates microglial activation by extracellular nucleotides. *Nature Neuroscience*. <https://doi.org/10.1038/nn1805>

- Heim, R., & Tsien, R. Y. (1996). Engineering green fluorescent protein for improved brightness, longer wavelengths and fluorescence resonance energy transfer. *Current Biology*. [https://doi.org/10.1016/S0960-9822\(02\)00450-5](https://doi.org/10.1016/S0960-9822(02)00450-5)
- Heitzer, T., Schlinzig, T., Krohn, K., Meinertz, T., & Münzel, T. (2001). Endothelial dysfunction, oxidative stress, and risk of cardiovascular events in patients with coronary artery disease. *Circulation*. <https://doi.org/10.1161/hc4601.099485>
- Heo, H. Y., Kim, K.-S., & Seol, W. (2010). Coordinate Regulation of Neurite Outgrowth by LRRK2 and Its Interactor, Rab5. *Experimental Neurobiology*. <https://doi.org/10.5607/en.2010.19.2.97>
- Herman, M. A., & Jahr, C. E. (2007). Extracellular glutamate concentration in hippocampal slice. *Journal of Neuroscience*, 27(36), 9736–9741. <https://doi.org/10.1523/JNEUROSCI.3009-07.2007>
- Higdon, A., Diers, A. R., Oh, J. Y., Landar, A., & Darley-Usmar, V. M. (2012). Cell signalling by reactive lipid species: New concepts and molecular mechanisms. *Biochemical Journal*. <https://doi.org/10.1042/BJ20111752>
- Hires, S. A., Zhu, Y., & Tsien, R. Y. (2008). Optical measurement of synaptic glutamate spillover and reuptake by linker optimized glutamate-sensitive fluorescent reporters. *Proceedings of the National Academy of Sciences of the United States of America*. <https://doi.org/10.1073/pnas.0712008105>
- Hirrlinger, J., Schulz, J. B., & Dringen, R. (2002). Glutathione release from cultured brain cells: Multidrug resistance protein 1 mediates the release of GSH from rat astroglial cells. *Journal of Neuroscience Research*, 69(3), 318–326. <https://doi.org/10.1002/jnr.10308>
- Ho, D. H., Je, A. R., Lee, H., Son, I., Kweon, H. S., Kim, H. G., & Seol, W. (2018). LRRK2 kinase activity induces mitochondrial fission in microglia via Drp1 and modulates neuroinflammation. *Experimental Neurobiology*. <https://doi.org/10.5607/en.2018.27.3.171>
- Hou, Y., Ouyang, X., Wan, R., Cheng, H., Mattson, M. P., & Cheng, A. (2012). Mitochondrial superoxide production negatively regulates neural progenitor proliferation and cerebral cortical development. *Stem Cells*, 30(11), 2535–2547. <https://doi.org/10.1002/stem.1213>
- Hsieh, C. H., Shaltouki, A., Gonzalez, A. E., Bettencourt da Cruz, A., Burbulla, L. F., St. Lawrence, E., ... Wang, X. (2016). Functional Impairment in Miro Degradation and Mitophagy Is a Shared Feature in Familial and Sporadic Parkinson's Disease. *Cell Stem Cell*, 19(6), 709–724. <https://doi.org/10.1016/j.stem.2016.08.002>
- Hsu, L J, Sagara, Y., Arroyo, A., Rockenstein, E., Sisk, A., Mallory, M., ... Masliah, E. (2000). Alpha-Synuclein Promotes Mitochondrial Deficit and Oxidative Stress. *The American Journal of Pathology*, 157(2), 401–410. [https://doi.org/10.1016/S0002-9440\(10\)64553-1](https://doi.org/10.1016/S0002-9440(10)64553-1)

- Hsu, Leigh J., Sagara, Y., Arroyo, A., Rockenstein, E., Sisk, A., Mallory, M., ... Masliah, E. (2000). A-Synuclein Promotes Mitochondrial Deficit and Oxidative Stress. *American Journal of Pathology*, 157(2), 401–410. [https://doi.org/10.1016/S0002-9440\(10\)64553-1](https://doi.org/10.1016/S0002-9440(10)64553-1)
- Hughes, A. J., Daniel, S. E., Kilford, L., & Lees, A. J. (1992). Accuracy of clinical diagnosis of idiopathic Parkinson's disease: A clinico-pathological study of 100 cases. *Journal of Neurology Neurosurgery and Psychiatry*. <https://doi.org/10.1136/jnnp.55.3.181>
- Hung, C. H.-L., Cheng, S. S.-Y., Cheung, Y.-T., Wuwongse, S., Zhang, N. Q., Ho, Y.-S., ... Chang, R. C.-C. (2018). A reciprocal relationship between reactive oxygen species and mitochondrial dynamics in neurodegeneration. *Redox Biology*, 14(July 2017), 7–19. <https://doi.org/10.1016/j.redox.2017.08.010>
- Ibrahimi, A., Velde, G. Vande, Reumers, V., Toelen, J., Thiry, I., Vandeputte, C., ... Gijssbers, R. (2009). Highly efficient multicistronic lentiviral vectors with peptide 2A sequences. *Human Gene Therapy*. <https://doi.org/10.1089/hum.2008.188>
- Idzko, M., Ferrari, D., & Eltzschig, H. K. (2014). Nucleotide signalling during inflammation. *Nature*. <https://doi.org/10.1038/nature13085>
- Iglesias, R. M., & Spray, D. C. (2012). Pannexin1-mediated ATP release provides signal transmission between Neuro2A cells. *Neurochemical Research*. <https://doi.org/10.1007/s11064-012-0720-6>
- Imamura, H., Nhat, K. P., Togawa, H., Saito, K., Iino, R., Kato-Yamada, Y., ... Noji, H. (2009). Visualization of ATP levels inside single living cells with fluorescence resonance energy transfer-based genetically encoded indicators. *Proc Natl Acad Sci U S A*, 106(37), 15651–15656. <https://doi.org/10.1073/pnas.0904764106>
- Imamura, Hiromi, Huynh Nhat, K. P., Togawa, H., Saito, K., Iino, R., Kato-Yamada, Y., ... Noji, H. (2009). Visualization of ATP levels inside single living cells with fluorescence resonance energy transfer-based genetically encoded indicators. *Proceedings of the National Academy of Sciences of the United States of America*. <https://doi.org/10.1073/pnas.0904764106>
- Inoue, M., Takeuchi, A., Horigane, S. I., Ohkura, M., Gengyo-Ando, K., Fujii, H., ... Bito, H. (2014). Rational design of a high-affinity, fast, red calcium indicator R-CaMP2. *Nature Methods*. <https://doi.org/10.1038/nmeth.3185>
- Iqbal, A., Arslan, S., Okumus, B., Wilson, T. J., Giraud, G., Norman, D. G., ... Lilley, D. M. J. (2008). Orientation dependence in fluorescent energy transfer between Cy3 and Cy5 terminally attached to double-stranded nucleic acids. *Proceedings of the National Academy of Sciences of the United States of America*. <https://doi.org/10.1073/pnas.0801707105>
- Janssen-Heininger, Y. M. W., Mossman, B. T., Heintz, N. H., Forman, H. J., Kalyanaraman, B., Finkel, T., ... van der Vliet, A. (2008). Redox-based regulation of signal transduction: Principles, pitfalls, and promises. *Free Radical Biology and Medicine*, 45(1), 1–17. <https://doi.org/10.1016/j.freeradbiomed.2008.03.011>

- Jin, S. M., & Youle, R. J. (2012). PINK1-and Parkin-mediated mitophagy at a glance. *Journal of Cell Science*. <https://doi.org/10.1242/jcs.093849>
- Jones, D. P., Go, Y.-M., Anderson, C. L., Ziegler, T. R., Kinkade, J. M., & Kirilin, W. G. (2004). Cysteine/cystine couple is a newly recognized node in the circuitry for biologic redox signaling and control. *The FASEB Journal*. <https://doi.org/10.1096/fj.03-0971fje>
- Junger, W. G. (2011). Immune cell regulation by autocrine purinergic signalling. *Nature Reviews Immunology*. <https://doi.org/10.1038/nri2938>
- Kamata, H., Honda, S. I., Maeda, S., Chang, L., Hirata, H., & Karin, M. (2005). Reactive oxygen species promote TNF $\alpha$ -induced death and sustained JNK activation by inhibiting MAP kinase phosphatases. *Cell*, 120(5), 649–661. <https://doi.org/10.1016/j.cell.2004.12.041>
- Kamp, F., Exner, N., Lutz, A. K., Wender, N., Hegermann, J., Brunner, B., ... Haass, C. (2010). Inhibition of mitochondrial fusion by  $\alpha$ -synuclein is rescued by PINK1, Parkin and DJ-1. *EMBO Journal*. <https://doi.org/10.1038/emboj.2010.223>
- Keeney, P. M. (2006). Parkinson's Disease Brain Mitochondrial Complex I Has Oxidatively Damaged Subunits and Is Functionally Impaired and Misassembled. *Journal of Neuroscience*, 26(19), 5256–5264. <https://doi.org/10.1523/JNEUROSCI.0984-06.2006>
- Khacho, M., Clark, A., Svoboda, D. S., Azzi, J., MacLaurin, J. G., Meghaizel, C., ... Slack, R. S. (2016). Mitochondrial Dynamics Impacts Stem Cell Identity and Fate Decisions by Regulating a Nuclear Transcriptional Program. *Cell Stem Cell*. <https://doi.org/10.1016/j.stem.2016.04.015>
- Khakh, B. S., & North, R. A. (2012). Neuromodulation by Extracellular ATP and P2X Receptors in the CNS. *Neuron*. <https://doi.org/10.1016/j.neuron.2012.09.024>
- Kiebertz, K., & Wunderle, K. B. (2013). Parkinson's disease: Evidence for environmental risk factors. *Movement Disorders*. <https://doi.org/10.1002/mds.25150>
- Klein, C., & Westenberger, A. (2012a). Genetics of Parkinson's disease. *Cold Spring Harbor Perspectives in Medicine*. <https://doi.org/10.1101/cshperspect.a008888>
- Klein, C., & Westenberger, A. (2012b). Genetics of Parkinson's disease. *Cold Spring Harbor Perspectives in Medicine*, 2(1). <https://doi.org/10.1101/cshperspect.a008888>
- Kolossov, V. L., Beaudoin, J. N., Ponnuraj, N., Diliberto, S. J., Hanafin, W. P., Kenis, P. J. A., & Rex Gaskins, H. (2015). Thiol-based antioxidants elicit mitochondrial oxidation via respiratory complex III. *American Journal of Physiology - Cell Physiology*, 309(2), C81–C91. <https://doi.org/10.1152/ajpcell.00006.2015>
- Korecka, J. A., van Kesteren, R. E., Blaas, E., Spitzer, S. O., Kamstra, J. H., Smit, A. B., ... Bossers, K. (2013). Phenotypic Characterization of Retinoic Acid Differentiated SH-SY5Y Cells by Transcriptional Profiling. *PLoS ONE*. <https://doi.org/10.1371/journal.pone.0063862>

- Kovalevich, J., & Langford, D. (2013). Considerations for the use of SH-SY5Y neuroblastoma cells in neurobiology. *Methods in Molecular Biology*. [https://doi.org/10.1007/978-1-62703-640-5\\_2](https://doi.org/10.1007/978-1-62703-640-5_2)
- Kraft, A. D. (2004). Nuclear Factor E2-Related Factor 2-Dependent Antioxidant Response Element Activation by tert-Butylhydroquinone and Sulforaphane Occurring Preferentially in Astrocytes Conditions Neurons against Oxidative Insult. *Journal of Neuroscience*, 24(5), 1101–1112. <https://doi.org/10.1523/JNEUROSCI.3817-03.2004>
- Kurishita, Y., Kohira, T., Ojida, A., & Hamachi, I. (2012). Organelle-localizable fluorescent chemosensors for site-specific multicolor imaging of nucleoside polyphosphate dynamics in living cells. *Journal of the American Chemical Society*. <https://doi.org/10.1021/ja308754g>
- Kushnareva, Y. E., Wiley, S. E., Ward, M. W., Andreyev, A. Y., & Murphy, A. N. (2005). Excitotoxic injury to mitochondria isolated from cultured neurons. *Journal of Biological Chemistry*. <https://doi.org/10.1074/jbc.M503090200>
- Lakshmi, S., & Joshi, P. G. (2006). Activation of src/kinase/phospholipase c/mitogenactivated protein kinase and induction of neurite expression by ATP, independent of nerve growth factor. *Neuroscience*. <https://doi.org/10.1016/j.neuroscience.2006.03.074>
- Lam, A. J., St-Pierre, F., Gong, Y., Marshall, J. D., Cranfill, P. J., Baird, M. A., ... Lin, M. Z. (2012). Improving FRET dynamic range with bright green and red fluorescent proteins. *Nature Methods*, 9(10), 1005–1012. <https://doi.org/10.1038/nmeth.2171>
- Langston, J., Ballard, P., Tetrud, J., & Irwin, I. (1983). Chronic Parkinsonism in humans due to a product of meperidine-analog synthesis. *Science*. <https://doi.org/10.1126/science.6823561>
- Langston, J. W. (2017). The MPTP story. *Journal of Parkinson's Disease*, 7, S11–S19. <https://doi.org/10.3233/JPD-179006>
- Langston, J. W., & Ballard, P. A. (1983). Parkinson's Disease in a Chemist Working with 1-Methyl-4-Phenyl-L,2,5,6-Tetrahydropyridine. *New England Journal of Medicine*. <https://doi.org/10.1056/NEJM198308043090511>
- Larsson, N. G., Wang, J., Wilhelmsson, H., Oldfors, A., Rustin, P., Lewandoski, M., ... Clayton, D. a. (1998). Length of huntingtin and its polyglutamine tract influences localization and frequency of intracellular aggregates. *Nature Genetics*. <https://doi.org/10.1038/ng0598-51>
- Lazarowski, E. R. (2012). Vesicular and conductive mechanisms of nucleotide release. *Purinergic Signalling*, 8(3), 359–373. <https://doi.org/10.1007/s11302-012-9304-9>
- Lazarowski, E. R., Boucher, R. C., & Harden, T. K. (2003). Mechanisms of release of nucleotides and integration of their action as P2X- and P2Y-receptor activating molecules. *Molecular Pharmacology*. <https://doi.org/10.1124/mol.64.4.785>

- Ledderose, C., Bao, Y., Lidicky, M., Zipperle, J., Li, L., Strasser, K., ... Junger, W. G. (2014). Mitochondria are gate-keepers of T cell function by producing the ATP that drives purinergic signaling. *Journal of Biological Chemistry*. <https://doi.org/10.1074/jbc.M114.575308>
- Lee, J. W., Tapias, V., Di Maio, R., Greenamyre, J. T., & Cannon, J. R. (2015). Behavioral, neurochemical, and pathologic alterations in bacterial artificial chromosome transgenic G2019S leucine-rich repeated kinase 2 rats. *Neurobiology of Aging*, *36*(1), 505–518. <https://doi.org/10.1016/j.neurobiolaging.2014.07.011>
- Lévesque, S. a, Lavoie, E. G., Lecka, J., Bigonnesse, F., & Sévigny, J. (2007). Specificity of the ecto-ATPase inhibitor ARL 67156 on human and mouse ectonucleotidases. *British Journal of Pharmacology*, *152*(1), 141–150. <https://doi.org/10.1038/sj.bjp.0707361>
- Levine, R. L., Garland, D., Oliver, C. N., Amici, A., Climent, I., Lenz, A. G., ... Stadtman, E. R. (1990). Determination of Carbonyl Content in Oxidatively Modified Proteins. *Methods in Enzymology*. [https://doi.org/10.1016/0076-6879\(90\)86141-H](https://doi.org/10.1016/0076-6879(90)86141-H)
- Li, N., Ragheb, K., Lawler, G., Sturgis, J., Rajwa, B., Melendez, J. A., & Robinson, J. P. (2003). Mitochondrial complex I inhibitor rotenone induces apoptosis through enhancing mitochondrial reactive oxygen species production. *Journal of Biological Chemistry*. <https://doi.org/10.1074/jbc.M210432200>
- Li, X., Patel, J. C., Wang, J., Avshalumov, M. V., Nicholson, C., Buxbaum, J. D., ... Yue, Z. (2010). Enhanced striatal dopamine transmission and motor performance with LRRK2 overexpression in mice is eliminated by familial Parkinson's disease mutation G2019S. *Journal of Neuroscience*. <https://doi.org/10.1523/JNEUROSCI.5604-09.2010>
- Li, Y., Liu, W., Oo, T. F., Wang, L., Tang, Y., Jackson-Lewis, V., ... Li, C. (2009). Mutant LRRK2R1441G BAC transgenic mice recapitulate cardinal features of Parkinson's disease. *Nature Neuroscience*. <https://doi.org/10.1038/nn.2349>
- Liemburg-Apers, D. C., Imamura, H., Forkink, M., Nootboom, M., Swarts, H. G., Brock, R., ... Koopman, W. J. H. (2011). Quantitative glucose and ATP sensing in mammalian cells. *Pharmaceutical Research*. <https://doi.org/10.1007/s11095-011-0492-8>
- Lin, M. T., & Beal, M. F. (2006). Mitochondrial dysfunction and oxidative stress in neurodegenerative diseases. *Nature*. <https://doi.org/10.1038/nature05292>
- Liou, A. K. F., Leak, R. K., Li, L., & Zigmond, M. J. (2008). Wild-type LRRK2 but not its mutant attenuates stress-induced cell death via ERK pathway. *Neurobiology of Disease*. <https://doi.org/10.1016/j.nbd.2008.06.016>
- Liu, H., Ho, P. W.-L., Leung, G. C., Lam, C. S., Pang, S. Y., Li, L., ... Ho, S.-L. (2017). Combined LRRK2 mutation, aging and chronic low dose oral rotenone as a model of Parkinson's disease. *Scientific Reports*, *7*(1), 40887. <https://doi.org/10.1038/srep40887>

- Liu, Z., Celotto, A. M., Romero, G., Wipf, P., & Palladino, M. J. (2012). Genetically encoded redox sensor identifies the role of ROS in degenerative and mitochondrial disease pathogenesis. *Neurobiology of Disease*. <https://doi.org/10.1016/j.nbd.2011.08.022>
- Llopis, J., McCaffery, J. M., Miyawaki, A., Farquhar, M. G., & Tsien, R. Y. (1998). Measurement of cytosolic, mitochondrial, and Golgi pH in single living cells with green fluorescent proteins. *Proceedings of the National Academy of Sciences of the United States of America*. <https://doi.org/10.1073/pnas.95.12.6803>
- Lohman, J. R., & Remington, S. J. (2008). Development of a family of redox-sensitive green fluorescent protein indicators for use in relatively oxidizing subcellular environments. *Biochemistry*, 47(33), 8678–8688. <https://doi.org/10.1021/bi800498g>
- Loo, J. M., Scherl, A., Nguyen, A., Man, F. Y., Weinberg, E., Zeng, Z., ... Tavazoie, S. F. (2015). Extracellular metabolic energetics can promote cancer progression. *Cell*. <https://doi.org/10.1016/j.cell.2014.12.018>
- Lopes, F. M., Schröder, R., Júnior, M. L. C. da F., Zanotto-Filho, A., Müller, C. B., Pires, A. S., ... Klamt, F. (2010). Comparison between proliferative and neuron-like SH-SY5Y cells as an in vitro model for Parkinson disease studies. *Brain Research*. <https://doi.org/10.1016/j.brainres.2010.03.102>
- Lorenz, V., Pinto, C. S., & Seifert, R. (2007). Complex changes in ecto-nucleoside 5'-triphosphate diphosphohydrolase expression in hypoxanthine phosphoribosyl transferase deficiency. *Neuroscience Letters*. <https://doi.org/10.1016/j.neulet.2007.04.004>
- Lou, N., Takano, T., Pei, Y., Xavier, A. L., Goldman, S. A., & Nedergaard, M. (2016). Purinergic receptor P2RY12-dependent microglial closure of the injured blood-brain barrier. *Proceedings of the National Academy of Sciences of the United States of America*. <https://doi.org/10.1073/pnas.1520398113>
- Lovatt, D., Xu, Q., Liu, W., Takano, T., Smith, N. A., Schnermann, J., ... Nedergaard, M. (2012). Neuronal adenosine release, and not astrocytic ATP release, mediates feedback inhibition of excitatory activity. *Proceedings of the National Academy of Sciences of the United States of America*. <https://doi.org/10.1073/pnas.1120997109>
- Lu, Y., Li, Q., Liu, Y. Y., Sun, K., Fan, J. Y., Wang, C. S., & Han, J. Y. (2015). Inhibitory effect of caffeic acid on ADP-induced thrombus formation and platelet activation involves mitogen-activated protein kinases. *Scientific Reports*. <https://doi.org/10.1038/srep13824>
- Lushchak, V. I. (2012). Glutathione Homeostasis and Functions: Potential Targets for Medical Interventions. *Journal of Amino Acids*, 2012, 1–26. <https://doi.org/10.1155/2012/736837>
- Luth, E. S., Stavrovskaya, I. G., Bartels, T., Kristal, B. S., & Selkoe, D. J. (2014). LRRK2 modulates vulnerability to mitochondrial dysfunction in *C. elegans*. *Journal of Biological Chemistry*. <https://doi.org/10.1074/jbc.M113.545749>

- MacDonald, C. L., Yu, D., Buibas, M., & Silva, G. A. (2008). Diffusion modeling of ATP signaling suggests a partially regenerative mechanism underlies astrocyte intercellular calcium waves. *Frontiers in Neuroengineering*. <https://doi.org/10.3389/neuro.16.001.2008>
- Magistretti, P. J., & Allaman, I. (2015). A Cellular Perspective on Brain Energy Metabolism and Functional Imaging. *Neuron*, *86*(4), 883–901. <https://doi.org/10.1016/j.neuron.2015.03.035>
- Mansfield, K. J., & Hughes, J. R. (2014). P2Y receptor modulation of ATP release in the urothelium. *BioMed Research International*. <https://doi.org/10.1155/2014/830374>
- Marras, C., Beck, J. C., Bower, J. H., Roberts, E., Ritz, B., Ross, G. W., ... Tanner, C. (2018). Prevalence of Parkinson's disease across North America. *Npj Parkinson's Disease*, *4*(1), 21. <https://doi.org/10.1038/s41531-018-0058-0>
- Martin, L. J. (1999). Neuronal death in amyotrophic lateral sclerosis is apoptosis: Possible contribution of a programmed cell death mechanism. *Journal of Neuropathology and Experimental Neurology*. <https://doi.org/10.1097/00005072-199905000-00005>
- Martindale, J. L., & Holbrook, N. J. (2002). Cellular response to oxidative stress: Signaling for suicide and survival. *Journal of Cellular Physiology*. <https://doi.org/10.1002/jcp.10119>
- Marvin, J. S., Borghuis, B. G., Tian, L., Cichon, J., Harnett, M. T., Akerboom, J., ... Looger, L. L. (2013). An optimized fluorescent probe for visualizing glutamate neurotransmission. *Nature Methods*. <https://doi.org/10.1038/nmeth.2333>
- Masgrau, R., Hurel, C., Papastefanaki, F., Georgopoulou, N., Thomaidou, D., & Matsas, R. (2009). BM88/Cend1 regulates stimuli-induced intracellular calcium mobilization. *Neuropharmacology*. <https://doi.org/10.1016/j.neuropharm.2008.10.015>
- Melani, A., Turchi, D., Vannucchi, M. G., Cipriani, S., Gianfriddo, M., & Pedata, F. (2005). ATP extracellular concentrations are increased in the rat striatum during in vivo ischemia. *Neurochemistry International*. <https://doi.org/10.1016/j.neuint.2005.05.014>
- Melrose, H. L., Dächsel, J. C., Behrouz, B., Lincoln, S. J., Yue, M., Hinkle, K. M., ... Farrer, M. J. (2010). Impaired dopaminergic neurotransmission and microtubule-associated protein tau alterations in human LRRK2 transgenic mice. *Neurobiology of Disease*. <https://doi.org/10.1016/j.nbd.2010.07.010>
- Meyer, A. J., Brach, T., Marty, L., Kreye, S., Rouhier, N., Jacquot, J. P., & Hell, R. (2007). Redox-sensitive GFP in *Arabidopsis thaliana* is a quantitative biosensor for the redox potential of the cellular glutathione redox buffer. *Plant Journal*. <https://doi.org/10.1111/j.1365-313X.2007.03280.x>
- Meyer, A. J., & Dick, T. P. (2010a). Fluorescent Protein-Based Redox Probes. *Antioxidants & Redox Signaling*, *13*(5), 621–650. <https://doi.org/10.1089/ars.2009.2948>
- Meyer, A. J., & Dick, T. P. (2010b). Fluorescent Protein-Based Redox Probes. *Antioxidants & Redox Signaling*, *13*(5), 621–650. <https://doi.org/10.1089/ars.2009.2948>

- Michaud, M., Martins, I., Sukkurwala, A. Q., Adjemian, S., Ma, Y., Pellegatti, P., ... Kroemer, G. (2011). Autophagy-dependent anticancer immune responses induced by chemotherapeutic agents in mice. *Science*. <https://doi.org/10.1126/science.1208347>
- Minich, T., Riemer, J., Schulz, J. B., Wielinga, P., Wijnholds, J., & Dringen, R. (2006). The multidrug resistance protein 1 (Mrp1), but not Mrp5, mediates export of glutathione and glutathione disulfide from brain astrocytes. *Journal of Neurochemistry*, *97*(2), 373–384. <https://doi.org/10.1111/j.1471-4159.2006.03737.x>
- Montgomery, E. B. (1995). Heavy metals and the etiology of Parkinson's disease and other movement disorders. *Toxicology*. [https://doi.org/10.1016/0300-483X\(94\)02962-T](https://doi.org/10.1016/0300-483X(94)02962-T)
- Morciano, G., Sarti, A. C., Marchi, S., Missiroli, S., Falzoni, S., Raffaghello, L., ... Pinton, P. (2017). Use of luciferase probes to measure ATP in living cells and animals. *Nature Protocols*. <https://doi.org/10.1038/nprot.2017.052>
- Morgan, B., Sobotta, M. C., & Dick, T. P. (2011). Measuring E GSH and H 2O 2 with roGFP2-based redox probes. *Free Radical Biology and Medicine*, *51*(11), 1943–1951. <https://doi.org/10.1016/j.freeradbiomed.2011.08.035>
- Mortiboys, H., Johansen, K. K., Aasly, J. O., & Bandmann, O. (2010). Mitochondrial impairment in patients with Parkinson disease with the G2019S mutation in LRRK2. *Neurology*. <https://doi.org/10.1212/WNL.0b013e3181ff9685>
- Munnamalai, V., & Suter, D. M. (2009). Reactive oxygen species regulate F-actin dynamics in neuronal growth cones and neurite outgrowth. *Journal of Neurochemistry*. <https://doi.org/10.1111/j.1471-4159.2008.05787.x>
- Murphy, M. P. (2012). Mitochondrial thiols in antioxidant protection and redox signaling: Distinct roles for glutathionylation and other thiol modifications. *Antioxidants and Redox Signaling*. <https://doi.org/10.1089/ars.2011.4289>
- Murphy, P. S., Wang, J., Bhagwat, S. P., Munger, J. C., Janssen, W. J., Wright, T. W., & Elliott, M. R. (2017). CD73 regulates anti-inflammatory signaling between apoptotic cells and endotoxin-conditioned tissue macrophages. *Cell Death and Differentiation*. <https://doi.org/10.1038/cdd.2016.159>
- Nagai, T., Sawano, A., Eun Sun Park, & Miyawaki, A. (2001). Circularly permuted green fluorescent proteins engineered to sense Ca<sup>2+</sup>. *Proceedings of the National Academy of Sciences of the United States of America*. <https://doi.org/10.1073/pnas.051636098>
- Neary, J. T., Kang, Y., Willoughby, K. A., & Ellis, E. F. (2003). Activation of extracellular signal-regulated kinase by stretch-induced injury in astrocytes involves extracellular ATP and P2 purinergic receptors. *Journal of Neuroscience*. <https://doi.org/10.1523/jneurosci.23-06-02348.2003>
- Newman, E. A. (2001). Propagation of intercellular calcium waves in retinal astrocytes and müler cells. *Journal of Neuroscience*. <https://doi.org/10.1523/jneurosci.21-07-02215.2001>

- Newman, E. A. (2003). Glial cell inhibition of neurons by release of ATP. *Journal of Neuroscience*. <https://doi.org/10.1523/jneurosci.23-05-01659.2003>
- Nguyen, H. N., Byers, B., Cord, B., Shcheglovitov, A., Byrne, J., Gujar, P., ... Pera, R. R. (2011). LRRK2 mutant iPSC-derived da neurons demonstrate increased susceptibility to oxidative stress. *Cell Stem Cell*, 8(3), 267–280. <https://doi.org/10.1016/j.stem.2011.01.013>
- Nicholls, D. G., Johnson-Cadwell, L., Vesce, S., Jekabsons, M., & Yadava, N. (2007). Bioenergetics of mitochondria in cultured neurons and their role in glutamate excitotoxicity. *Journal of Neuroscience Research*, 85(15), 3206–3212. <https://doi.org/10.1002/jnr.21290>
- Niu, J., Yu, M., Wang, C., & Xu, Z. (2012). Leucine-rich repeat kinase 2 disturbs mitochondrial dynamics via dynamin-like protein. *Journal of Neurochemistry*. <https://doi.org/10.1111/j.1471-4159.2012.07809.x>
- Norcross, S., Trull, K. J., Snaider, J., Doan, S., Tat, K., Huang, L., & Tantama, M. (2017). Extending roGFP Emission via Förster-Type Resonance Energy Transfer Relay Enables Simultaneous Dual Compartment Ratiometric Redox Imaging in Live Cells. *ACS Sensors*, 2(11), 1721–1729. <https://doi.org/10.1021/acssensors.7b00689>
- Okumoto, S., Looger, L. L., Micheva, K. D., Reimer, R. J., Smith, S. J., & Frommer, W. B. (2005). Detection of glutamate release from neurons by genetically encoded surface-displayed FRET nanosensors. *Proceedings of the National Academy of Sciences of the United States of America*. <https://doi.org/10.1073/pnas.0503274102>
- Østergaard, H., Henriksen, A., Hansen, F. G., & Winther, J. R. (2001a). Shedding light on disulfide bond formation: Engineering a redox switch in green fluorescent protein. *EMBO Journal*, 20(21), 5853–5862. <https://doi.org/10.1093/emboj/20.21.5853>
- Østergaard, H., Henriksen, A., Hansen, F. G., & Winther, J. R. (2001b). Shedding light on disulfide bond formation: Engineering a redox switch in green fluorescent protein. *EMBO Journal*. <https://doi.org/10.1093/emboj/20.21.5853>
- Paisán-Ruíz, C., Jain, S., Evans, E. W., Gilks, W. P., Simón, J., Van Der Brug, M., ... Singleton, A. B. (2004). Cloning of the gene containing mutations that cause PARK8-linked Parkinson's disease. *Neuron*. <https://doi.org/10.1016/j.neuron.2004.10.023>
- Panatier, A., Vallée, J., Haber, M., Murai, K. K., Lacaille, J. C., & Robitaille, R. (2011). Astrocytes are endogenous regulators of basal transmission at central synapses. *Cell*, 146(5), 785–798. <https://doi.org/10.1016/j.cell.2011.07.022>
- Pangršič, T., Potokar, M., Stenovec, M., Kreft, M., Fabbretti, E., Nistri, A., ... Zorec, R. (2007). Exocytotic release of ATP from cultured astrocytes. *Journal of Biological Chemistry*, 282(39), 28749–28758. <https://doi.org/10.1074/jbc.M700290200>
- Panieri, E., & Santoro, M. M. (2016). Ros homeostasis and metabolism: A dangerous liason in cancer cells. *Cell Death and Disease*. <https://doi.org/10.1038/cddis.2016.105>

- Papkovskaia, T. D., Chau, K. Y., Inesta-vaquera, F., Papkovsky, D. B., Healy, D. G., Nishio, K., Cooper, J. M. (2012). G2019s leucine-rich repeat kinase 2 causes uncoupling protein-mediated mitochondrial depolarization. *Human Molecular Genetics*, *21*(19), 4201–4213. <https://doi.org/10.1093/hmg/dds244>
- Parkinson, J. (1817). *An essay on shaking palsy*. Sherwood, Neely and Jones.
- Pellegatti, P., Falzoni, S., Pinton, P., Rizzuto, R., & Di Virgilio, F. (2005). A novel recombinant plasma membrane-targeted luciferase reveals a new pathway for ATP secretion. *Molecular Biology of the Cell*. <https://doi.org/10.1091/mbc.E05-03-0222>
- Pellegatti, P., Raffaghello, L., Bianchi, G., Piccardi, F., Pistoia, V., & Di Virgilio, F. (2008). Increased level of extracellular ATP at tumor sites: In vivo imaging with plasma membrane luciferase. *PLoS ONE*. <https://doi.org/10.1371/journal.pone.0002599>
- Pelletier, J., & Sonenberg, N. (1988). Internal initiation of translation of eukaryotic mRNA directed by a sequence derived from poliovirus RNA. *Nature*. <https://doi.org/10.1038/334320a0>
- Pham, E., Chiang, J., Li, I., Shum, W., & Truong, K. (2007). A Computational Tool for Designing FRET Protein Biosensors by Rigid-Body Sampling of Their Conformational Space. *Structure*. <https://doi.org/10.1016/j.str.2007.03.009>
- Piattoni, C. V., Sardi, F., Klein, F., Pantano, S., Bollati-Fogolin, M., & Comini, M. (2019). New red-shifted fluorescent biosensor for monitoring intracellular redox changes. *Free Radical Biology and Medicine*, *134*(January 2019), 545–554. <https://doi.org/10.1016/j.freeradbiomed.2019.01.035>
- Pietrocola, F., Pol, J., Vacchelli, E., Rao, S., Enot, D. P., Baracco, E. E., ... Kroemer, G. (2016). Caloric Restriction Mimetics Enhance Anticancer Immunosurveillance. *Cancer Cell*. <https://doi.org/10.1016/j.ccell.2016.05.016>
- Pougnat, J. T., Toulme, E., Martinez, A., Choquet, D., Hosy, E., & Boué-Grabot, E. (2014). ATP P2X receptors downregulate AMPA receptor trafficking and postsynaptic efficacy in hippocampal neurons. *Neuron*. <https://doi.org/10.1016/j.neuron.2014.06.005>
- Powers, K. M., Smith-Weller, T., Franklin, G. M., Longstreth, J. T., Swanson, P. D., & Checkoway, H. (2009). Dietary fats, cholesterol and iron as risk factors for Parkinson's disease. *Parkinsonism and Related Disorders*. <https://doi.org/10.1016/j.parkreldis.2008.03.002>
- Praetorius, H. A., & Leipziger, J. (2009). ATP release from non-excitabile cells. *Purinergic Signalling*. <https://doi.org/10.1007/s11302-009-9146-2>
- Rahman, I., Kode, A., & Biswas, S. K. (2007). Assay for quantitative determination of glutathione and glutathione disulfide levels using enzymatic recycling method. *Nature Protocols*, *1*(6), 3159–3165. <https://doi.org/10.1038/nprot.2006.378>

- Rajendran, M., Dane, E., Conley, J., & Tantama, M. (2016). Imaging adenosine triphosphate (ATP). *Biological Bulletin*. <https://doi.org/10.1086/689592>
- Ralevic, V., & Burnstock, G. (1998). Receptors for purines and pyrimidines. *Pharmacological Reviews*. [https://doi.org/10.1007/978-3-642-28863-0\\_5](https://doi.org/10.1007/978-3-642-28863-0_5)
- Rama, R., & Garcia Rodriguez, J. C. (2012). Excitotoxicity and Oxidative Stress in Acute Ischemic Stroke. In *Acute Ischemic Stroke* (Vol. 395, pp. 116–124). InTech. <https://doi.org/10.5772/28300>
- Ramonet, D., Daher, J. P. L., Lin, B. M., Stafa, K., Kim, J., Banerjee, R., ... Moore, D. J. (2011). Dopaminergic Neuronal loss, Reduced Neurite Complexity and Autophagic Abnormalities in Transgenic Mice Expressing G2019S Mutant LRRK2. *PLoS ONE*. <https://doi.org/10.1371/journal.pone.0018568>
- Ray Dorsey, E., Elbaz, A., Nichols, E., Abd-Allah, F., Abdelalim, A., Adsuar, J. C., ... Murray, C. J. L. (2018). Global, regional, and national burden of Parkinson's disease, 1990–2016: a systematic analysis for the Global Burden of Disease Study 2016. *The Lancet Neurology*. [https://doi.org/10.1016/S1474-4422\(18\)30295-3](https://doi.org/10.1016/S1474-4422(18)30295-3)
- Reigada, D., Navarro-Ruiz, R. M., Caballero-López, M. J., Del Águila, Á., Muñoz-Galdeano, T., Maza, R. M., & Nieto-Díaz, M. (2017). Diadenosine tetraphosphate (Ap<sub>4</sub>A) inhibits ATP-induced excitotoxicity: a neuroprotective strategy for traumatic spinal cord injury treatment. *Purinergic Signalling*. <https://doi.org/10.1007/s11302-016-9541-4>
- Reinhardt, P., Schmid, B., Burbulla, L. F., Schöndorf, D. C., Wagner, L., Glatza, M., ... Sternecker, J. (2013). Genetic correction of a *lrrk2* mutation in human iPSCs links parkinsonian neurodegeneration to ERK-dependent changes in gene expression. *Cell Stem Cell*, 12(3). <https://doi.org/10.1016/j.stem.2013.01.008>
- Reynolds, I. J., & Hastings, T. G. (1995). Glutamate induces the production of reactive oxygen species in cultured forebrain neurons following NMDA receptor activation. *Journal of Neuroscience*, 15(5 D), 3318–3327. <https://doi.org/10.1523/jneurosci.15-05-03318.1995>
- Richardson, J. R., Quan, Y., Sherer, T. B., Greenamyre, J. T., & Miller, G. W. (2005). Paraquat neurotoxicity is distinct from that of MPTP and rotenone. *Toxicological Sciences*. <https://doi.org/10.1093/toxsci/kfi304>
- Robinson, K. M., Janes, M. S., Pehar, M., Monette, J. S., Ross, M. F., Hagen, T. M., ... Beckman, J. S. (2006). Selective fluorescent imaging of superoxide in vivo using ethidium-based probes. *Proceedings of the National Academy of Sciences of the United States of America*. <https://doi.org/10.1073/pnas.0601945103>
- Robson, S. C., Sévigny, J., & Zimmermann, H. (2006). The E-NTPDase family of ectonucleotidases: Structure function relationships and pathophysiological significance. *Purinergic Signalling*, 2(2), 409–430. <https://doi.org/10.1007/s11302-006-9003-5>

- Rothe, G., & Valet, G. (1990). Flow cytometric analysis of respiratory burst activity in phagocytes with hydroethidine and 2',7'-dichlorofluorescein. *Journal of Leukocyte Biology*. <https://doi.org/10.1002/jlb.47.5.440>
- Rothman, D. L., Sibson, N. R., Hyder, F., Shen, J., Behar, K. L., & Shulman, R. G. (1999). In vivo nuclear magnetic resonance spectroscopy studies of the relationship between the glutamate-glutamine neurotransmitter cycle and functional neuroenergetics. *Philosophical Transactions of the Royal Society B: Biological Sciences*. <https://doi.org/10.1098/rstb.1999.0472>
- Rothstein, J. D., Dykes-Hoberg, M., Pardo, C. A., Bristol, L. A., Jin, L., Kuncl, R. W., ... Welty, D. F. (1996). Knockout of glutamate transporters reveals a major role for astroglial transport in excitotoxicity and clearance of glutamate. *Neuron*. [https://doi.org/10.1016/S0896-6273\(00\)80086-0](https://doi.org/10.1016/S0896-6273(00)80086-0)
- Sanders, L. H., Laganière, J., Cooper, O., Mak, S. K., Vu, B. J., Huang, Y. A., ... Schüle, B. (2014). LRRK2 mutations cause mitochondrial DNA damage in iPSC-derived neural cells from Parkinson's disease patients: Reversal by gene correction. *Neurobiology of Disease*, 62. <https://doi.org/10.1016/j.nbd.2013.10.013>
- Saxena, S., & Caroni, P. (2011). Selective Neuronal Vulnerability in Neurodegenerative Diseases: From Stressor Thresholds to Degeneration. *Neuron*. <https://doi.org/10.1016/j.neuron.2011.06.031>
- Schapira, A. H. V., Cooper, J. M., Dexter, D., Clark, J. B., Jenner, P., & Marsden, C. D. (1990). Mitochondrial Complex I Deficiency in Parkinson's Disease. *Journal of Neurochemistry*, 54(3), 823–827. <https://doi.org/10.1111/j.1471-4159.1990.tb02325.x>
- Schieber, M., & Chandel, N. S. (2014). ROS Function in Redox Signaling and Oxidative Stress. *Current Biology*, 24(10), R453–R462. <https://doi.org/10.1016/j.cub.2014.03.034>
- Sedlak, J., & Lindsay, R. H. (1968). Estimation of total, protein-bound, and nonprotein sulfhydryl groups in tissue with Ellman's reagent. *Analytical Biochemistry*. [https://doi.org/10.1016/0003-2697\(68\)90092-4](https://doi.org/10.1016/0003-2697(68)90092-4)
- Sedlak, T. W., Paul, B. D., Parker, G. M., Hester, L. D., Snowman, A. M., Taniguchi, Y., ... Sawa, A. (2019). The glutathione cycle shapes synaptic glutamate activity. *Proceedings of the National Academy of Sciences of the United States of America*. <https://doi.org/10.1073/pnas.1817885116>
- Shadel, G. S., & Horvath, T. L. (2015). Mitochondrial ROS Signaling in Organismal Homeostasis. *Cell*. <https://doi.org/10.1016/j.cell.2015.10.001>
- Shaner, N. C., Campbell, R. E., Steinbach, P. A., Giepmans, B. N. G., Palmer, A. E., & Tsien, R. Y. (2004). Improved monomeric red, orange and yellow fluorescent proteins derived from *Discosoma* sp. red fluorescent protein. *Nature Biotechnology*, 22(12), 1567–1572. <https://doi.org/10.1038/nbt1037>

- Shaner, N. C., Lin, M. Z., McKeown, M. R., Steinbach, P. A., Hazelwood, K. L., Davidson, M. W., & Tsien, R. Y. (2008). Improving the photostability of bright monomeric orange and red fluorescent proteins. *Nature Methods*, 5(6), 545–551. <https://doi.org/10.1038/nmeth.1209>
- Shcherbakova, D. M., Baloban, M., Emelyanov, A. V., Brenowitz, M., Guo, P., & Verkhusha, V. V. (2016). Bright monomeric near-infrared fluorescent proteins as tags and biosensors for multiscale imaging. *Nature Communications*. <https://doi.org/10.1038/ncomms12405>
- Sherer, T. B., Betarbet, R., Testa, C. M., Seo, B. B., Richardson, J. R., Kim, J. H., ... Greenamyre, J. T. (2003). Mechanism of Toxicity in Rotenone Models of Parkinson's Disease. *Journal of Neuroscience*. <https://doi.org/10.1523/jneurosci.23-34-10756.2003>
- Shigenaga, M. K., Park, J. W., Cundy, K. C., Gimeno, C. J., & Ames, B. N. (1990). In Vivo Oxidative DNA damage: Measurement of 8-Hydroxy-2'-deoxyguanosine in DNA and urine by high-performance liquid chromatography with electrochemical detection. *Methods in Enzymology*. [https://doi.org/10.1016/0076-6879\(90\)86146-M](https://doi.org/10.1016/0076-6879(90)86146-M)
- Shigetomi, E., Kracun, S., Sofroniew, M. V., & Khakh, B. S. (2010). A genetically targeted optical sensor to monitor calcium signals in astrocyte processes. *Nature Neuroscience*. <https://doi.org/10.1038/nn.2557>
- Shih, A. Y., Johnson, D. A., Wong, G., Kraft, A. D., Jiang, L., Erb, H., ... Murphy, T. H. (2003). Coordinate Regulation of Glutathione Biosynthesis and Release by Nrf2-Expressing Glia Potently Protects Neurons from Oxidative Stress. *The Journal of Neuroscience*, 23(8), 3394–3406. <https://doi.org/10.1523/JNEUROSCI.23-08-03394.2003>
- Shokhina, A. G., Belousov, V. V., & Bilan, D. S. (2019). A genetically encoded biosensor rokate for monitoring the redox state of the glutathione pool. *Bulletin of Russian State Medical University*, (1), 86–92. <https://doi.org/10.24075/brsmu.2019.013>
- Shokhina, Arina G., Kostyuk, A. I., Ermakova, Y. G., Panova, A. S., Staroverov, D. B., Egorov, E. S., ... Bilan, D. S. (2019). Red fluorescent redox-sensitive biosensor Grx1-roCherry. *Redox Biology*. <https://doi.org/10.1016/j.redox.2018.101071>
- Shulaev, V., & Oliver, D. J. (2006). Metabolic and proteomic markers for oxidative stress. New tools for reactive oxygen species research. *Plant Physiology*. <https://doi.org/10.1104/pp.106.077925>
- Shults, C. W., Haas, R. H., Passov, D., & Beal, M. F. (1997). Coenzyme Q10 levels correlate with the activities of complexes I and II/III in mitochondria from Parkinsonian and nonparkinsonian subjects. *Annals of Neurology*, 42(2), 261–264. <https://doi.org/10.1002/ana.410420221>
- Signaling, S., Harden, K., Boyer, J. L., & Nicholas, R. A. (1995). P2-PURINERGIC RECEPTORS :

- Smith, W. W., Pei, Z., Jiang, H., Moore, D. J., Liang, Y., West, A. B., ... Ross, C. A. (2005). Leucine-rich repeat kinase 2 (LRRK2) interacts with parkin, and mutant LRRK2 induces neuronal degeneration. *Proceedings of the National Academy of Sciences of the United States of America*. <https://doi.org/10.1073/pnas.0508052102>
- Sohal, R. S., & Orr, W. C. (2012). The redox stress hypothesis of aging. *Free Radical Biology and Medicine*. <https://doi.org/10.1016/j.freeradbiomed.2011.10.445>
- Spitz, D. R., Azzam, E. I., Li, J. J., & Gius, D. (2004). Metabolic oxidation/reduction reactions and cellular responses to ionizing radiation: A unifying concept in stress response biology. *Cancer and Metastasis Reviews*. <https://doi.org/10.1023/B:CANC.0000031769.14728.bc>
- Steger, M., Tonelli, F., Ito, G., Davies, P., Trost, M., Vetter, M., ... Mann, M. (2016). Phosphoproteomics reveals that Parkinson's disease kinase LRRK2 regulates a subset of Rab GTPases. *ELife*. <https://doi.org/10.7554/elife.12813>
- Sulzer, D., & Surmeier, D. J. (2013). Neuronal vulnerability, pathogenesis, and Parkinson's disease. *Movement Disorders*, 28(1), 41–50. <https://doi.org/10.1002/mds.25095>
- Surmeier, D. J., Guzman, J. N., Sanchez-Padilla, J., & Schumacker, P. T. (2011). The role of calcium and mitochondrial oxidant stress in the loss of substantia nigra pars compacta dopaminergic neurons in Parkinson's disease. *Neuroscience*. <https://doi.org/10.1016/j.neuroscience.2011.08.045>
- Surmeier, D. James, Guzman, J. N., Sanchez-Padilla, J., & Goldberg, J. A. (2010). *What causes the death of dopaminergic neurons in Parkinson's disease? Progress in Brain Research* (Vol. 183). Elsevier B.V. [https://doi.org/10.1016/S0079-6123\(10\)83004-3](https://doi.org/10.1016/S0079-6123(10)83004-3)
- Suzen, S., Gurer-Orhan, H., & Saso, L. (2017). Detection of reactive oxygen and nitrogen species by electron paramagnetic resonance (EPR) technique. *Molecules*, 22(1), 1–9. <https://doi.org/10.3390/molecules22010181>
- Swain, L., Kesemeyer, A., Meyer-Roxlau, S., Vettel, C., Zieseniss, A., Güntsch, A., ... Katschinski, D. M. (2016). Redox Imaging Using Cardiac Myocyte-Specific Transgenic Biosensor Mice. *Circulation Research*. <https://doi.org/10.1161/CIRCRESAHA.116.309551>
- Sweet, E. S., Saunier-Rebori, B., Yue, Z., & Blitzer, R. D. (2015). The Parkinson's disease-associated mutation LRRK2-G2019S impairs synaptic plasticity in mouse hippocampus. *Journal of Neuroscience*. <https://doi.org/10.1523/JNEUROSCI.0040-15.2015>
- Tajeddine, N. (2016). How do reactive oxygen species and calcium trigger mitochondrial membrane permeabilisation? *Biochimica et Biophysica Acta - General Subjects*, 1860(6), 1079–1088. <https://doi.org/10.1016/j.bbagen.2016.02.013>
- Tan, Z., Liu, Y., Xi, W., Lou, H. F., Zhu, L., Guo, Z., ... Duan, S. (2017). Glia-derived ATP inversely regulates excitability of pyramidal and CCK-positive neurons. *Nature Communications*. <https://doi.org/10.1038/ncomms13772>

- Tantama, M., Hung, Y. P., & Yellen, G. (2011). Imaging intracellular pH in live cells with a genetically encoded red fluorescent protein sensor. *Journal of the American Chemical Society*. <https://doi.org/10.1021/ja202902d>
- Tantama, M., Martínez-François, J. R., Mongeon, R., & Yellen, G. (2013). Imaging energy status in live cells with a fluorescent biosensor of the intracellular ATP-to-ADP ratio. *Nature Communications*. <https://doi.org/10.1038/ncomms3550>
- Testa, C. M., Sherer, T. B., & Greenamyre, J. T. (2005). Rotenone induces oxidative stress and dopaminergic neuron damage in organotypic substantia nigra cultures. *Molecular Brain Research*. <https://doi.org/10.1016/j.molbrainres.2004.11.007>
- Thestrup, T., Litzlbauer, J., Bartholomäus, I., Mues, M., Russo, L., Dana, H., ... Griesbeck, O. (2014). Optimized ratiometric calcium sensors for functional in vivo imaging of neurons and T lymphocytes. *Nature Methods*. <https://doi.org/10.1038/nmeth.2773>
- Thomas, B., & Flint Beal, M. (2007). Parkinson's disease. *Human Molecular Genetics*. <https://doi.org/10.1093/hmg/ddm159>
- Timme-Laragy, A. R., Goldstone, J. V., Imhoff, B. R., Stegeman, J. J., Hahn, M. E., & Hansen, J. M. (2013). Glutathione redox dynamics and expression of glutathione-related genes in the developing embryo. *Free Radical Biology and Medicine*. <https://doi.org/10.1016/j.freeradbiomed.2013.06.011>
- Torres, A., Wang, F., Xu, Q., Fujita, T., Dobrowolski, R., Willecke, K., ... Nedergaard, M. (2012). Extracellular Ca<sup>2+</sup> acts as a mediator of communication from neurons to glia. *Science Signaling*. <https://doi.org/10.1126/scisignal.2002160>
- Tozzi, A., Tantucci, M., Marchi, S., Mazzocchetti, P., Morari, M., Pinton, P., ... Calabresi, P. (2018). Dopamine D2 receptor-mediated neuroprotection in a G2019S Lrrk2 genetic model of Parkinson's disease. *Cell Death and Disease*. <https://doi.org/10.1038/s41419-017-0221-2>
- Trouillon, R., & Ewing, A. G. (2013). Single cell amperometry reveals glycocalyx hinders the release of neurotransmitters during exocytosis. *Analytical Chemistry*. <https://doi.org/10.1021/ac4008682>
- Tsien, R. Y. (1998). THE GREEN FLUORESCENT PROTEIN. *Annual Review of Biochemistry*. <https://doi.org/10.1146/annurev.biochem.67.1.509>
- Tsika, E., Kannan, M., Foo, C. S. Y., Dikeman, D., Glauser, L., Gellhaar, S., ... Moore, D. J. (2014). Conditional expression of Parkinson's disease-related R1441C LRRK2 in midbrain dopaminergic neurons of mice causes nuclear abnormalities without neurodegeneration. *Neurobiology of Disease*. <https://doi.org/10.1016/j.nbd.2014.08.027>
- Tsika, E., Nguyen, A. P. T., Dusonchet, J., Colin, P., Schneider, B. L., & Moore, D. J. (2015). Adenoviral-mediated expression of G2019S LRRK2 induces striatal pathology in a kinase-dependent manner in a rat model of Parkinson's disease. *Neurobiology of Disease*. <https://doi.org/10.1016/j.nbd.2015.02.019>

- Vaahtera, L., Brosché, M., Wrzaczek, M., & Kangasjärvi, J. (2014). Specificity in ROS signaling and transcript signatures. *Antioxidants & Redox Signaling*. <https://doi.org/10.1089/ars.2013.5662>
- van Hoesen, G. W., Hyman, B. T., & Damasio, A. R. (1991). Entorhinal cortex pathology in Alzheimer's disease. *Hippocampus*. <https://doi.org/10.1002/hipo.450010102>
- Vargas, M. R., Johnson, D. A., Sirkis, D. W., Messing, A., & Johnson, J. A. (2008). Nrf2 activation in astrocytes protects against neurodegeneration in mouse models of familial amyotrophic lateral sclerosis. *Journal of Neuroscience*. <https://doi.org/10.1523/JNEUROSCI.4099-08.2008>
- Verma, M., Callio, J., Otero, P. A., Sekler, I., Wills, Z. P., & Chu, C. T. (2017). Mitochondrial Calcium Dysregulation Contributes to Dendrite Degeneration Mediated by PD/LBD-Associated LRRK2 Mutants. *The Journal of Neuroscience*, 37(46), 11151–11165. <https://doi.org/10.1523/jneurosci.3791-16.2017>
- Vesce, S., Jekabsons, M. B., Johnson-Cadwell, L. I., & Nicholls, D. G. (2005). Acute glutathione depletion restricts mitochondrial ATP export in cerebellar granule neurons. *Journal of Biological Chemistry*, 280(46), 38720–38728. <https://doi.org/10.1074/jbc.M506575200>
- Villamena, F. A., & Zweier, J. L. (2004). Detection of Reactive Oxygen and Nitrogen Species by EPR Spin Trapping. *Antioxidants & Redox Signaling*, 6(3), 619–629. <https://doi.org/10.1089/152308604773934387>
- Vishnu, N., Khan, M. J., Karsten, F., Groschner, L. N., Waldeck-Weiermair, M., Rost, R., ... Malli, R. (2014). ATP increases within the lumen of the endoplasmic reticulum upon intracellular Ca<sup>2+</sup> release. *Molecular Biology of the Cell*. <https://doi.org/10.1091/mbc.E13-07-0433>
- von Schack, D., Agostino, M. J., Murray, B. S., Li, Y., Reddy, P. S., Chen, J., ... Ajit, S. K. (2011). Dynamic changes in the microRNA expression profile reveal multiple regulatory mechanisms in the spinal nerve ligation model of neuropathic pain. *PLoS ONE*. <https://doi.org/10.1371/journal.pone.0017670>
- Wagener, K. C., Kolbrink, B., Dietrich, K., Kizina, K. M., Terwitte, L. S., Kempkes, B., ... Müller, M. (2016). Redox Indicator Mice Stably Expressing Genetically Encoded Neuronal roGFP: Versatile Tools to Decipher Subcellular Redox Dynamics in Neuropathophysiology. *Antioxidants and Redox Signaling*, 25(1), 41–58. <https://doi.org/10.1089/ars.2015.6587>
- Wang, Xianhua, Fang, H., Huang, Z., Shang, W., Hou, T., Cheng, A., & Cheng, H. (2013). Imaging ROS signaling in cells and animals. *Journal of Molecular Medicine*, 91(8), 917–927. <https://doi.org/10.1007/s00109-013-1067-4>
- Wang, Xinglong, Yan, M. H., Fujioka, H., Liu, J., Wilson-delfosse, A., Chen, S. G., ... Zhu, X. (2012a). LRRK2 regulates mitochondrial dynamics and function through direct interaction with DLP1. *Human Molecular Genetics*. <https://doi.org/10.1093/hmg/dds003>

- Wang, Xinglong, Yan, M. H., Fujioka, H., Liu, J., Wilson-delfosse, A., Chen, S. G., ... Zhu, X. (2012b). LRRK2 regulates mitochondrial dynamics and function through direct interaction with DLP1. *Human Molecular Genetics*, 21(9), 1931–1944. <https://doi.org/10.1093/hmg/dds003>
- Wang, Xinkun, & Michaelis, E. K. (2010). Selective neuronal vulnerability to oxidative stress in the brain. *Frontiers in Aging Neuroscience*, 2(MAR), 1–13. <https://doi.org/10.3389/fnagi.2010.00012>
- Weber, F. C., Esser, P. R., Müller, T., Ganesan, J., Pellegatti, P., Simon, M. M., ... Martin, S. F. (2010). Lack of the purinergic receptor P2X7 results in resistance to contact hypersensitivity. *Journal of Experimental Medicine*. <https://doi.org/10.1084/jem.20092489>
- West, A. B., Moore, D. J., Biskup, S., Bugayenko, A., Smith, W. W., Ross, C. A., ... Dawson, T. M. (2005a). Parkinson's disease-associated mutations in leucine-rich repeat kinase 2 augment kinase activity. *Proceedings of the National Academy of Sciences of the United States of America*. <https://doi.org/10.1073/pnas.0507360102>
- West, A. B., Moore, D. J., Biskup, S., Bugayenko, A., Smith, W. W., Ross, C. A., ... Dawson, T. M. (2005b). Parkinson's disease-associated mutations in leucine-rich repeat kinase 2 augment kinase activity.
- Weydert, C. J., & Cullen, J. J. (2010). Measurement of superoxide dismutase, catalase and glutathione peroxidase in cultured cells and tissue. *Nature Protocols*, 5(1), 51–66. <https://doi.org/10.1038/nprot.2009.197>
- Wilhelm, K., Ganesan, J., Müller, T., Dürr, C., Grimm, M., Beilhack, A., ... Zeiser, R. (2010). Graft-versus-host disease is enhanced by extracellular ATP activating P2X7R. *Nature Medicine*. <https://doi.org/10.1038/nm.2242>
- Wilson, J. X. (1997). Antioxidant defense of the brain: A role for astrocytes. *Canadian Journal of Physiology and Pharmacology*. <https://doi.org/10.1139/y97-146>
- Winterbourn, C. C., & Hampton, M. B. (2008). Thiol chemistry and specificity in redox signaling. *Free Radical Biology and Medicine*, 45(5), 549–561. <https://doi.org/10.1016/j.freeradbiomed.2008.05.004>
- Wolf, A. M., Nishimaki, K., Kamimura, N., & Ohta, S. (2014). Real-time monitoring of oxidative stress in live mouse skin. *Journal of Investigative Dermatology*. <https://doi.org/10.1038/jid.2013.428>
- Wu, J., Abdelfattah, A. S., Miraucourt, L. S., Kutsarova, E., Ruangkittisakul, A., Zhou, H., ... Campbell, R. E. (2014). A long Stokes shift red fluorescent Ca<sup>2+</sup> indicator protein for two-photon and ratiometric imaging. *Nature Communications*. <https://doi.org/10.1038/ncomms6262>

- Xie, W., & Chung, K. K. K. (2012). Alpha-synuclein impairs normal dynamics of mitochondria in cell and animal models of Parkinson's disease. *Journal of Neurochemistry*. <https://doi.org/10.1111/j.1471-4159.2012.07769.x>
- Yadava, N., & Nicholls, D. G. (2007). Spare respiratory capacity rather than oxidative stress regulates glutamate excitotoxicity after partial respiratory inhibition of mitochondrial complex I with rotenone. *Journal of Neuroscience*. <https://doi.org/10.1523/JNEUROSCI.0212-07.2007>
- Yaginuma, H., Kawai, S., Tabata, K. V., Tomiyama, K., Kakizuka, A., Komatsuzaki, T., ... Imamura, H. (2014). Diversity in ATP concentrations in a single bacterial cell population revealed by quantitative single-cell imaging. *Scientific Reports*. <https://doi.org/10.1038/srep06522>
- Yano, T., Oku, M., Akeyama, N., Itoyama, A., Yurimoto, H., Kuge, S., ... Sakai, Y. (2010). A Novel Fluorescent Sensor Protein for Visualization of Redox States in the Cytoplasm and in Peroxisomes. *Molecular and Cellular Biology*, 30(15), 3758–3766. <https://doi.org/10.1128/MCB.00121-10>
- Yue, M., Hinkle, K. M., Davies, P., Trushina, E., Fiesel, F. C., Christenson, T. A., ... Melrose, H. L. (2015). Progressive dopaminergic alterations and mitochondrial abnormalities in LRRK2 G2019S knock-in mice. *Neurobiology of Disease*, 78, 172–195. <https://doi.org/10.1016/j.nbd.2015.02.031>
- Zhang, H., Limphong, P., Pieper, J., Liu, Q., Rodesch, C. K., Christians, E., & Benjamin, I. J. (2012). Glutathione-dependent reductive stress triggers mitochondrial oxidation and cytotoxicity. *The FASEB Journal*. <https://doi.org/10.1096/fj.11-199869>
- Zhang, J., Campbell, R. E., Ting, A. Y., & Tsien, R. Y. (2002). Creating new fluorescent probes for cell biology. *Nature Reviews Molecular Cell Biology*. <https://doi.org/10.1038/nrm976>
- Zhang, Y., Phillips, G. J., Li, Q., & Yeung, E. S. (2008). Imaging localized astrocyte ATP release with firefly luciferase beads attached to the cell surface. *Analytical Chemistry*. <https://doi.org/10.1021/ac801701w>
- Zhang, Z., Chen, G., Zhou, W., Song, A., Xu, T., Luo, Q., ... Duan, S. (2007a). Regulated ATP release from astrocytes through lysosome exocytosis. *Nature Cell Biology*, 9(8), 945–953. <https://doi.org/10.1038/ncb1620>
- Zhang, Z., Chen, G., Zhou, W., Song, A., Xu, T., Luo, Q., ... Duan, S. (2007b). Regulated ATP release from astrocytes through lysosome exocytosis. *Nature Cell Biology*. <https://doi.org/10.1038/ncb1620>
- Zhao, Y., Araki, S., Wu, J., Teramoto, T., Chang, Y. F., Nakano, M., ... Campbell, R. E. (2011). An expanded palette of genetically encoded Ca<sup>2+</sup> indicators. *Science*. <https://doi.org/10.1126/science.1208592>

- Zielonka, J., & Kalyanaraman, B. (2010). Hydroethidine- and MitoSOX-derived red fluorescence is not a reliable indicator of intracellular superoxide formation: Another inconvenient truth. *Free Radical Biology and Medicine*. <https://doi.org/10.1016/j.freeradbiomed.2010.01.028>
- Zimprich, A., Biskup, S., Leitner, P., Lichtner, P., Farrer, M., Lincoln, S., ... Gasser, T. (2004). Mutations in LRRK2 Cause Autosomal-Dominant Parkinsonism with Pleomorphic Pathology, *44*, 601–607.
- Zündorf, G., Kahlert, S., & Reiser, G. (2007). Gap-junction blocker carbenoxolone differentially enhances NMDA-induced cell death in hippocampal neurons and astrocytes in co-culture. *Journal of Neurochemistry*, *102*(2), 508–521. <https://doi.org/10.1111/j.1471-4159.2007.04509.x>

## VITA

Saranya Radhakrishnan was born in Chennai, India. She obtained her bachelor's degree in Bioengineering at SASTRA University, India in 2012. She spent a year as a research intern at the Brigham and Women's Hospital, Boston studying the association of copy number variants with methylation variation. In 2013, she worked as a junior research fellow at the Center for Neuroscience in the Indian Institute of Science where she studied the development of disease pathology in microcephaly. She joined Purdue University as a graduate student through the PULSe program. She joined the Tantama lab in June 2016. Saranya will continue her research career as a postdoctoral research fellow at the National Institute of Mental Health in Bethesda, Maryland.

## PUBLICATIONS

Radhakrishnan S, Norley J, Wendt S, LeRoy N, Hall Hana, Norcross S, Doan S, Snaider J, MacVicar B.A., Weake V.M., Huang L., Tantama M. Neuron activity-dependent redox compartmentation revealed with a second generation red-shifted ratiometric sensor. *Manuscript under review*

Conley, J. M., Radhakrishnan, S., Valentino, S. A., & Tantama, M. (2017). Imaging extracellular ATP with a genetically-encoded, ratiometric fluorescent sensor. *PLoS ONE*, 12(11), 1–24.